ZERO GRAVITY TWO-PHASE FLOW REGIME TRANSITION MODELING COMPARED WITH DATA AND RELAP5-3D PREDICTIONS

A Thesis

by

MELISSA RENEE GHRIST

Submitted to the Office of Graduate Studies of
Texas A&M University
in partial fulfillment of the requirements for the degree of

MASTER OF SCIENCE

December 2008

Major Subject: Nuclear Engineering

ZERO GRAVITY TWO-PHASE FLOW REGIME TRANSITION MODELING COMPARED WITH DATA AND RELAP5-3D PREDICTIONS

A Thesis

by

MELISSA RENEE GHRIST

Submitted to the Office of Graduate Studies of
Texas A&M University
in partial fulfillment of the requirements for the degree of

MASTER OF SCIENCE

Approved by:

Chair of Committee,	Frederick R. Best
Committee Members,	Yassin Hassan
	Debjyoti Banerjee
Head of Department,	Raymond Juzaitis

December 2008

Major Subject: Nuclear Engineering

ABSTRACT

Zero Gravity Two-Phase Flow Regime Transition Modeling Compared with Data and RELAP5-3D Predictions. (December 2008)

Melissa Renee Ghrist, B.S., Texas A&M University

Chair of Advisory Committee: Dr Frederick R. Best

This thesis compares air/water two-phase flow regime transition models in zero gravity with data and makes recommendations for zero gravity models to incorporate into the RELAP5-3D thermal hydraulic computer code. Data from numerous researchers and experiments are compiled into a large database. A RELAP5-3D model is built to replicate the zero gravity experiments, and flow regime results from the RELAP5-3D code are compared with data. The comparison demonstrates that the current flow regime maps used in the computer code do not scale to zero gravity. A new flow regime map is needed for zero gravity conditions.

Three bubbly-to-slug transition models and four slug-to-annular transition models are analyzed and compared with the data. A mathematical method is developed using least squares to objectively compare the accuracy of the models with the data. The models are graded by how well each represents the data. Agreement with data validates the recommendations made for changes to the RELAP5-3D computer code models. For smaller diameter tubes, Dukler's bubbly-to-slug model best fits the data. For the larger

tubes, the Drift Flux model is a better fit. The slug-to-annular transition is modeled best by Creare for small tubes and Reinarts for larger tubes.

A major finding of this thesis work is that more air/water data is needed at equally distributed flow velocities and a greater variety of tube diameters. More data is specifically needed in the predicted transition regions made in this study.

DEDICATION

I would like to dedicate all of my work to my mother, Sandra L. Ghrist. She is the strongest, most selfless, and hardest working woman I have ever known. Without her, I would not have had the inspiration to push myself so far. Without her, I wouldn't be the person I am today. I love you Mama and wish only to make you proud.

ACKNOWLEDGEMENTS

I would like to express my gratitude to my advisor and committee chairman, Dr. Frederick R. Best. He has spent many hours of his time discussing my thesis progress and reading through my work. He has supported me and believed in me from the moment I expressed interest in space power and two-phase flow. He has also encouraged me more than any other professor I had at Texas A&M. I would also like to thank the members of my committee for their efforts throughout the process, including Dr. Yassin Hassan and Debjyoti Banerjee.

I would also like to thank Cable Kurwitz and Ryoji Oinuma who have helped me through my entire career at Texas A&M. They both always made time for my questions even when they were overwhelmed with their own studies and work. I thoroughly enjoyed working and studying with these two wonderful people.

Sincere appreciation goes to the previous researchers who have spent their careers developing the models that I have analyzed in my work. I would also like to thank all of the people at NASA who encourage reduced gravity research.

Lastly I would like to thank my friends and family who have encouraged and believed in me. I know I would have never been able to get as far as I have without every single one of you.

NOMENCLATURE

Symbol	Description
a	Magnitude of acceleration (m/s^2)
A	Cross sectional area of tube (m^2)
Bo	Dimensionless Bond number
Co	Velocity distribution coefficient
D	Tube inner diameter (m)
f_i	Friction factor at gas-liquid interface
f_{wg}	Frition factor at gas-wall interface
f_{wl}	Friction factor at liquid-wall interface
F	Dimensionless Froude number
g	gravitational constant (m/s^2)
G_m	Average mixture mass flux (kg/m^2-s)
jg	Superficial velocity of the gas phase (m/s)
jf	Superficial velocity of the liquid phase (m/s)
k	Turbulence coefficient
Kg	Dimensionless Kutateladze number
M	Dimensionless superficial velocity ratio
We	Dimensionless Weber number
X	Dimensionless Martinelli parameter
Y	Dimensionless pipe inclination parameter

α_{BS}	Transition void fraction from bubbly to slug flow
α_{DE}	Transition void fraction from slug to slug/annular flow
α_{SA}	Transition void fraction from slug/annular to annular
α_{AM}	Transition void fraction from annular to dispersed flow
v_{crit}	Critical void fraction
v_g	Gas velocity (m/s)
v_f	Fluid velocity (m/s)
v_m	Mixing velocity (m/s)
ρ_g	Gas density (kg/m^3)
ρ_f	Fluid density (kg/m^3)
ρ_m	Mixture density (kg/m^3)
θ	Central angle

TABLE OF CONTENTS

Page

CHAPTER Page

LIST OF FIGURES

Page

Page

Page

Page

Page

Page

Page

LIST OF TABLES

Page

CHAPTER I

INTRODUCTION AND BACKGROUND

1.1 Microgravity Two-Phase Flow

Co-current two phase flows are expected to occur in a wide variety of space hardware including thermal management systems, storage and transfer of cryogenic fluids, and condensation and boiling in two phase power systems for space craft or lunar power plants (Ref 1). Therefore the study of gas-liquid flow in microgravity has a wide range of space applications. Space reactors are necessary for both long duration exploration and habitation in space. Future space exploration will require power systems that deliver one to several kilowatts of power for mission durations in excess of days (Ref 1). Nuclear power is an attractive option to meet power requirements and provide design flexibility that other power sources do not offer such as tolerance to external radiation, spacecraft orientation (in relation to the sun) independence, and attractive power-to-mass ratios. Lunar and Martian surface power are also of high interest. The interest in developing a lunar outpost has been increasing since the first lunar landing over 30 years ago. Lunar habitation would require a reliable power system to support energy demands. Nuclear power proves to be advantageous for such a system (Ref 1).

Due to the high thermal loads of proposed nuclear and associated power conversion systems, advanced thermal management techniques that utilize two-phase flow are required in order to achieve the projected efficiencies and mass/volume goals.

This thesis follows the style of *Nuclear Technology.*

On earth (1-g), the flow regime of a gas/liquid mixture is understood and pressure drop and heat transfer correlations are based on this knowledge. However, the flow regime models have strong gravity dependence and cannot be extended into reduced gravity conditions. As gravity is reduced, the mechanics of the flow change significantly. Gravity has a substantial effect on the flows due to the large density differences which exist between gas and liquid flows (Ref 2). Both pressure drop and heat transfer are dependent on the flow regime (Ref 3). To design two-phase systems for 0-g or other reduced accelerations, such as Lunar (~1/6-g) or Martian (~1/3-g) accelerations, flow regime prediction will be required in order to accurately model relevant thermal-hydraulic phenomena.

In vertical flows, gravity causes slip between phases and can cause periodic flow reversals such as in slug or churn flow (Ref 4). In horizontal flow, the force of gravity causes asymmetry of the flow, otherwise known as stratification. This occurs when the liquid flows at the bottom of the channel and the gas flows at the top of the channel. The stratified flow regime begins to disappear as gravity is reduced and does not appear at all in 0-g. Annular flow is observed at lower superficial velocities relative to 1-g flow. Annular flow occurs in 1-g at high vapor velocities where inertial forces overwhelm gravitational forces and at most velocities in small tubes where surface tension forces overwhelm gravitational forces. In zero gravity, annular flow occurs where stratified flow would occur on earth (Ref 5). Thicker liquid films on the wall during annular flow will affect heat transfer through the mixture. Because of these differences, reduced gravity flow regime models are needed. Computer codes, such as RELAP5-3D,

incorporate flow regime modeling in their calculations. Code flow regime models may prove inaccurate in reduced gravity conditions.

1.2 Introduction to RELAP5-3D

The purpose of this study is to evaluate the RELAP5-3D computer code's capability to predict flow regimes in reduced gravity and make suggestions for changes to the code models. The RELAP5-3D code is a thermal hydraulics code developed at Idaho National Laboratory (Ref 6) under sponsorship of the U.S. Department of Energy, the U.S. Regulatory Commission, members of the International Code Assessment and Applications Program (ICAP), members of the Code Applications and Maintenance Program (CAMP), and the members of the International RELAP5 Users Group (IRUG) (Ref 6). The code was developed to couple the reactor cooling system and the core in order to simulate transients in light water reactor (LWR) systems. These transients include loss of coolant accidents (LOCA), anticipated transients without scram (ATWS), and operational transients such as the loss of offsite power, loss of feedwater, blackout, and turbine trip (Ref 6). The RELAP5-3D code uses a generic modeling approach and can analyze the behavior of both nuclear and non-nuclear system transients including mixtures of vapor and liquid, non-condensable gases, and non-volatile solute.

The RELAP5-3D computer code has proven very accurate in modeling flow regimes for systems on the earth's surface. However, if the code is ever to be used to model system transients for space systems, the flow regime modeling will need to be altered to accurately predict flow regimes in reduced gravity conditions. INL has

recently become more involved in the space program. Therefore, it is highly desirable that the code developed at INL be modified to correctly address reduced gravity conditions.

1.3 Research Strategy and Thesis Outline

This study will consist of two main areas: first, a review of past work done in the area of reduced gravity flow regime modeling and the compilation of a database of reduced gravity two phase flow data, and second, a comparison of the flow regime prediction from RELAP5-3D with data, including modeling improvement recommendations.

The first chapter reviews applicable literature covering RELAP53-D flow regime models along with previous reduced gravity modeling efforts. The second chapter describes the experiments used to collect the data presented in the database. The database is presented in Chapter III. Chapter IV presents the flow regime models used in RELAP5-3D, and the Chapter V discusses current zero gravity flow regime models. The objective comparison of the current models is presented in chapter VI, and final recommendations are given in chapter VII.

1.4 Flow Regime Mapping

The technology of predicting flow regimes for co-current gas and liquid flows is a continuously developing field. There are many different models currently in use (Collier). One approach commonly used is the collection of flow data along with the visual identification of the flow regime. The data along with the visually observed flow regime are used to map transition boundaries between flow regimes. The maps are typically based on parameters of the flow such as superficial velocity or void fraction. Theoretical models have also been created using a force balance approach to predict the flow regime. The dominant forces acting on the fluid are identified, and then the balances between the forces are used to describe the transitions between flow regimes. These force balances include: the balance of buoyancy and inertial forces, and the balance of surface tension and inertial forces.

The generally accepted flow regimes for 1-g vertical flow are bubbly flow, slug flow, and annular flow but some researches have defined other flow regimes in between such as churn flow and wispy-annular flow (Ref 7). The vertical flow regimes are illustrated below in Figure 1.

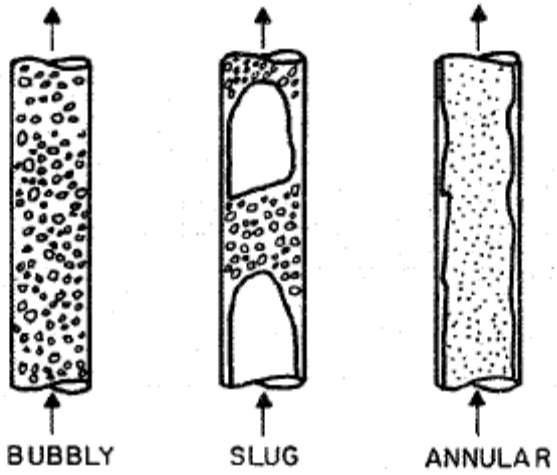

Figure 1 Vertical Flow Regime (Ref 8)

In bubbly flow, the vapor flow is distributed in distinct bubbles. The bubbles can be small and spherical or large with a spherical cap. In slug flow, the vapor bubbles are approximately the diameter of the pipe but are separated from the wall by a thin liquid film. The bubble is bullet shaped and the length of the bubbles can vary. Churn flow begins as the bubbles begin to break down and the flow becomes more chaotic. Wispy-annular flow exists when the flow has a relatively thick liquid film on the wall along with a significant amount of liquid entrained in a vapor core. Annular flow occurs when the vapor core is continuous (Ref 7). In horizontal flow, the generally accepted flow regimes are stratified flow, slug flow, and bubbly flow but are sometimes extended to include plug flow and wavy flow. Plug flow is similar to slug flow except that the bubbles flow in the upper half of the pipe. Stratified flow occurs at lower flow rates and is identified by the two phases being completely separated with the liquid in the lower part of the pipe, and the vapor at the top. As the vapor velocity increases, waves begin

to form in the direction of the flow. This is known as wavy flow. The horizontal flow regimes are shown in Figure 2.

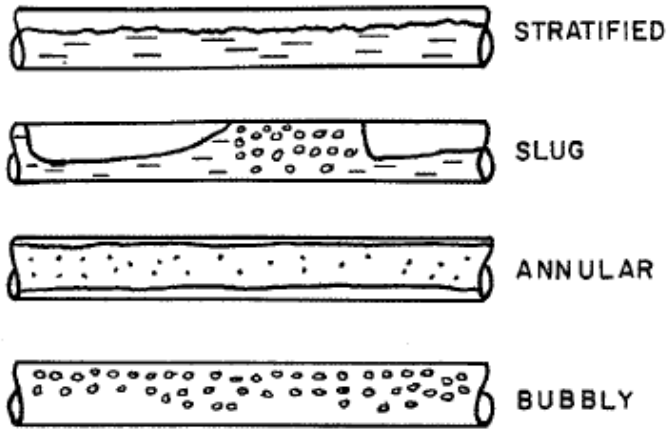

Figure 2: Horizontal Flow Regimes (Ref 8)

While flow regime mapping is common and well understood in normal gravity conditions, reduced gravity flow regime mapping is a work in progress. There is significantly less reduced gravity two phase flow data compared with the amount of 1-g data due partially to the fact that data are difficult to collect. There has been work done collecting reduced gravity data aboard NASA's reduced gravity aircraft, the space shuttle, and International Space Center (ISS) (Ref 9). The data has been analyzed and several different flow regime models have been developed to predict flow regime and flow regime transitions. It has been shown that only three basic flow regimes exist in microgravity: bubbly, slug, and annular flows. Figure 3 below shows the common flow regimes observed in microgravity.

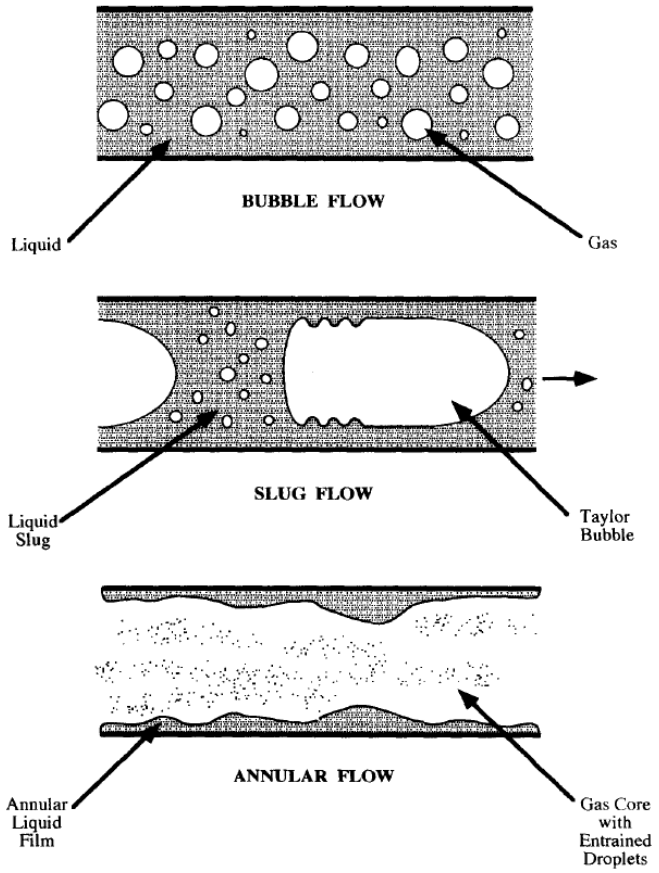

Figure 3: Microgravity Flow Regimes (Ref 9)

The Interphase Transport Phenomena (ITP) Laboratory of Texas A&M University has been studying two-phase flow in reduced gravity since 1986. Given that the database of low gravity two-phase flow is small, work has been carried out at Texas A&M to provide two-phase data for Lunar, Martian, and zero gravities. A database of reduced gravity multiphase flow data collected aboard the reduced gravity aircraft has been compiled along with the data collected from other researchers. The database includes void fraction, pressure drop, and flow rates for varying gravity fields (lunar, Martian, and zero) and for both air/water systems as well as refrigerants. This data can

be used to create flow regime maps which are a function of gravity field as well as to develop flow regime models scaled for various gravity conditions (Ref 10).

1.5 Summary

This flow regime study will consist of three major contributions: a zero-G flow regime data base and previous modeling efforts, a comparison of RELAP5-3D's flow regime output with the zero-G data and models, and suggestions for improvement of the code's flow regime models. This chapter introduced the importance of flow regime modeling in all gravity fields. The following chapter discusses the models utilized by RELAP5-3D along with the reasons why the models may fail in zero gravity conditions.

CHAPTER II

RELAP5-3D FLOW REGIME MAPPING

2.1 Introduction

RELAP5-3D has four flow regime maps built into the code: a horizontal map for flow in pipes, a vertical map for flow in pipes, annuli and bundles, a high mixing map for flow through pumps, and an emergency core coolant (ECC) mixer map for flow in the horizontal pipes near the ECC injection port. These flow regime maps are based on work done by Taitel and Dukler (Ref 6). Void fraction is the primary parameter used to characterize the flow regimes in the code.

2.2 Horizontal Flow Regime Map

The horizontal flow regime map is used for volumes with an inclination less than 30 degrees. This map is shown in Figure 4 where the shaded regions represent transition regions.

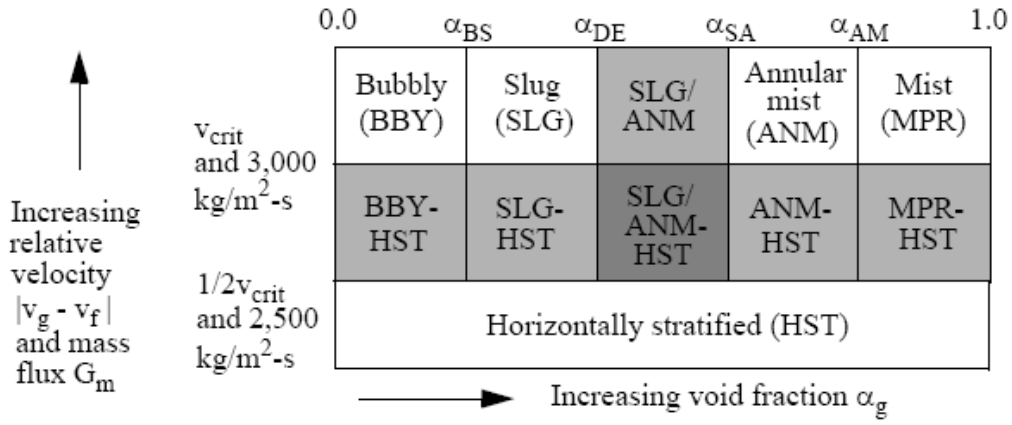

Figure 4: Schematic of Horizontal Flow Regime Map Used in RELAP5-3D (Ref 6)

The parameters shown in the horizontal flow regime map are defined below. G_m is the average mixture mass flux, α_{BS} is the transition void fraction from bubbly-to-slug flow, α_{DE} is the void fraction transition from slug flow to slug/annular mist flow, α_{SA} is the transition void fraction from slug/annular mist flow to annular mist flow, and α_{AM} is the transition void fraction between annular mist flow and dispersed (mist) flow.

$$G_m = \alpha_g \rho_g \left| v_g \right| + \alpha_f \rho_f \left| v_f \right|$$

Equation 1

$$\begin{aligned} \alpha_{BS} &= 0.25 \quad G_m \le 2{,}000 \text{ kg/m}^2 - s \\ &= 0.25 + 0.00025(G_m - 2{,}000) \quad 2{,}000 < G_m < 3{,}000 \text{ kg/m}^2 - s \\ &= 0.5 \quad G_m \ge 3{,}000 \text{ kg/m}^2 - s \end{aligned}$$

Equation 2

The graphical interpretation of Equation 2 is illustrated below in Figure 5 showing that the transition void fraction is constant at 0.25 until the mass flux reaches 2000 kg/m^{2}s. At that point it increases linearly until at 3000 kg/m2s it is constant again

at 0.5. The lower limit of 0.25 void fraction is based on the conclusion by previous researchers that coalescence increases sharply when bubble spacing decreases to about half the bubble radius which corresponds to 25% void (Ref 6). RELAP5-3D uses 0.5 as an upper limit on void fraction based on a conclusion that 0.52 is the absolute maximum attainable void fraction for bubbly flow. This assumption is based on the presence of vigorous turbulent diffusion (Ref 6). The linear increase from 0.25 to 0.5 void fraction is RELAP5-3D's attempt to account for an increase in the maximum bubbly void fraction due to turbulence (Ref 6).

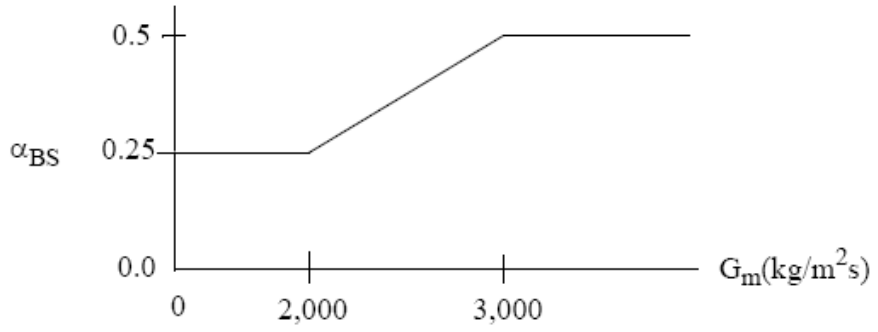

Figure 5: Horizontal Bubbly-to-Slug Void Fraction Transition in RELAP5-3D (Ref 6)

The RELAP5-3D code uses a void fraction range of 0.75 and 0.8 (as shown in Equation 3 and Equation 4) for the slug-to-annular mist transition region. This is based on research performed that implies that annular flow can occur for a void fraction greater than 0.76 (Ref 6). The research indicates that for co-current up flow, the transition criteria give reasonable agreement with air/water systems at atmospheric conditions for a 2.5 and 5.1 cm diameter tube, and Freon for a 2.5 cm tube (Ref 6).

$$\alpha_{DE} = 0.75$$

Equation 3

$$\alpha_{SA} = 0.8$$

Equation 4

Equation 5 shows the void fraction for which annular mist flow no longer exists and dispersed flow takes over. This void fraction was chosen to allow a smooth transition to single phase vapor/gas flow.

$$\alpha_{AM} = 0.9999$$

Equation 5

The critical void fraction, v_{crit}, shown in Equation 6 represents the gas velocity above which waves form (Ref 6). The critical void fraction is used to determine if the flow is stratified or not. In zero gravity conditions, stratified flow would not be expected.

$$v_{crit} = \frac{1}{2}\left[\frac{\left(\rho_f - \rho_g\right) g \alpha_g A}{\rho_g D \sin\theta}\right]^{1/2} \left(1 - \cos\theta\right)$$

Equation 6

The central angle θ shown in Equation 6 and Equation 7 is related to the liquid level with respect to the bottom of the volume (Ref 6). This relationship is illustrated in Figure 6 below.

$$\pi\alpha_g = \theta - \sin\theta\cos\theta$$

Equation 7

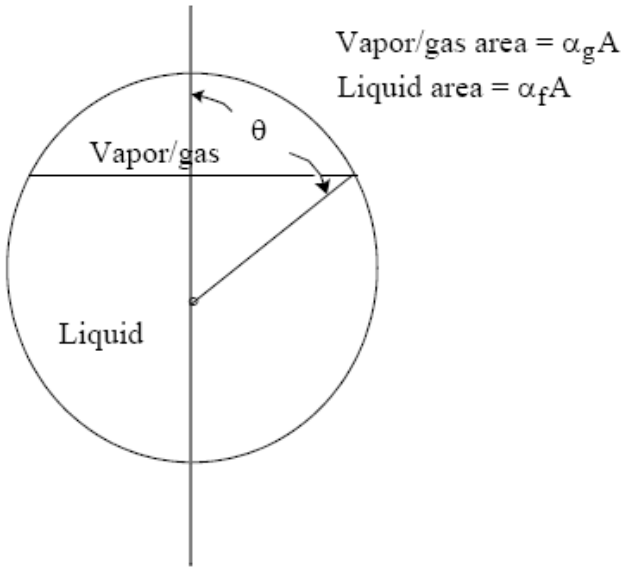

Figure 6: Relation of Central Angle to Void Fraction (Ref 6)

In Taitel and Dukler's model, horizontal stratification occurs when the following Equation is satisfied.

$$|v_g| < v_{crit}$$

Equation 8

However, the RELAP5-3D flow regime model modified this condition to relax the assumption of stagnant flow made by Taitel and Dukler (Ref 6). The modified horizontal stratification Equation is shown in Equation 9 and Equation 10.

$$|v_g - v_f| < v_{crit}$$

Equation 9

$$G_m < 3{,}000 \text{ kg/m}^2\text{-s}$$

Equation 10

If these two Equations are true, the flow regime will be horizontally stratified (HST) represented by the lower portion of the flow regime map in Figure 4. If the

conditions are not true, the flow will be bubbly, slug, annular mist, or dispersed flow regimes represented by the upper portion of the flow regime map in Figure 4.

This horizontal flow regime model fails in zero gravity conditions. In the Equation defining critical velocity, the gravity acceleration constant is multiplied with void fraction and density parameters in the numerator. In the case of a zero gravity constant, the critical void fraction would be zero and no transition would be defined. Therefore for purposes of this study, the acceleration constant used in RELAP5-3D will be 0.001 g instead of 0g. At this reduced gravity, v_{crit} defined in Equation 6 will be reduced to a small number. This will remove the possibility of stratified flow due to the relationship shown in Equation 9. The method of constant void fraction for bubbly-to-slug flow is a common method that is utilized by many researchers. However, research in zero gravity conditions that will be outlined in upcoming sections show a void fraction for the transition to be between 0.4 and 0.45 for zero gravity. This differs from the transition void fraction utilized by RELAP5-3D's value beginning at 0.25 for lower mass fluxes. This disparity will show in the comparison of the zero gravity data compared with RELAP5-3D's output.

2.3 Vertical Flow Regime Map

The vertical flow regime map used in the RELAP5-3D code is used for both directions (up flow and down flow) as well as countercurrent flow in volumes with an inclination angle between 60 and 90 degrees. For inclinations between 30 degrees and 60 degrees, an interpolation is used between the vertical and horizontal flow maps. A schematic of the vertical flow regime map is shown below in Figure 7 .

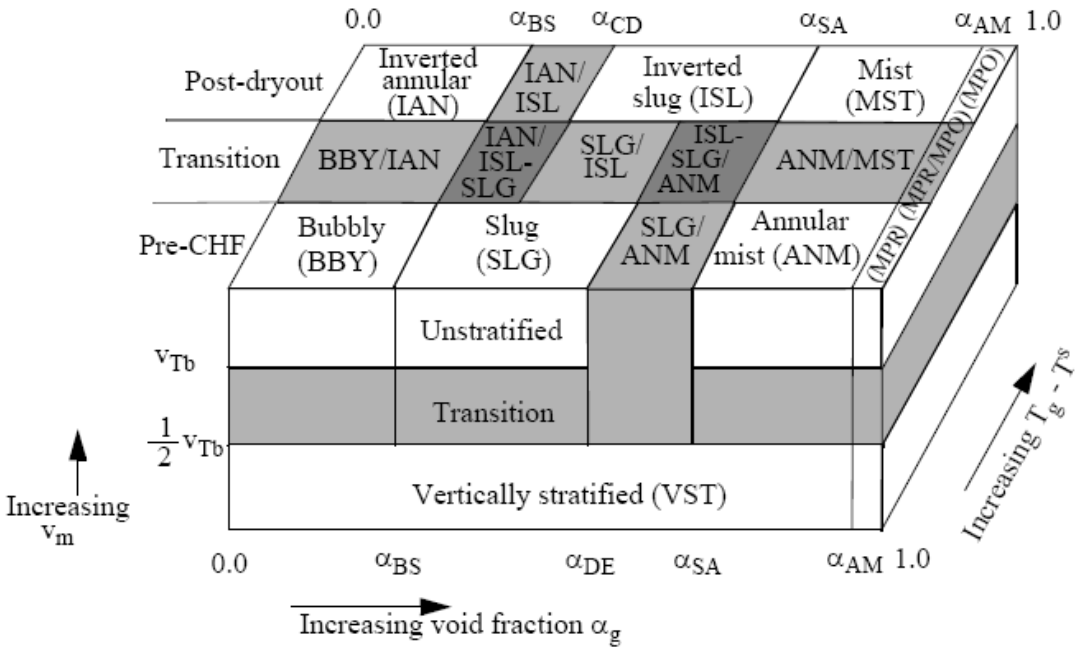

Figure 7: Schematic of Vertical Flow Regime Map Used in RELAP5-3 (Ref 6)

The vertical flow regime map is three dimensional and based on void fraction, average mixing velocity v_m, and boiling regime. The mixing velocity is defined as the mass flux of the mixture divided by the density of the mixture as shown in Equation 11.

$$v_m = \frac{G_m}{\rho_m} \text{ where}$$

$$G_m = \alpha_g \rho_g |v_g| + \alpha_f \rho_f |v_f|$$

and

$$\rho_m = \alpha_g \rho_g + \alpha_f \rho_f$$

Equation 11

The map shown in Figure 7 consists of bubbly, slug, annular mist, and dispersed flows in the pre-critical heat flux regime; inverted annular, inverted slug, and dispersed

flows in post-dryout, and vertically stratified for sufficiently low mixture velocity (Ref 6). For purposes of the present research only the pre-CHF regimes and transitions will be studied. The parameters and Equations governing the flow regime transitions for the vertical flow regime map are listed and explained below.

For the bubbly-to-slug transition, the vertical model is the same as the horizontal method except for a provision for small diameter tubes. Taitel and Dukler's model suggests that bubbly flow may not exist in small diameter tubes where the velocity of the small bubbles is higher than the velocity of the Taylor bubbles (Ref 6). The Equations for the rise velocity of the small bubbles and the Taylor bubbles are shown in Equation 12 and Equation 13 respectively.

$$v_{sb} = 1.53\left[\frac{g(\rho_f - \rho_g)\sigma}{\rho_f^2}\right]^{1/4}$$

Equation 12

$$v_{TB} = 0.35\left[\frac{gD(\rho_f - \rho_g)}{\rho_f}\right]^{1/2}$$

Equation 13

Therefore in the condition that v_{TB} is less than v_{sb}, bubbly flow will not exist since the bubbles will approach the trailing edges of the Taylor bubbles and coalesce (Ref 6). Equating Equation 12 and Equation 13 results in a critical diameter for bubbly flow below which bubbly flow is presumed not to exist (Ref 6). This is shown in Equation 14.

$$D_{crit} = 19.11\left[\frac{\sigma}{g\left(\rho_f - \rho_g\right)}\right]^{1/4}$$

Equation 14

D^* is the dimensionless tube diameter (Bond number) given by Equation 15.

$$D^* = D\left[\frac{g(\rho_f - \rho_g)}{\sigma}\right]^{1/2}$$

Equation 15

The limit on the dimensionless tube diameter allowing bubbly flow is $D^* \geq 19.11$. In the RELAP5-3D coding, the limit has been changed from 19.11 to 22.22 for better agreement with the data compared in the code's development (Ref 6). Therefore, for flow conditions allowing bubbly flow, the bubbly-to-slug transition is defined in Equation 16 where the exponential power of 8 is used to provide a smooth variation of α_{BS}^*.

$$\alpha_g = \left\{0.25 \min[1.0, \left(\frac{D^*}{22.22}\right)^8]\right\}$$

Equation 16

At high mass fluxes, bubbly flow with finely dispersed bubbles can exist up to a void fraction of 0.5 (Ref 6). If the criterion is linearly interpolated between the upper and lower void limits, the bubbly-to-slug flow transition can be written as the following Equation 17 through Equation 19.

$$\alpha_{BS} = \alpha_{BS}^* \quad \text{for } G_m \leq 2{,}000 \text{ kg/m}^2 - s$$

Equation 17

$$\alpha_{BS} = \alpha_{BS}^* + \frac{(0.5 - \alpha_{BS}^*)}{1{,}000}(G_m - 2{,}000) \quad \text{for } 2{,}000 < G_m < 3{,}000 \text{ kg/m}^2 - s$$

Equation 18

$$\alpha_{BS} = 0.5 \quad \text{for } G_m \geq 3{,}000 \text{ kg/m}^2 - s$$

Equation 19

Where α_{BS}^{*} is the lower void limit defined below in Equation 20.

$$\alpha_{BS}^{*} = \max\left\{0.25 \min[1, (0.045 D^{*})^{8}], 10^{-3}\right\}$$

Equation 20

For the slug-to-annular flow regime transition, Taitel's model for annular transition upflow is governed by Equation 21 and Equation 22 where j_g is the vapor superficial velocity and Ku_g is the Kutateladze number.

$$j_g^{*} = \frac{\alpha_g v_g}{\left[\dfrac{gD\left(\rho_f - \rho_g\right)}{\rho_g}\right]^{1/2}} \geq j_{g,crit}^{*}$$

Equation 21

$$Ku_g = \frac{\alpha_g v_g}{\left[\dfrac{g\sigma\left(\rho_f - \rho_g\right)}{\rho_g^2}\right]^{1/4}} \geq Ku_{g,crit}$$

Equation 22

Equation 21 (flow reversal) controls the transition in small tubes and the second Equation 22 (droplet entrainment) controls the transition in large tubes (Ref 6). The critical values are given in Equation 23 and Equation 24.

$$j_{g,crit}^{*} = 1$$

Equation 23

$$Ku_{g,crit} = 3.2$$

Equation 24

Small tubes are depicted as having a diameter less than the value calculated in Equation 25.

$$D_{h,\lim} = 10.24\left[\frac{\sigma}{g(\rho_f - \rho_g)}\right]^{1/2}$$

Equation 25

The large tubes governed by Equation 22 should have a diameter larger than Equation 25. The two criterion can be expressed as the following Equations for the transition between slug and annular flow.

$$\alpha_{SA} = \min\left(\alpha_{crit}^{f}, \alpha_{crit}^{e}\right)$$

Equation 26

Equation 27 is the void fraction for flow reversal and is found by combining Equation 21 and Equation 23 (INL).

$$\alpha_{crit}^{f} = \left\{\frac{1}{v_g}\left[\frac{gD\left(\rho_f - \rho_g\right)}{\rho_g}\right]^{1/2}\right\} \quad \text{for upflow}$$

Equation 27

$$\alpha_{crit}^{f} = 0.75 \quad \text{for downflow and countercurrent flow}$$

Equation 28

Equation 29 is the void fraction for droplet entrainment found by combining Equation 22 and Equation 24.

$$\alpha_{crit}^{e} = \left\{ \frac{3.2}{v_g} \left[\frac{g\sigma\left(\rho_f - \rho_g\right)}{\rho_g^2} \right]^{1/4} \right\}$$

Equation 29

The final transition criterion used in the RELAP5-3D code is

$$\alpha_{SA} = \max[\alpha_{AM}^{\min}, \min(\alpha_{crit}^{f}, \alpha_{crit}^{e}, \alpha_{BS}^{\max})]$$

where:

$$\alpha_{AM}^{\min} = \begin{Bmatrix} 0.5\ pipes \\ 0.8\ bundles \end{Bmatrix}$$

$$\alpha_{BS}^{\max} = 0.9$$

Equation 30

The vertical flow regime map used in RELAP5-3D has the gravity constant built into several Equations. In the Equations for the rise velocity of the small bubbles and the Taylor bubbles (Equation 12 and Equation 13), the gravity constant is multiplied by the difference in density and the surface tension. At zero gravity, this would result in a rise velocity of zero. Using the value of 0.001g for the comparison would make the rise velocity very small. Studies would need to be completed in order to validate the rise velocity in reduced gravities. This may introduce inaccuracies into the RELAP5-3D flow regime mapping.

The gravitation constant again is multiplied in the calculation for the dimensionless tube diameter in Equation 15 reducing the dimensionless diameter substantially as gravity is reduced.

In true zero gravity conditions, there is no need for two separate flow regime maps (horizontal and vertical). Because the data used in this study were oriented horizontally in the aircraft, the RELAP5-3D model was built for horizontal flow. The vertical flow regime map is not utilized for comparison. This could possibly be a suggestion for further study.

2.4 Summary

Because RELAP5-3D's flow regime maps are based on normal gravity conditions, the code is expected to fail in the prediction of flow regime as gravity is reduced. Flow regimes have been shown to be sometimes significantly different in the absence of gravity. For example, if the code predicts a stratified flow for a system operating in space, all future calculations based on the flow regime will be incorrect as there does not exist a stratified flow in microgravity. Furthermore, in microgravity there are no horizontal or vertical effects on flow regime. The hypothesis made in this thesis is that the RELAP5-3D flow regime output will diverge from the data as gravity is reduced. In zero gravity, the RELAP5-3D output is predicted to be highly divergent from the experimental results. In this study, only zero gravity data will be compared due to the fact that refrigerant property data is not available in RELAP5-3D. A future study could include varying gravity fields once refrigerants are added to the code, obtaining more reduced gravity data for varying tube diameters, and comparing the results of RELAP5-3D's vertical flow regime map with the zero gravity data.

CHAPTER III

EXPERIMENTAL RESULTS

3.1 Introduction

In this chapter, the reduced gravity data used in the RELAP5-3D comparison will be presented. The data used in this RELAP5-3D comparison consists of only the air/water data. However, for future phases of this research project when refrigerants are readily available in the program, more of the data can be used for comparison. Because refrigerants have more suitable fluid properties for the short experiment duration, most of the recent experiments utilize them. There is varying gravity field data available for refrigerants; however the air/water data is 0g only.

3.2 Experimental Methods

The data used in this research comes from numerous reduced gravity experiments conducted by a variety of researchers. The general method of how the data discussed in this chapter was collected will be briefly discussed.

The National Aeronautics and Space Administration (NASA) uses a reduced gravity flight pattern to achieve varying gravity fields. The experiments were flown aboard the NASA-Johnson Space Center (JSC) KC-135 aircraft or a similar aircraft at another NASA location. The KC-135 airplane flies alternating periods of high gravity (~1.8g) and reduced gravity by flying a parabolic path. The aircraft is capable of providing microgravity (~0g), or, a partial gravity environment including Lunar (0.16g) and Martian (0.38g) levels. Figure 8 is a diagram of a KC-135 flight parabola.

Hardware was built and taken aboard the aircraft for experimentation. Flow meters for both nitrogen and water measure the flow rates of the gas and liquid. A clear test section is available in the experiment where visual inspection and/or high speed imagery is used to determine the flow regime at each data point.

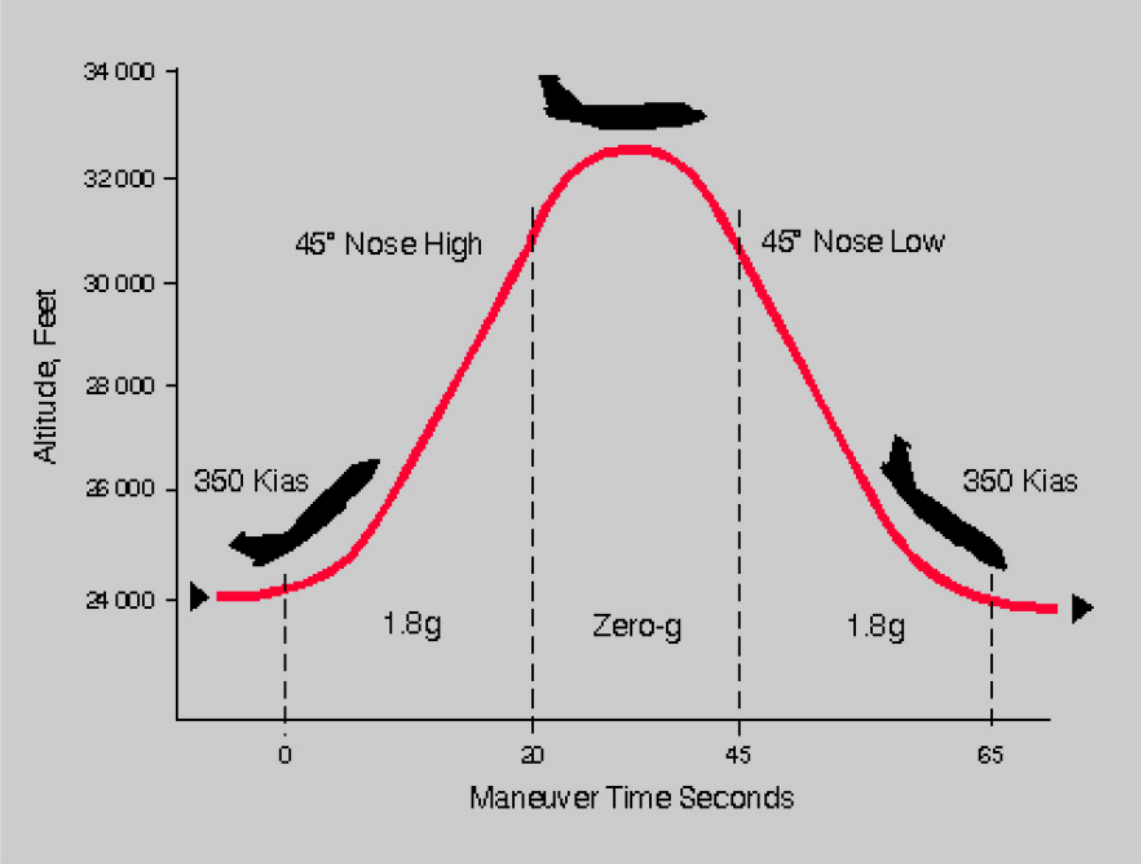

Figure 8: Parabola Diagram (Ref 11)

3.3 Air/Water Data

The following data tables present the data that are used to compare with the RELAP5-3D flow regime output. The tables are divided into tube diameter and researcher. Each table is followed by its corresponding flow regime map.

3.3.1 Air/Water 0g Data ID=9.525

Huckerby and Rezkallah mapped microgravity air and water flow regimes in a 9.525 mm inner diameter tube in 1992 aboard NASA's KC-135 aircraft. The two-phase flow was recorded and photographed after passing through 79 L/Ds (0.75 m) as a measure to ensure steady state flow (Ref 12). The superficial velocities and flow regime results are shown in Table 1 and plotted in Figure 9: Huckerby/Rezkallah ID=9.525mm. In this experiment, no annular points were identified. The transition between bubbly-to-slug flow is apparent, but there are some inconsistencies in the flow regime data from this experiment. Rezkallah performs another experiment with Zhao the following year which produces much more defined results. This will be shown next.

Table 1: Huckerby/Rezkallah 0g air/water data

j-l (m/s)	j-g (m/s)	flow regime
0.087	0.181	bubbly
0.288	0.251	bubbly
0.312	0.153	bubbly
0.714	0.222	bubbly
0.75	0.274	bubbly
0.825	0.275	bubbly
1.66	0.33	bubbly
3.2	0.115	bubbly
2.02	0.641	bubbly/slug
2.1676	0.815	bubbly/slug
2.17	0.521	bubbly/slug
0.624	0.498	bubbly/slug
0.6607	0.305	bubbly/slug
1.313	0.522	bubbly/slug
2.1198	0.413	bubbly/slug
0.13	1.72	slug
0.138	1.035	slug
0.167	1.152	slug
0.232	0.753	slug
0.2377	0.746	slug
0.28	2.46	slug
0.324	2.984	slug
0.355	5.945	slug
0.388	4.95	slug
0.4465	1.892	slug
0.48	1.894	slug
0.5178	0.693	slug
0.5433	0.531	slug
0.6118	3.978	slug
0.6346	1.428	slug
0.648	1.987	slug
0.69	1.922	slug
0.8536	2.425	slug
0.973	1.077	slug
0.9879	1.063	slug
1.112	0.973	slug
1.31	0.786	slug
2.39	0.718	slug
2.861	0.373	slug
0.24	4.91	slug/annular
0.283	3.89	slug/annular

Table 1: Continued

j-l (m/s)	j-g (m/s)	flow regime
0.308	5.78	slug/annular
0.373	4.82	slug/annular
0.374	5.89	slug/annular
0.409	2.93	slug/annular
0.477	2.95	slug/annular
0.817	2.978	slug/annular
1.055	3.928	slug/annular

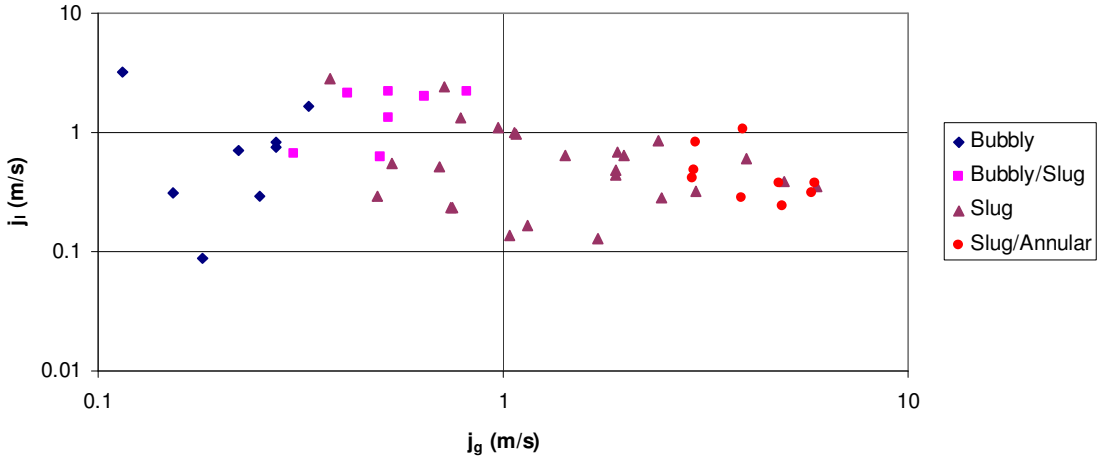

Figure 9: Huckerby/Rezkallah ID=9.525mm

Zhao and Rezkallah studied air/water flow regimes in 1993 using the same apparatus Rezkallah used in his 1992 study with Huckerby. There are some unexplained discrepancies between his two studies. The 1993 study shows much more agreement with Bousman's and Dukler's data. Clear regions of bubbly, slug, and annular flow are shown through Zhao and Rezkallah's new data. This data are shown in Table 2 and plotted in Figure 10: Zhao and Rezkallah ID =9.525mm.

Table 2: Zhao and Rezkallah 0g Data ID=12.7 mm

j-l (m/s)	j-g (m/s)	flow regime
13.39	0.09	Annular
16.37	0.09	Annular
18.95	0.09	Annular
21.51	0.09	Annular
23.31	0.09	Annular
14.26	0.09	Annular
16.39	0.09	Annular
18.86	0.09	Annular
19.14	0.09	Annular
22.35	0.09	Annular
16.74	0.13	Annular
19.31	0.13	Annular
19.9	0.14	Annular
23.02	0.13	Annular
17.1	0.2	Annular
19.66	0.17	Annular
19.72	0.19	Annular
18.73	0.19	Annular
22.66	0.19	Annular
27.86	0.14	Annular
32.17	0.11	Annular
0.3	2.27	Bubble
0.29	3.46	Bubble
0.66	3.45	Bubble
0.75	3.73	Bubble
1	3.71	Bubble
0.47	0.92	Slug
0.72	0.89	Slug
0.95	0.95	Slug
1.56	0.86	Slug
2.76	0.88	Slug
0.42	2.39	Slug
0.65	2.26	Slug
0.81	2.35	Slug
1.13	2.33	Slug
2.49	2.33	Slug
2.42	3.34	Slug
0.33	0.09	Slug
0.53	0.09	Slug
0.67	0.09	Slug

Table 2: Continued

j-l (m/s)	j-g (m/s)	flow regime
0.39	0.13	Slug
0.47	0.11	Slug
0.66	0.12	Slug
1.05	0.13	Slug
1.41	0.13	Slug
0.14	0.21	Slug
0.21	0.21	Slug
0.27	0.21	Slug
0.65	0.2	Slug
0.97	0.2	Slug
1.82	0.2	Slug
0.5	0.3	Slug
0.57	0.3	Slug
0.77	0.3	Slug
1.75	0.3	Slug
0.54	0.09	Slug
0.81	0.09	Slug
1.26	0.09	Slug
0.37	0.09	Slug
0.71	0.09	Slug
1.05	0.09	Slug
0.37	0.45	Slug
0.42	0.43	Slug
0.52	0.43	Slug
1.06	0.4	Slug
2.02	0.44	Slug
2.58	0.5	Slug
0.4	0.47	Slug
0.64	0.44	Slug
0.71	0.47	Slug
1.04	0.47	Slug
1.93	0.46	Slug
5.36	0.92	Slug-Annular
7.5	0.85	Slug-Annular
9.95	0.9	Slug-Annular
12.25	0.85	Slug-Annular
14.97	1.02	Slug-Annular
11.53	0.56	Slug-Annular
13.22	1.38	Slug-Annular
4.9	1.97	Slug-Annular
6.72	2.18	Slug-Annular

Table 2: Continued

j-l (m/s)	j-g (m/s)	flow regime
9.08	2.13	Slug-Annular
10.46	2.08	Slug-Annular
4.65	3.06	Slug-Annular
6.62	2.83	Slug-Annular
8.56	2.59	Slug-Annular
10.42	2.39	Slug-Annular
1.26	0.09	Slug-Annular
1.68	0.09	Slug-Annular
2.63	0.09	Slug-Annular
4.1	0.09	Slug-Annular
6.58	0.09	Slug-Annular
8.96	0.09	Slug-Annular
12.48	0.09	Slug-Annular
2.63	0.13	Slug-Annular
3.85	0.13	Slug-Annular
6.51	0.13	Slug-Annular
8.99	0.13	Slug-Annular
12.29	0.13	Slug-Annular
3.15	0.2	Slug-Annular
5.53	0.2	Slug-Annular
9.11	0.19	Slug-Annular
11.89	0.21	Slug-Annular
3.14	0.29	Slug-Annular
5.43	0.29	Slug-Annular
7.35	0.29	Slug-Annular
9.98	0.3	Slug-Annular
12.37	0.29	Slug-Annular
1.91	0.09	Slug-Annular
2.26	0.09	Slug-Annular
3.39	0.09	Slug-Annular
4.58	0.09	Slug-Annular
6.42	0.09	Slug-Annular
8.9	0.09	Slug-Annular
12.52	0.09	Slug-Annular
1.6	0.09	Slug-Annular
2.2	0.09	Slug-Annular
3.21	0.09	Slug-Annular
4.58	0.09	Slug-Annular
6.46	0.09	Slug-Annular
8.81	0.09	Slug-Annular
12.37	0.09	Slug-Annular

Table 2: Continued

j-l (m/s)	j-g (m/s)	flow regime
13.8	0.14	Slug-Annular
15.02	0.2	Slug-Annular
4.36	0.43	Slug-Annular
7.51	0.42	Slug-Annular
10.15	0.42	Slug-Annular
12.01	0.42	Slug-Annular
3.81	0.38	Slug-Annular
7.44	0.38	Slug-Annular
9.74	0.36	Slug-Annular
11.96	0.36	Slug-Annular
16.51	0.22	Slug-Annular
4.61	0.2	Slug-Annular
6.69	0.41	Slug-Annular

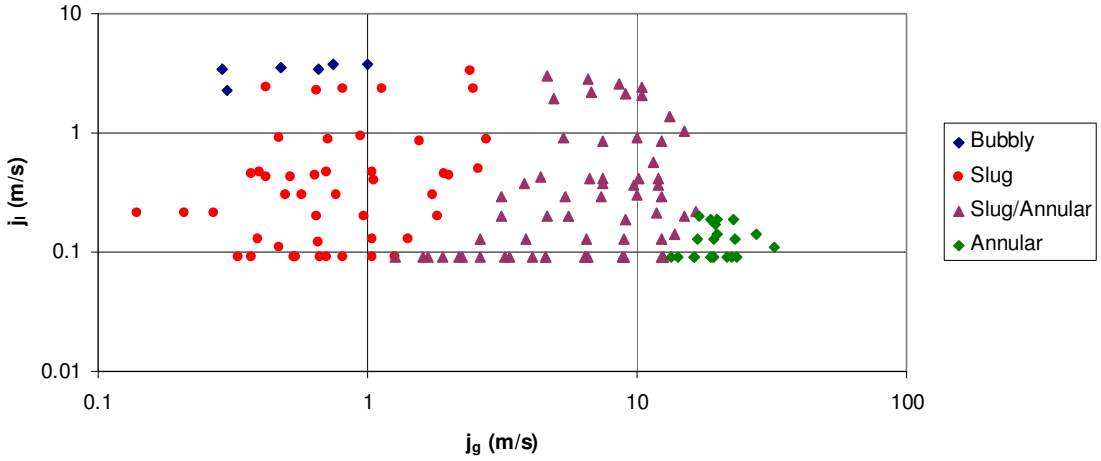

Figure 10: Zhao and Rezkallah ID =9.525mm

3.3.2 Air/water 0g data ID = 12.7 mm

Dukler performed his research aboard NASA Lewis Research Center (LRC) Learjet using air and water in a 12.7 mm tube with a test section 83 L/Ds (1.060 m) long (Ref 12). Dukler's data spans a greater range of gas superficial velocity than liquid superficial velocity. Several annular flow regime data points were achieved at these higher superficial vapor velocities. Dukler's data are shown below in Table 3 and

plotted in Figure 11. The transitions between bubbly-to-slug and slug-to-annular are fairly well defined in his data. There exists only one transition point in Dukler's experiment.

Table 3: Dukler 0g Data ID=12.7 mm

j-l (m/s)	j-g (m/s)	flow regime
0.08	25.32	annular
0.45	11.44	annular
0.08	7.97	annular
0.08	2.22	annular
0.44	2.99	annular
0.42	23	annular
0.08	11.4	annular
0.08	10.1	annular
0.08	0.77	annular
0.08	3.42	annular
0.48	3.4	annular
0.08	20.4	annular
0.46	19.7	annular
0.1	1.8	annular/slug
0.48	0.09	bubbly
0.94	0.65	bubbly
0.88	0.13	bubbly
0.46	0.13	bubbly
1.06	0.64	bubbly
1.09	0.2	bubbly
0.08	0.61	slug
0.08	0.22	slug
0.08	0.64	slug
0.46	1.09	slug
0.45	1.75	slug
0.92	1.9	slug
0.08	0.7	slug
0.45	0.65	slug
0.08	0.16	slug
0.47	0.71	slug
0.08	0.21	slug
0.08	0.2	slug
0.08	0.175	slug
1.04	1.15	slug
0.08	0.22	slug

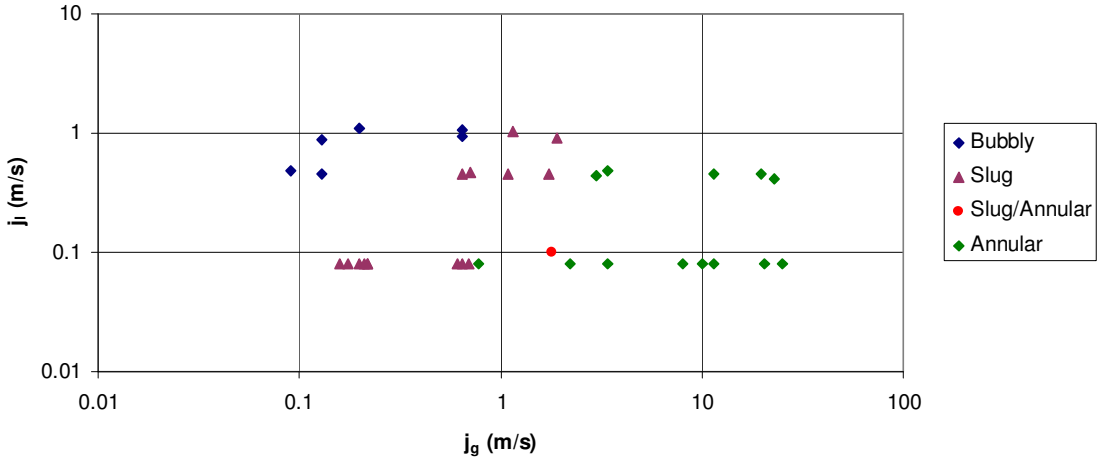

Figure 11: Dukler ID=12.7 mm

Bousman completed his dissertation work in 1994 by studying microgravity flow regimes and the effect of liquid viscosity, surface tension, and tube diameter on the locations of the flow regime transitions. He used void fraction and Weber number transition criteria to produce a successful transition model (Ref 13). He collected void fraction and flow regime data with air/water, air/water/glycerin, and air/water/zonyl FSP. For this study, only the air/water data will be used. Bousman's air/water data for the 12.7 mm tube is shown below in Table 4 and plotted in Figure 12. Bousman's data shows similar results to Dukler's map. While Dukler's data has few transition points, the areas of each flow regime are clearly defined. Bousman's data shows numerous transition points from bubbly-to-slug flow and from slug-to-annular flow. This is useful in determining which model best matches the data.

Table 4: Bousman 0g Data ID=12.7mm

j-l (m/s)	j-g (m/s)	flow regime
0.067	5.302	Annular
0.185	4.403	Annular
0.407	7.503	Annular
0.192	11.567	Annular
0.206	7.672	Annular
0.099	10.828	Annular
0.349	10.138	Annular
0.514	9.23	Annular
0.073	10.067	Annular
0.058	4.685	Annular
0.765	10.238	Annular
0.197	24.75	Annular
0.077	10.825	Annular
0.12	10.395	Annular
0.209	10.325	Annular
0.121	15.665	Annular
0.549	9.264	Annular
0.07	15.665	Annular
0.114	15.68	Annular
0.198	15.179	Annular
0.134	10.299	Annular
0.134	5.278	Annular
0.498	22.43	Annular
0.07	26.183	Annular
0.105	25.5	Annular
0.069	5.476	Annular
0.121	5.378	Annular
0.207	5.285	Annular
0.067	25.079	Annular
0.111	25.453	Annular
0.399	23.517	Annular
0.074	10.441	Annular
0.542	10.008	Annular
0.9	0.234	Bubble
0.608	0.249	Bubble
0.805	0.487	Bubble
0.504	0.109	Bubble
0.532	0.312	Bubble
0.807	0.362	Bubble
0.806	0.118	Bubble
0.717	0.195	Bubble
0.715	0.114	Bubble
0.49	0.126	Bubble

Table 4: Continued

j-l (m/s)	j-g (m/s)	flow regime
0.805	0.487	Bubble
0.504	0.109	Bubble
0.532	0.312	Bubble
0.807	0.362	Bubble
0.806	0.118	Bubble
0.177	0.22	Bubble-Slug
0.101	0.114	Bubble-Slug
0.34	0.182	Bubble-Slug
0.861	0.597	Bubble-Slug
0.204	0.118	Bubble-Slug
0.519	0.576	Bubble-Slug
0.53	0.543	Bubble-Slug
0.444	0.192	Bubble-Slug
0.34	0.11	Bubble-Slug
0.516	0.221	Bubble-Slug
0.177	0.22	Bubble-Slug
0.101	0.114	Bubble-Slug
0.34	0.182	Bubble-Slug
0.861	0.597	Bubble-Slug
0.204	0.118	Bubble-Slug
0.519	0.576	Bubble-Slug
0.072	0.43	Slug
0.073	0.147	Slug
0.203	1.11	Slug
0.082	0.396	Slug
0.207	0.506	Slug
0.143	0.36	Slug
0.335	0.589	Slug
0.341	1.154	Slug
0.163	1.433	Slug
0.104	0.9	Slug
0.055	0.202	Slug
0.878	1.118	Slug
0.601	0.77	Slug
0.581	1.674	Slug
0.527	0.981	Slug
0.203	0.291	Slug
0.065	0.345	Slug
0.792	2.034	Slug
0.197	1.244	Slug
0.203	0.624	Slug
0.789	1.205	Slug
0.515	2.18	Slug

Table 4: Continued

j-l (m/s)	j-g (m/s)	flow regime
0.121	0.987	Slug
0.071	0.533	Slug
0.526	1.071	Slug
0.193	1.075	Slug
0.195	0.536	Slug
0.113	1.064	Slug
0.113	0.546	Slug
0.53	2.059	Slug
0.663	0.47	Slug
0.674	2	Slug
0.662	1.01	Slug
0.097	0.124	Slug
0.12	0.506	Slug
0.128	0.215	Slug
0.492	0.984	Slug
0.508	2.07	Slug
0.141	0.5	Slug
0.255	0.104	Slug
0.172	0.196	Slug
0.2	0.509	Slug
0.226	1.03	Slug
0.349	0.533	Slug
0.345	1.02	Slug
0.33	0.195	Slug
0.3	0.305	Slug
0.71	2.98	Slug
0.673	0.732	Slug
0.53	0.738	Slug
0.485	2.02	Slug
0.484	0.468	Slug
0.485	0.786	Slug
0.55	0.545	Slug
0.142	0.509	Slug
0.165	0.205	Slug
0.23	0.497	Slug
0.157	0.211	Slug
0.182	0.085	Slug
0.21	0.503	Slug
0.072	0.43	Slug
0.203	1.11	Slug
0.082	0.396	Slug
0.207	0.506	Slug
0.143	0.36	Slug

Table 4: Continued

j-l (m/s)	j-g (m/s)	flow regime
0.335	0.589	Slug
0.341	1.154	Slug
0.104	0.9	Slug
0.055	0.202	Slug
0.878	1.118	Slug
0.601	0.77	Slug
0.581	1.674	Slug
0.527	0.981	Slug
0.203	0.291	Slug
0.065	0.345	Slug
0.792	2.034	Slug
0.197	1.244	Slug
0.203	0.624	Slug
0.789	1.205	Slug
0.515	2.18	Slug
0.121	0.987	Slug
0.11	2.099	Slug
0.069	2.103	Slug
0.071	1.089	Slug
0.071	0.533	Slug
0.526	1.071	Slug
0.53	0.543	Slug
0.192	2.1	Slug
0.193	1.075	Slug
0.195	0.536	Slug
0.113	0.064	Slug
0.113	0.546	Slug
0.53	2.059	Slug
0.069	2.194	Slug-Annular
0.082	1.773	Slug-Annular
0.102	1.666	Slug-Annular
0.861	4.294	Slug-Annular
0.095	2.208	Slug-Annular
0.328	4.595	Slug-Annular
0.153	2.486	Slug-Annular
0.603	5.784	Slug-Annular
0.069	1.116	Slug-Annular
0.068	2.251	Slug-Annular
0.506	4.426	Slug-Annular
0.198	2.01	Slug-Annular
0.8	4.433	Slug-Annular
0.2	3.987	Slug-Annular
0.545	5.106	Slug-Annular

Table 4: Continued

j-l (m/s)	j-g (m/s)	flow regime
0.11	2.099	Slug-Annular
0.069	2.103	Slug-Annular
0.071	1.089	Slug-Annular
0.192	2.1	Slug-Annular

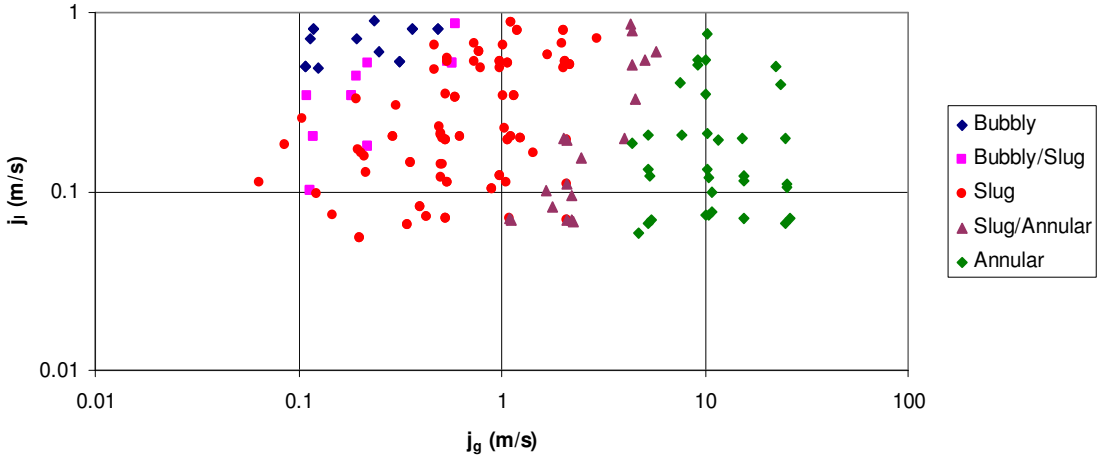

Figure 12: Bousman Data ID=12.7mm

3.3.3 Air/water 0g data ID=24.5 mm

Bousman's research also included data with ID = 25.4 mm. These data are shown below in Table 5 and Figure 13. The majority of his data in this tube size are slug and slug/annular. There are just a few bubbly data points, no bubbly/slug points, and a handful of annular points.

Table 5: Bousman 0g Data ID=24.5 mm

j-l (m/s)	j-g (m/s)	flow regime
0.604	9.57	Annular
0.1	10.8	Annular
0.123	14.7	Annular
0.118	5.04	Annular
0.442	10.8	Annular
0.095	10.8	Annular
0.237	10.5	Annular
0.193	5.07	Annular
0.348	10.8	Annular
0.345	7.35	Annular
0.21	16.35	Annular
0.465	10.3	Annular
0.127	5.23	Annular
0.25	7.02	Annular
0.06	4.69	Annular
0.07	5.48	Annular
0.07	10.07	Annular
0.07	10.44	Annular
0.08	10.83	Annular
0.07	15.66	Annular
0.07	25.08	Annular
0.07	26.18	Annular
0.13	5.28	Annular
0.12	5.38	Annular
0.13	10.3	Annular
0.12	10.4	Annular
0.12	15.67	Annular
0.11	15.68	Annular
0.11	25.45	Annular
0.11	25.5	Annular
0.2	3.99	Annular
0.21	5.29	Annular
0.21	10.33	Annular
0.2	15.18	Annular
0.2	24.75	Annular
0.55	5.11	Annular
0.51	9.23	Annular
0.55	9.26	Annular
0.54	10.01	Annular
0.5	22.43	Annular
0.4	23.52	Annular
0.717	0.195	Bubble
0.715	0.114	Bubble

Table 5: Continued

j-l (m/s)	j-g (m/s)	flow regime
0.49	0.126	Bubble
0.444	0.192	Bubble-Slug
0.34	0.11	Bubble-Slug
0.516	0.221	Bubble-Slug
0.663	0.47	Slug
0.674	2	Slug
0.662	1.01	Slug
0.097	0.124	Slug
0.12	0.506	Slug
0.128	0.215	Slug
0.492	0.984	Slug
0.508	2.07	Slug
0.141	0.5	Slug
0.255	0.104	Slug
0.172	0.196	Slug
0.2	0.509	Slug
0.226	1.03	Slug
0.349	0.533	Slug
0.345	1.02	Slug
0.33	0.195	Slug
0.3	0.305	Slug
0.71	2.98	Slug
0.673	0.732	Slug
0.53	0.738	Slug
0.485	2.02	Slug
0.484	0.468	Slug
0.485	0.786	Slug
0.55	0.545	Slug
0.142	0.509	Slug
0.165	0.205	Slug
0.23	0.497	Slug
0.157	0.211	Slug
0.182	0.085	Slug
0.21	0.503	Slug
0.623	4.74	Slug-Annular
0.098	2.08	Slug-Annular
0.459	4.92	Slug-Annular
0.256	2.02	Slug-Annular
0.34	2.03	Slug-Annular
0.311	2.99	Slug-Annular
0.69	6.83	Slug-Annular
0.49	3	Slug-Annular
0.46	6.74	Slug-Annular

Table 5: Continued

j-l (m/s)	j-g (m/s)	flow regime
0.14	2.03	Slug-Annular
0.185	1.55	Slug-Annular
0.124	3.06	Slug-Annular
0.18	3	Slug-Annular

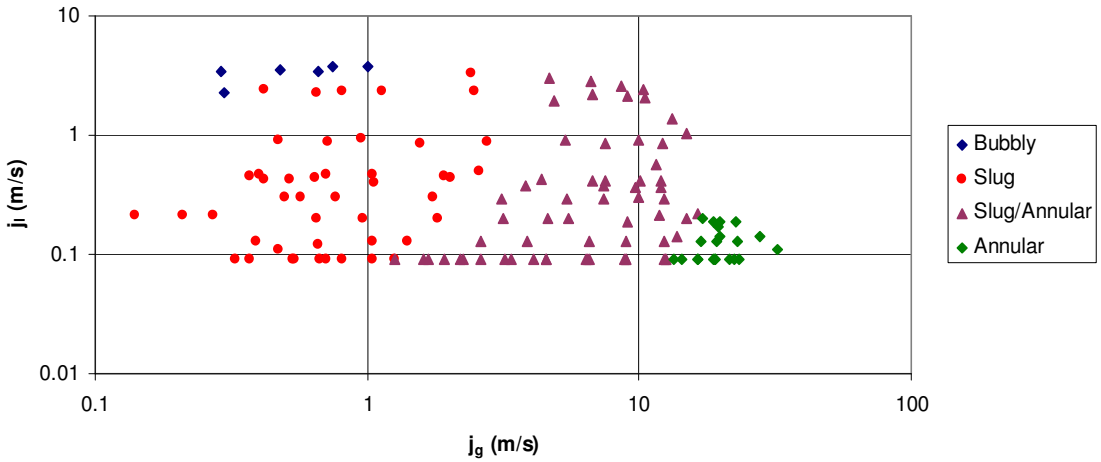

Figure 13: Bousman Data ID=25.4mm

3.3.4 Air/water 0g data ID=40 mm

Colin performed microgravity flow regime mapping experiments with air and water in a 40 mm tube aboard the French Caravelle plane which is similar to the reduced gravity aircraft at NASA (Ref 12). The test section was 79 L/Ds (0.3170 m) in length and flow regime recordings as well as high speed photography were taken at the end of the test section (Ref 12). Bubbly and slug flow data were gathered through this experiment.

Because this experiment involved such a large diameter tube and needed a longer developing length, the experiment was oriented along the major axis of the plane in the fore/aft direction. This arrangement is different than the other experiments discussed in this thesis work. The fore/aft accelerations that occur immediately before each parabola

make this arrangement undesirable due to the longer time to reach equilibrium (Ref 12). Furthermore, in this experiment only vertical acceleration data were collected therefore the effects of the fore/aft accelerations cannot be quantified. The data may show signs of these effects. In Figure 14 below, there are some flow regime points that are not well grouped. Several bubbly flow points appear in the slug flow region and vise versa. However in general the bubbly-to-slug transition region is defined in the data shown in Table 6 and Figure 14. This data is presented in this thesis work regardless of the potential for acceleration effects because of the larger diameter. As long as the effects are considered in the results, the data can still be viable data.

Table 6: Colin 0g Data ID=40mm

j-l (m/s)	j-g (m/s)	flow regime
0.494	0.08	bubbly
0.551	0.123	bubbly
0.531	0.159	bubbly
0.692	0.044	bubbly
0.653	0.114	bubbly
0.627	0.159	bubbly
0.61	0.193	bubbly
0.591	0.246	bubbly
0.881	0.054	bubbly
0.845	0.116	bubbly
0.819	0.174	bubbly
0.766	0.247	bubbly
1.104	0.086	bubbly
1.058	0.153	bubbly
1.001	0.191	bubbly
0.971	0.274	bubbly
0.331	0.045	bubbly
0.306	0.063	bubbly
0.309	0.052	bubbly
0.319	0.065	bubbly
0.313	0.124	bubbly
0.448	0.049	bubbly
0.418	0.06	bubbly
0.881	0.159	bubbly
0.268	0.047	bubbly
0.256	0.059	bubbly
0.489	0.047	bubbly
0.958	0.05	bubbly
0.931	0.067	bubbly
0.954	0.128	bubbly
0.937	0.219	bubbly
0.336	0.129	bubbly
0.865	0.129	bubbly
0.839	0.128	bubbly
0.835	0.129	bubbly
0.822	0.13	bubbly
0.809	0.132	bubbly
0.938	0.061	bubbly
0.918	0.06	bubbly
0.902	0.058	bubbly
0.888	0.058	bubbly
0.878	0.057	bubbly
0.865	0.056	bubbly

Table 6: Continued

j-l (m/s)	j-g (m/s)	flow regime
1.485	0.123	bubbly
0.243	0.038	bubbly
0.233	0.021	bubbly
0.263	0.021	bubbly
0.251	0.024	bubbly
0.241	0.015	bubbly
0.381	0.108	bubbly
0.257	0.11	bubbly
0.408	0.11	bubbly
0.965	0.037	bubbly
0.994	0.045	bubbly
0.992	0.039	bubbly
0.887	0.11	bubbly
0.854	0.05	bubbly
0.839	0.043	bubbly
0.793	0.125	bubbly
0.757	0.134	bubbly
0.448	0.062	bubbly
0.445	0.076	bubbly
0.883	0.069	bubbly
0.872	0.093	bubbly
0.862	0.092	bubbly
0.84	0.127	bubbly
0.834	0.164	bubbly
0.833	0.165	bubbly
0.54	0.215	bubbly
0.535	0.217	bubbly
0.468	0.132	bubbly
0.862	0.124	bubbly
0.842	0.223	bubbly
0.815	0.377	bubbly
0.803	0.47	bubbly
0.821	0.564	bubbly
0.804	0.563	bubbly
0.806	0.624	bubbly
0.673	0.178	bubbly
0.682	0.281	bubbly
0.668	0.47	bubbly
0.665	0.455	bubbly
0.486	0.192	slug
0.292	0.301	slug
0.555	0.292	slug
0.487	0.323	slug

Table 6: Continued

j-l (m/s)	j-g (m/s)	flow regime
0.304	0.226	slug
0.284	0.466	slug
0.29	0.485	slug
0.304	0.23	slug
0.278	0.121	slug
0.271	0.201	slug
0.278	0.436	slug
0.475	0.065	slug
0.46	0.124	slug
0.914	0.353	slug
0.952	0.55	slug
0.258	0.127	slug
0.33	0.128	slug
0.304	0.128	slug
0.469	0.129	slug
0.461	0.129	slug
0.46	0.129	slug
0.543	0.129	slug
0.244	0.097	slug
0.322	0.209	slug
0.441	0.125	slug
0.438	0.124	slug
0.43	0.188	slug
0.427	0.188	slug
0.41	0.19	slug
0.467	0.231	slug
0.464	0.229	slug
0.462	0.231	slug
0.448	0.284	slug
0.539	0.252	slug
0.528	0.319	slug
0.214	0.137	slug
0.216	0.136	slug
0.204	0.206	slug
0.205	0.292	slug
0.206	0.387	slug
0.184	0.305	slug
0.174	0.258	slug
0.467	0.176	slug
0.469	0.23	slug
0.464	0.318	slug
0.457	0.414	slug

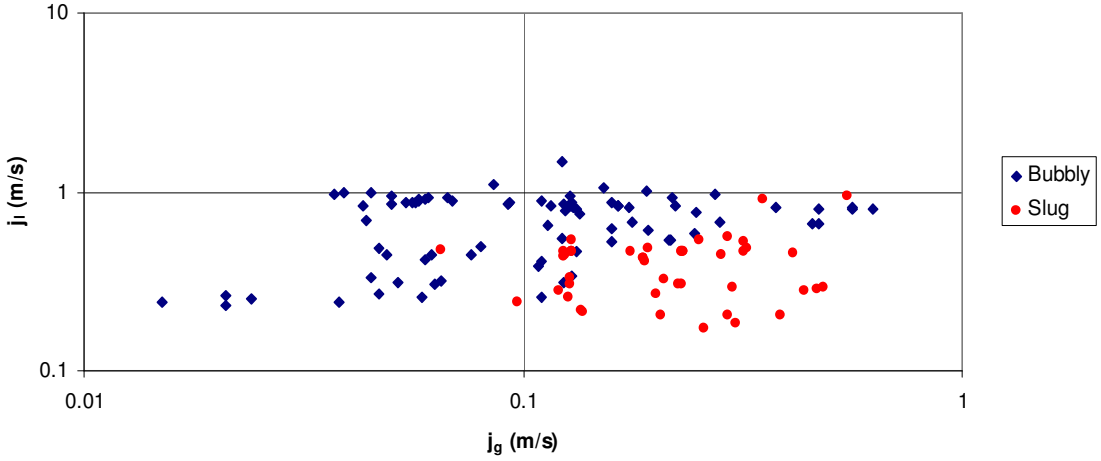

Figure 14: Colin 0g Data ID=40mm

3.3 Summary

This chapter presented the data that will be used to validate the conclusion that RELAP5-3D needs a new flow regime model for reduced gravity conditions. The data presented in this chapter will also be used to find the existing flow regime model that will be recommended for use in the RELAP5-3D computer program. The next chapter will take the data points and compare the visual flow regime identifications with the RELAP5-3D results.

CHAPTER IV

RELAP5-3D MODEL AND RESULTS

4.1 Introduction

Now that the experimental zero gravity data have been presented, the results will be compared with RELAP5-3D's flow regime output. A model was created using RELAP5-3D to simulate the experiments. The program has the capability to reduce the gravity field, however, the energy Equations embedded in the program do not allow the gravity to be set to zero. Therefore, in the RELAP5-3D model a value of 0.001g will be used. The graphical user interface showing the model is shown below in Figure 15. The model test section was set to the length and diameter of each experiment. Conditions such as temperature, pressure, quality, and both liquid and vapor mass flow rates were set at the inlet of the test section to match experimental conditions. The test section is broken into 15 nodes, and a flow regime output is generated for each node. The flow regime predictions in the last 5 nodes were used in the comparison as this was the section where flow regime records were taken in the experiments to ensure steady state flow. In Figure **15** the test section is oriented horizontally. For 1g ground test comparisons, the orientation of the test section can be rotated as needed to imitate vertical up flow and match experimental methods.

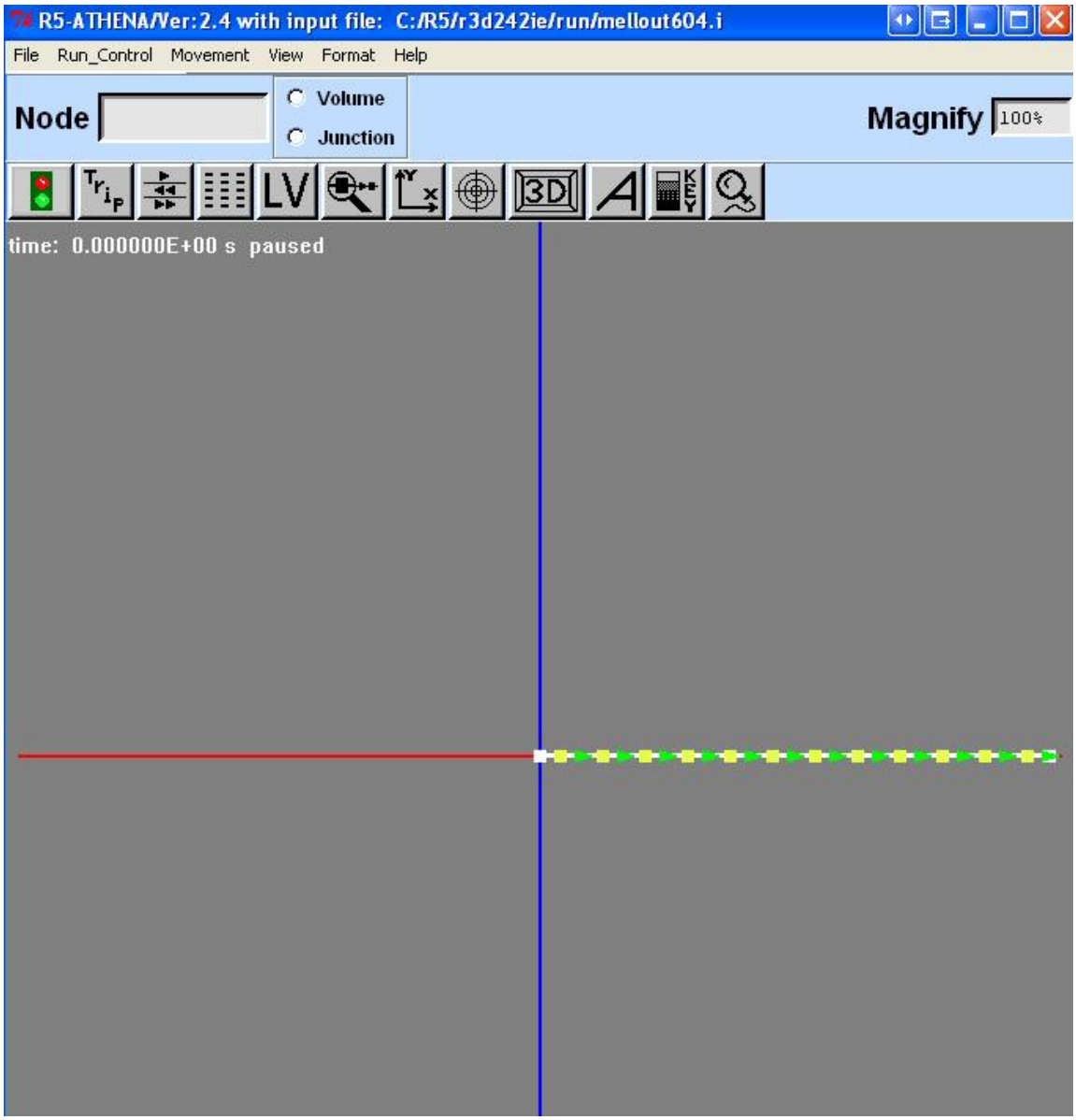

Figure 15: RELAP5-3D Graphical Interface

4.2 RELAP5-3D Flow Regime Output

In Figure 16 through Figure 23, the RELAP5-3D flow regime output is shown at each diameter tubing following the plot of the experimental results. Comparing the two

results side by side allows a visual interpretation of the relationship between actual experimental results and the computer code's output. The RELAP5-3D flow regime mapping shows obvious discontinuity with the experimental results

Figure 16 and Figure 17 both show data points for the 9.525 mm diameter tube. Figure 16 shows the visual flow regime results identified during the experiment. Figure 17 shows the flow regime results from RELAP5-3D using the same combinations of superficial velocities that were gathered in the experimental study. Comparing the two figures shows very clear distinctions and differences. The experimental results show fairly well defined transition regions while the RELAP5-3D transition regions are unclear. This could possibly be because the data points do not fall within the RELAP5-3D defined transition region. Nearly all of the transition points from bubbly-to-slug and slug-to-annular result in slug and annular flow in RELAP5-3D. The annular flow regime as identified from the RELAP5-3D output begins at much lower flow velocities than in the experimental results. At the 9.525 mm diameter, the RELAP5-3D results do not follow the experimental results very well.

Figure 18 and Figure 19 show similar results as the previous two figures for the 12.7 mm diameter. Once again, the RELAP5-3D flow regime output does not follow the experimental very well. No bubbly flow regime points are identified and no transition points are identified in the RELAP5-3D output.

Figure 20 and Figure 21 show experimental and RELAP5-3D output for the 25.4 mm diameter tube. The RELAP5-3D flow regime results fail to identify the bubbly or bubbly/slug flow regime shown in Figure 20. The slug-to-annular and annular flow regime regions are very close between the two figures. The transition region is closely

identified by the RELAP5-3D output. There are closer resemblances between this larger diameter tube than the previous smaller diameter tubing.

Finally Figure 22 and Figure 23 show results for the 40 mm diameter tubing. Because of the difficulties in collecting this data, the comparison is more difficult to make at this diameter. However, the general slug flow regime region matches between the experimental and the RELAP5-3D output. The RELAP5-3D shows the transition between bubbly and slug flow regimes happens at lower gas superficial velocities than is shown in the experimental results. Many of the bubbly data points are identified as slug points from the RELAP5-3D code.

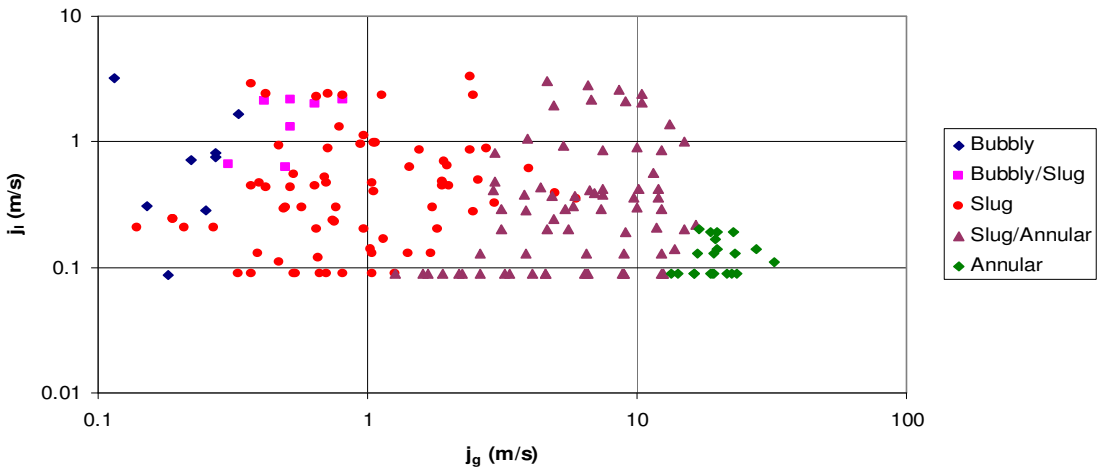

Figure 16: Zero Gravity Experimental Results ID=9.525 mm

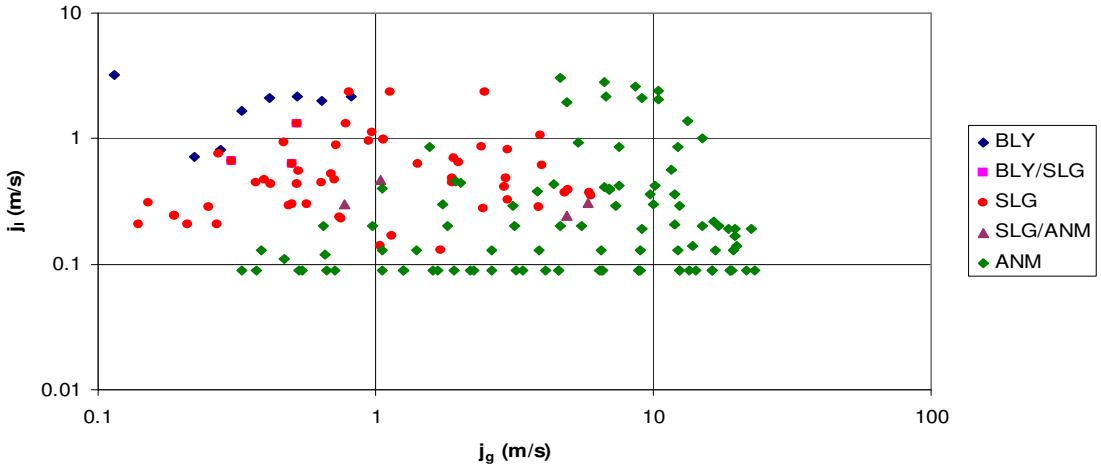

Figure 17: Zero Gravity RELAP5-3D Results ID=9.525mm

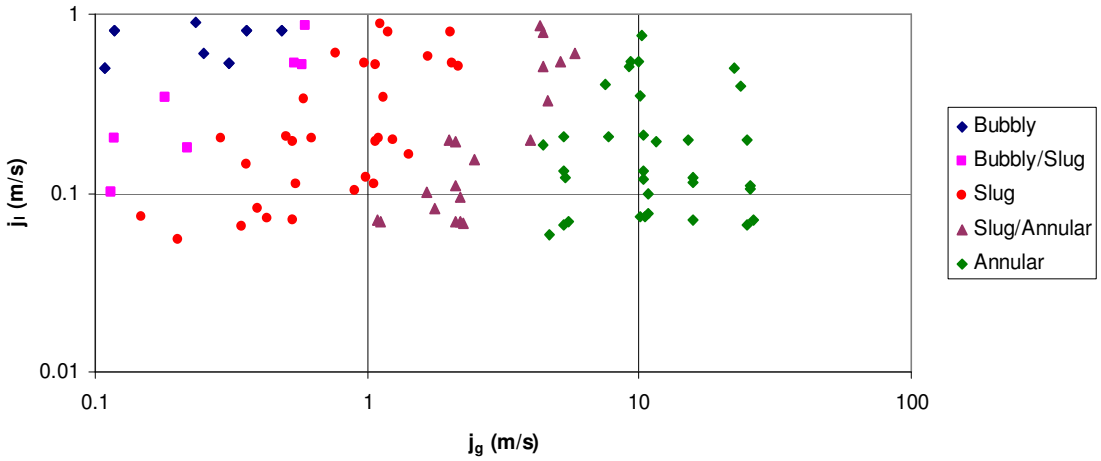

Figure 18: Zero Gravity Experimental Results ID=12.7mm

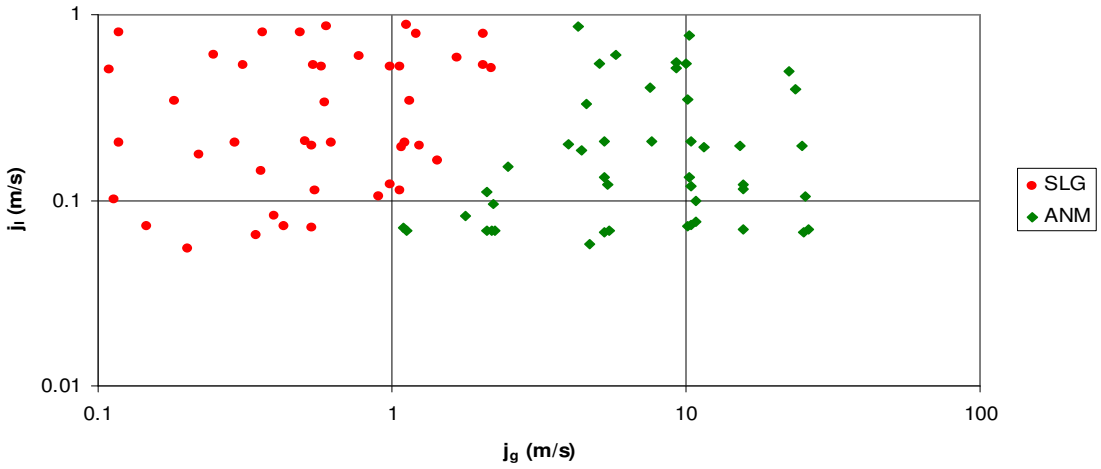

Figure 19: Zero Gravity RELAP5-3D Results ID=12.7 mm

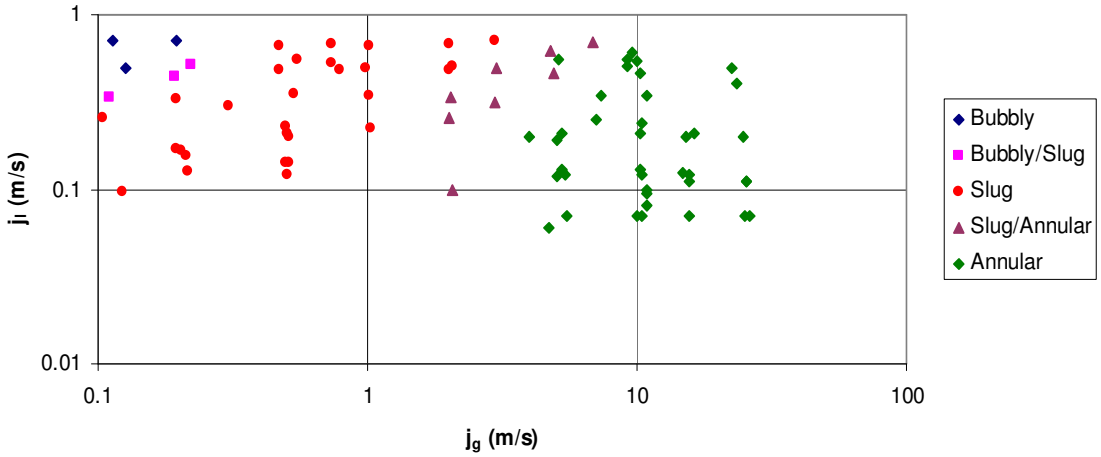

Figure 20: Zero Gravity Experimental Results ID=25.4 mm

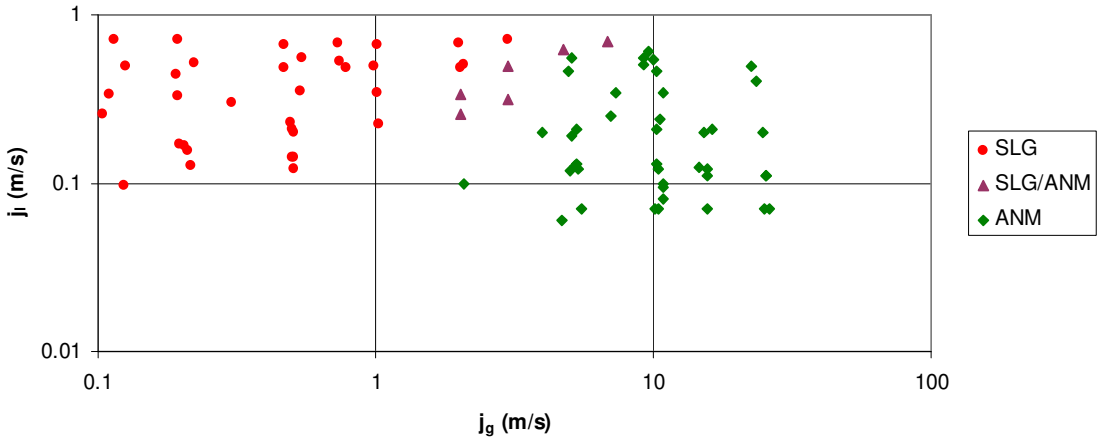

Figure 21: Zero Gravity RELAP5-3D Results ID=25.4 mm

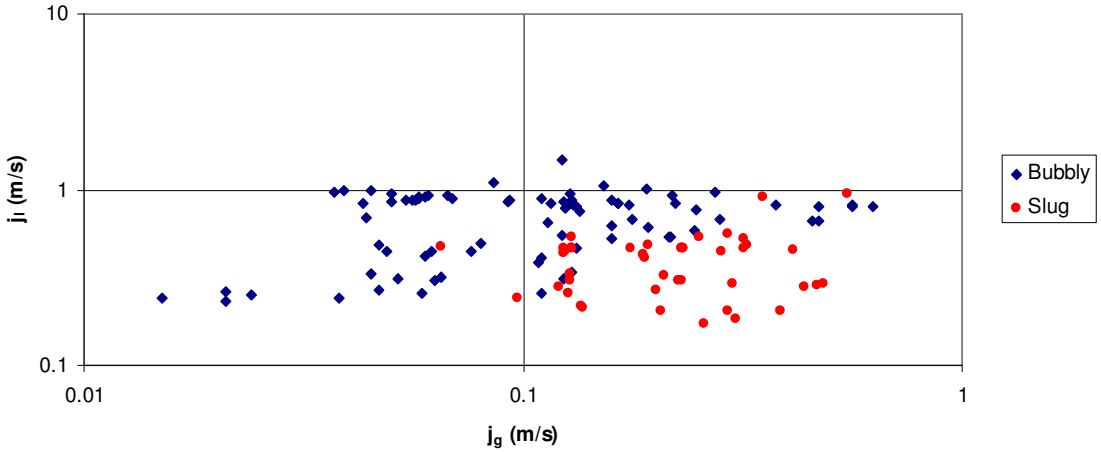

Figure 22: Zero Gravity Experimental Results ID=40 mm

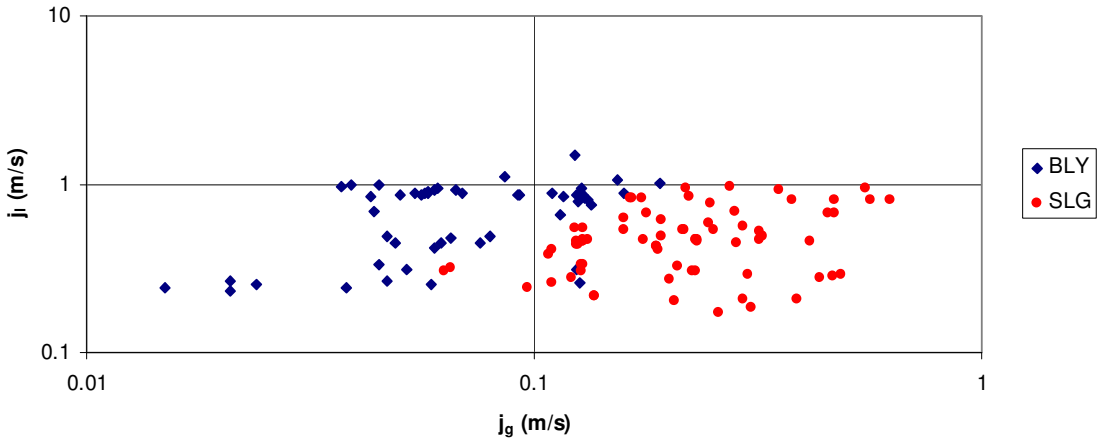

Figure 23: Zero Gravity RELAP5-3D Results ID=40mm

4.3 Summary

The RELAP5-3D flow regime results have a stronger correlation with the experimental flow regime results at the larger diameter tubes than at the smaller diameter tubes. The transition regions are poorly defined in the RELAP5-3D flow regime models for reduced gravity conditions. The bubbly and bubbly-to-slug regions are the regions that have the highest mismatch between the computer code's output and the experimental results. In the RELAP5-3D flow regime map, the transition from bubbly-to-slug takes place at a void fraction as low as 0.25 whereas in reduced gravity experimental research the transition is shown to take place between 0.35 and 0.45. This is the reason that very few bubbly flow regime points exist in the RELAP5-3D results shown in this chapter.

A new flow regime model is needed in the RELAP5-3D computer code to account for reduced and zero gravity conditions. This chapter has shown visual evidence that the current models do not represent the data well. The following chapters will compare several existing models to the data to find the model that best represents the experimental results.

CHAPTER V

PREVIOUS REDUCED GRAVITY FLOW REGIME MODELING

5.1 Introduction

This chapter presents several zero gravity models from different researchers and explains the logic behind each of them. First the bubbly-to-slug models will be discussed and shown with the data. The slug-to-annular models will also be discussed and shown with the data. The following chapter will begin to compare the models to the data. This chapter is a presentation and explanation of transition models.

5.2 Bubbly-to-Slug Transition Models

Three bubbly-to-slug transition models are presented in this section. These include Dukler, Drift-Flux, and Creare models.

5.2.1 Dukler Bubbly-to-Slug Model

One of the earlier and more popular flow regime modeling efforts was performed by Taitel and Dukler (Ref 13). This flow regime model is used in the RELAP5-3D program. Taitel and Dukler's model stemmed from a momentum balance performed on both the vapor and liquid phases of the flow. The model was extended into zero-G for the bubbly-to-slug and slug-to-annular transition. The bubbly-to-slug transition was predicted to occur when the void fraction is such that the bubbles reach a maximum packing density where the bubbles encounter each other and coalesce due to surface tension (Ref 13). This implies that the transition should occur at a constant void fraction.

At void fractions lower than the critical void fraction, bubbly flow exists. After this transition void fraction is reached, the bubbles coalesce into slugs and slug flow exists. Dukler set the transition void fraction at a value of 0.45 which was determined from high speed imagery experimental flight video and data. The governing Equation for the Dukler model is shown in Equation 31.

$$j_l = \frac{1-\alpha_{crit}}{\alpha_{crit}} j_g$$

Equation 31

Dukler's bubbly-to-slug transition model is plotted with the data for the various tube diameters shown below in Figure 24 through Figure 27.

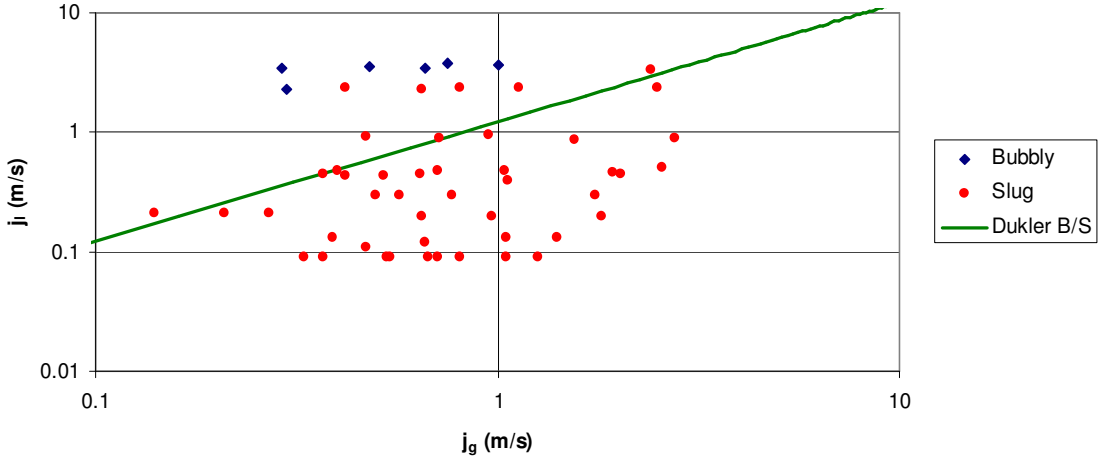

Figure 24: Dukler Model with Data ID=9.525mm

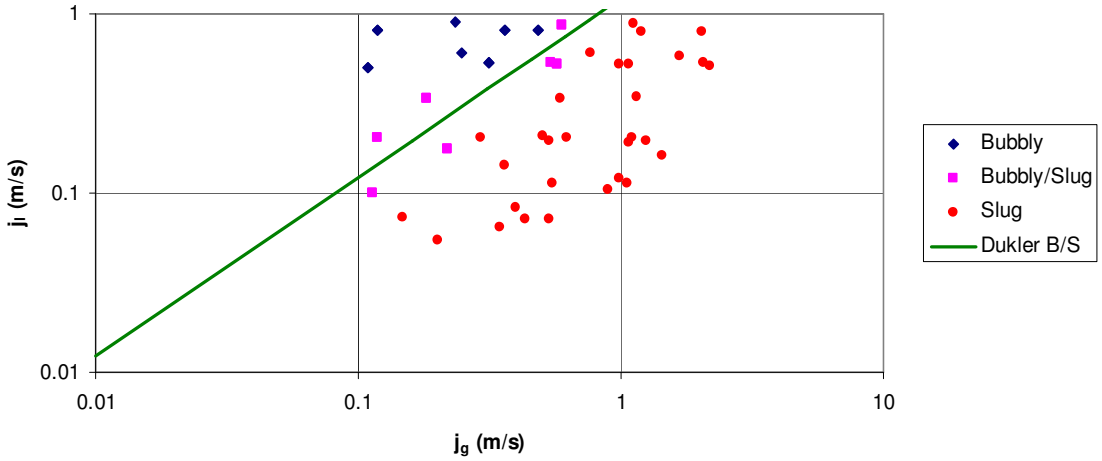

Figure 25: Dukler Model with Data ID=12.7mm

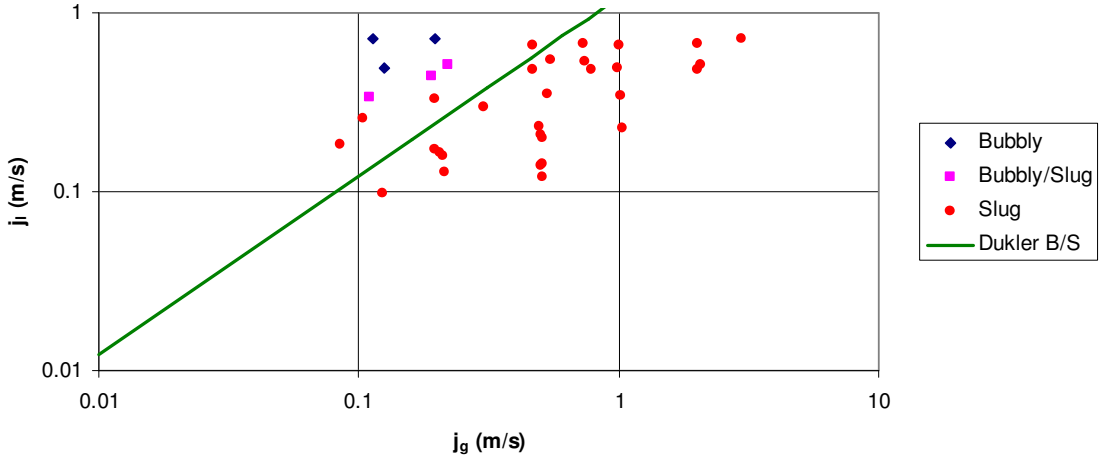

Figure 26: Dukler Model with Data ID=25.4mm

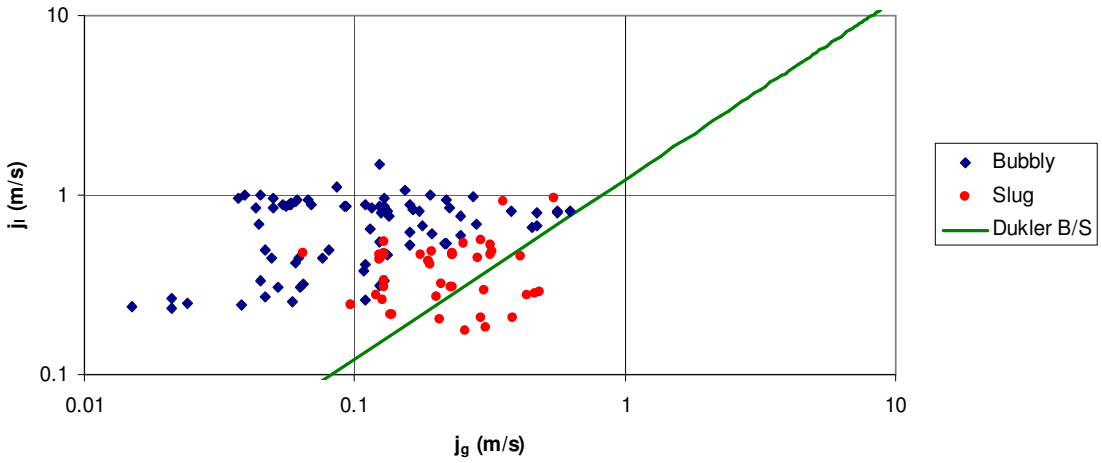

Figure 27: Dukler Model with Data ID=40mm

5.2.2 Drift-Flux Bubbly-to-Slug Model

The drift-flux model is a void fraction based flow regime model developed primarily by Zuber and Findlay in 1965 (Ref 7). The average superficial velocities of the vapor and liquid can be related to the cross sectional average gas and liquid velocities and the cross sectional average void fraction by Equation 32 through Equation 33.

$$j_g = \langle \alpha \rangle \langle v_g \rangle$$

Equation 32

$$j_l = (1 - \langle \alpha \rangle) \langle v_l \rangle$$

Equation 33

The total superficial velocity, j, is defined in Equation 34 as the sum of the vapor superficial velocity and the liquid superficial velocity.

$$j = j_g + j_l$$

Equation 34

The average gas velocity can be calculated through a mass balance as a sum of a flux term and a drift term. The average net drift velocity, v_0, is negligible in microgravity as proven through movie films of bubble and slug flows (Ref 13). This is due to the lack of buoyancy between the liquid and gas in the absence of gravity. Therefore in Equation 35 below, the drift term will be neglected.

$$\langle v_g \rangle = \frac{\langle \alpha j \rangle}{\langle \alpha \rangle} + \frac{\langle \alpha v_o \rangle}{\langle \alpha \rangle}$$

Equation 35

Zuber and Findlay defined a distribution coefficient to correct the one-dimensional homogeneous theory and account for non-uniform distribution of the void fraction across the cross section of the channel (Ref 7). This term, C_0, is defned in Equation 36.

$$C_o = \frac{\langle \alpha j \rangle}{\langle \alpha \rangle \langle j \rangle}$$

Equation 36

Once a value for this distribution coefficient is known, this gives a method for predicting the cross sectional average void fraction from the vapor and liquid superficial velocities. This relationship is shown in Equation 37.

$$\frac{j_g}{j} = C_0 \langle \alpha \rangle$$

Equation 37

An acceptable value for C_0 for air/water systems is 1.21 (Ref 13). This value was determined from velocity measurements in work done by Bousman. The above drift flux Equations can be rearranged to develop a void fraction based bubbly flow to slug flow transition model. This is shown in Equation 38.

$$j_l = \frac{\left(1 - C_0 \langle \alpha \rangle\right)}{C_0 \langle \alpha \rangle} j_g$$

Equation 38

This Equation can be used if void fraction data are available. The void fraction data available for microgravity air/water systems is very limited. Most of the void fraction data available are with refrigerants as the working fluid. Bousman has void fraction data available for bubbly and slug flows for the 12.7 mm tube. The center point void fraction found in his research for bubbly-to-slug transition was 0.4 (Ref 13). This value will be used in Equation 38 to calculate the transition model. Figure 28 shows the results of the drift flux model predictions of bubbly-to-slug transition with the data points taken in the 12.7 mm tube.

Bousman's void fraction data for the 25.4 mm tube were unreliable. However, he could see from his data that the larger tube diameter resulted in a lower transition void fraction for air/water (Ref 13). Using Equation 38 and solving for <α>, the transition void fraction can be estimated for the 25.4 mm tube. The distribution coefficient value

of 1.21 is used again. The reason for this is that work completed by Colin in 1990 showed that a distribution coefficient of 1.2 was reported for microgravity bubble and slug flows in a 40 mm inner diameter tube (Ref 13). This suggests that the value for the distribution coefficient does not depend on tube diameter. By solving Equation 38 for the average void fraction, a result of 0.23 is found for the 25.4 mm tube. Figure 29 shows the results of the drift flux model predicting the bubbly-to-slug transition for the 25.4 mm tube.

The same process for estimating average void fraction that was used for Bousman's 25.4 mm inner diameter tube is utilized to estimate an average void fraction for a 40 mm tube as well as a 9.525 mm tube. The estimated average void fraction for the 40 mm tube is calculated to be 0.198. The results are shown in Figure 30. The estimated average void fraction for the 9.525 mm tube is calculated to be 0.51. The results of the drift flux model predicting the bubbly-to-slug transition for the 9.525 tube are shown in Figure 31.

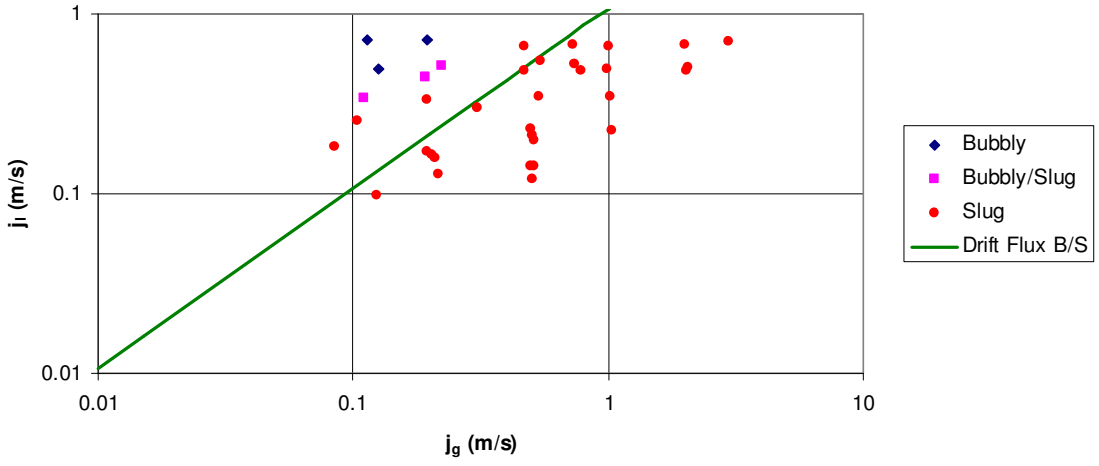

Figure 28: Drift Flux Model with Data ID=12.7 mm

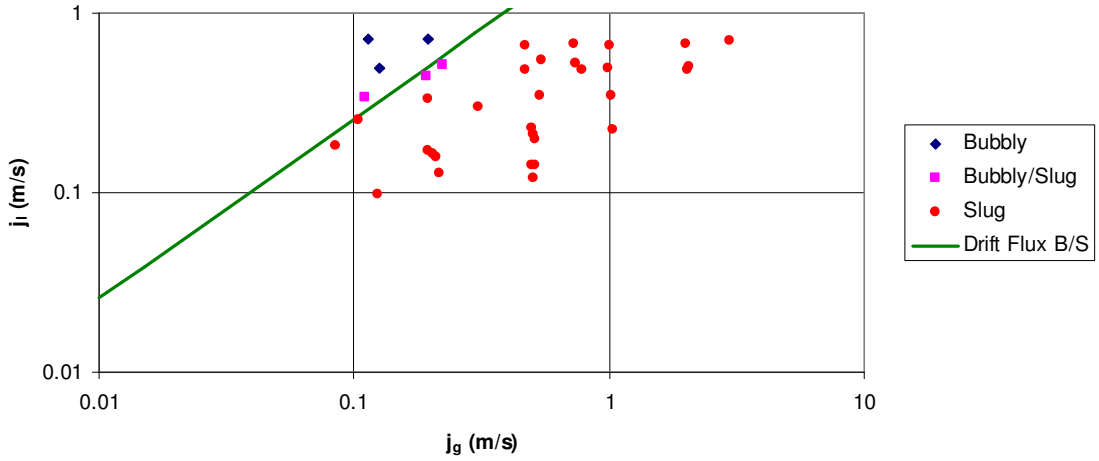

Figure 29: Drift Flux Model ID=25.4 mm

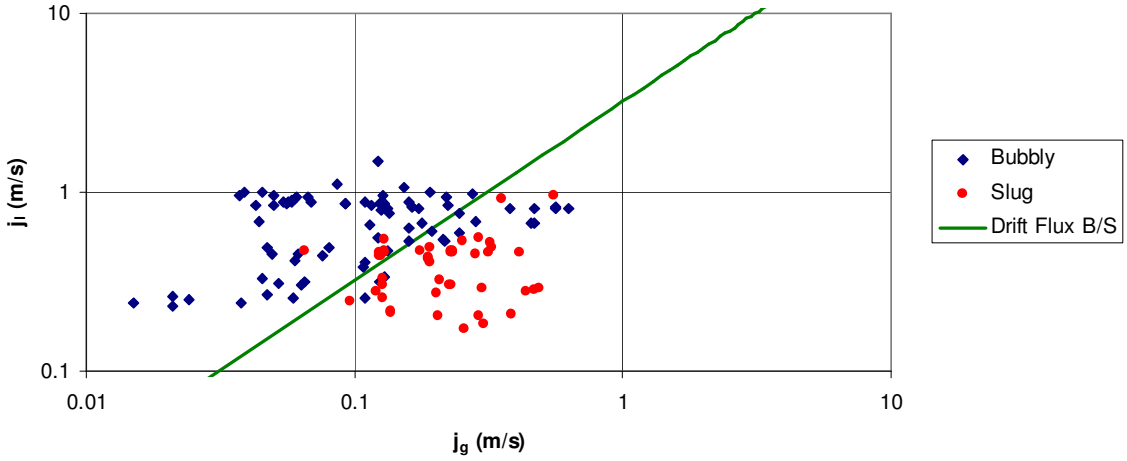

Figure 30: Drift Flux Model with Data ID=40mm

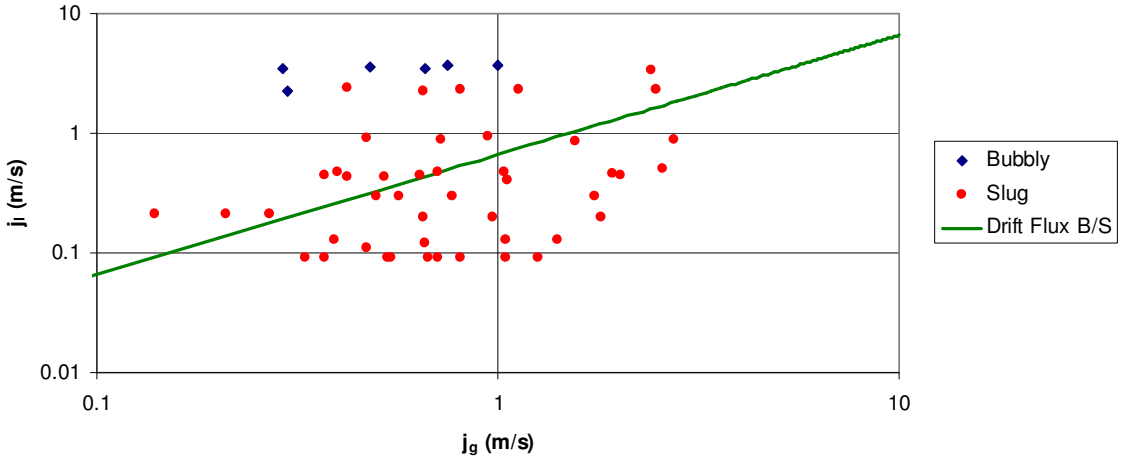

Figure 31: Drift Flux Model ID=9.525mm

5.2.3 Creare Bubbly-to-Slug

The Creare models are unique in that the software uses the same models for all accelerations. The models scale from zero gravity to earth gravity. The recommended models were extensively compared with data (Ref 14). The bubbly-to-slug flow regime transition consists of two parts: a transition based on turbulence and a transition based on critical void fraction. In order to determine whether the flow regime is bubbly flow or slug flow, both criteria must be checked. First dimensionless Weber and Bond numbers are determined through Equation 39 and Equation 40.

$$We = \left[\frac{\rho_l D_j^2}{\sigma}\right] = \left[\frac{\rho_l D\left(j_g + j_l\right)^2}{\sigma}\right]$$

Equation 39

$$Bo = \left[\frac{aD^2\left(\rho_l - \rho_g\right)}{\sigma}\right]$$

Equation 40

The point with coordinates (Bo, We) is then located on Figure 32. If the point is above the transition line in the figure, then the regime may be bubbly flow. However, the other criterion of critical void fraction must be checked before that determination is made (Ref 14).

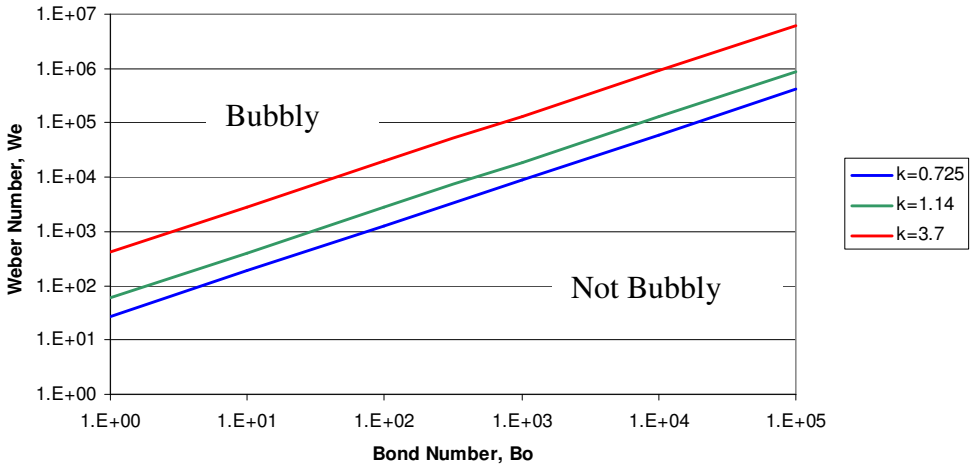

Figure 32: Dimensionless Design Map for Bubbly to Slug Transition Turbulence Criterion

The three lines in Figure 32 illustrate a range of uncertainty for the transition from bubbly flow regime to slug flow regime. The Equations of the three lines are the dimensionless Equation shown in Equation 41 where k is a constant in the range of 0.725 to 3.7 (Ref 14) and f_{wl} is a friction factor with a value of 0.005.

$$We = \left[\frac{1.2k}{f_{wl}^{0.4}}\right]^{1.67} Bo^{0.835}$$

Equation 41

Given the definition of the two phase Weber number in Equation 39, the previous Equation can be rewritten to solve for the superficial liquid velocity which can be used to map the transition according to superficial velocities by selecting a range of gas

superficial velocities and calculating the corresponding liquid superficial velocities. This is shown below in Equation 42.

$$j_l = \left[\frac{We\sigma}{\rho_l D}\right]^{0.5} - j_g$$

Equation 42

If the point is below all three transition lines shown in Figure 32, then the slug-to-annular flow regime transition must be checked (Ref 14). This will be described in the next several paragraphs.

Next, the critical void fraction criterion must be checked to determine if the flow regime is bubbly or slug flow. Equation 43 through Equation 46 show the dimensionless parameters used for the critical void fraction determination. M is the dimensionless superficial velocity ratio, K_g is the dimensionless gas Froude number, ρ* is the dimensionless density ratio, and H is the dimensionless Bubble Drift Velocity.

$$M = \frac{j_l}{j_g}$$

Equation 43

$$K_g = \frac{\rho_g^{0.5} j_g}{\left[a\sigma\left(\rho_l - \rho_g\right)\right]^{0.25}}$$

Equation 44

$$\rho^* = \frac{\rho_l}{\rho_g}$$

Equation 45

$$H = \frac{1.4}{K_g}\sqrt{\rho^*}$$

Equation 46

The transition from bubbly-to-slug flow comes from the basic drift flux Equation for bubbly flow shown in Equation 47.

$$\frac{j_g}{\alpha_c} = C_0\left(j_g + j_l\right) + 1.41\left(\frac{a\sigma\left(\rho_l - \rho_g\right)}{\rho_l^2}\right)^{0.25}$$

Equation 47

This Equation can be written in dimensionless form as Equation 48 which can be written another way to solve for superficial liquid velocity in Equation 49.

$$\left[\frac{j_l}{j_g}\right] = \left[\frac{1}{C_o\alpha_c} - 1\right] - \frac{1.41}{K_g}\left[\frac{\rho_g}{\rho_l}\right]^{0.5}$$

Equation 48

$$j_l = \left(\left[\frac{1}{C_o\alpha_c} - 1\right]j_g - \left[\frac{1.41}{C_o}\right]\left[\frac{a\sigma\left(\rho_l - \rho_g\right)}{\rho_l^2}\right]^{0.25}\right)$$

Equation 49

Figure 33 shows the design map for the critical void fraction criterion with coordinates $\left(H, M\right)$. If the point is below the line, the flow regime is bubbly (Ref 14). If the point is above the line, the slug-to-annular transition needs to be evaluated. The region between the two lines in Figure 33 represents an uncertain region. This uncertainty region lies between critical void fraction values of 0.4 and 0.52.

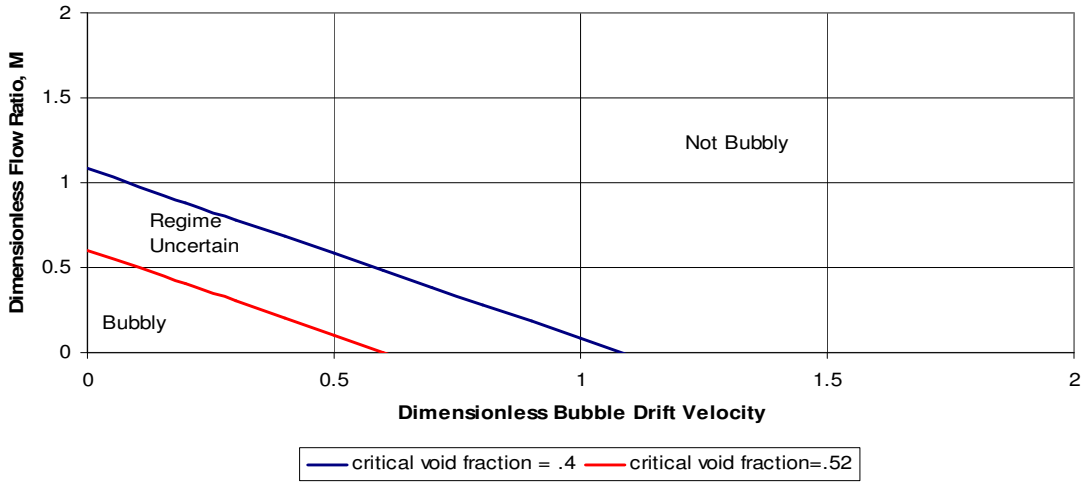

Figure 33: Dimensionless Design Map for Slug to Bubbly Transition (Void Fraction Criterion)

The criterion chosen (turbulence or critical void fraction) is the criterion with the higher liquid velocity at a given gas velocity. This will determine if Equation 42 or Equation 49 will be used (Ref 14). In Figure 34 through Figure 37, the air/water data are plotted with the Creare transition line for the various tube diameters.

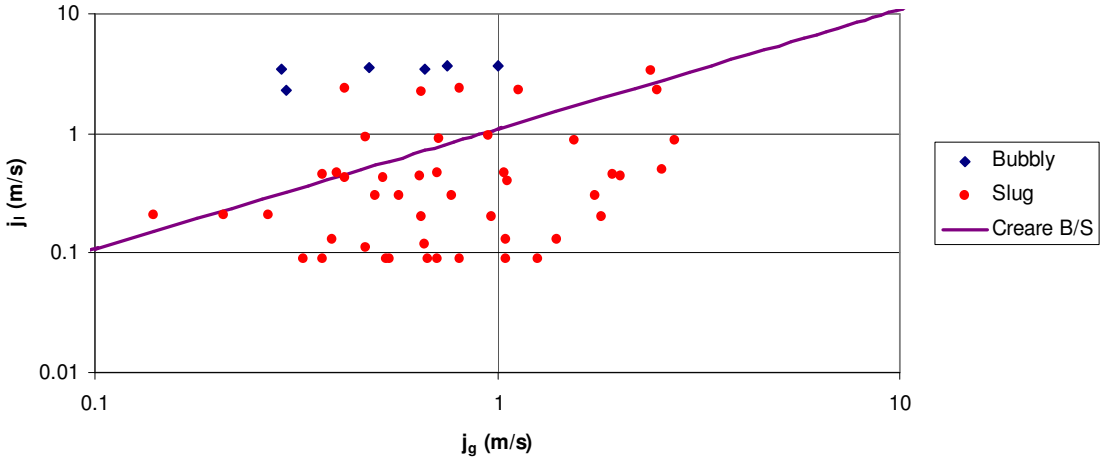

Figure 34: Creare Bubby-to-Slug Model with Data ID=9.525mm

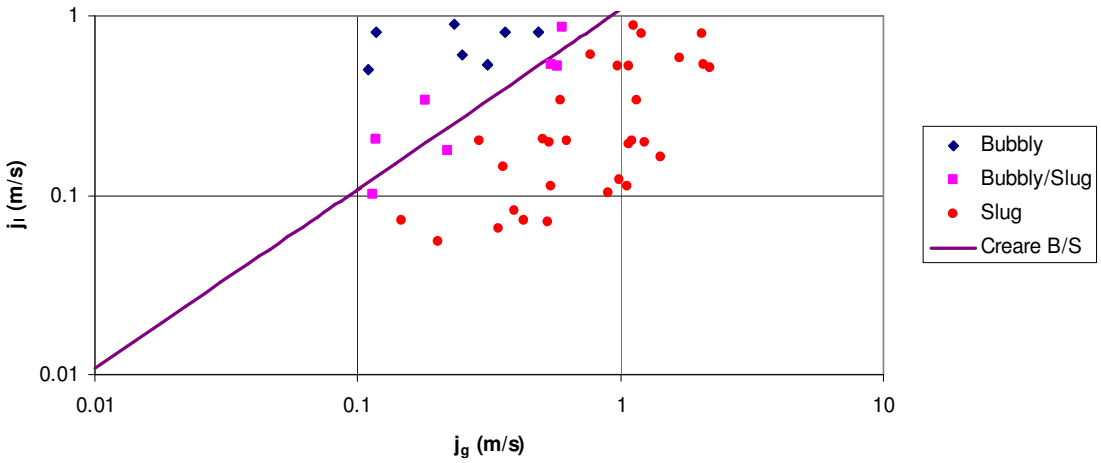

Figure 35: Creare Bubby-to-Slug Model with Data ID=12.7mm

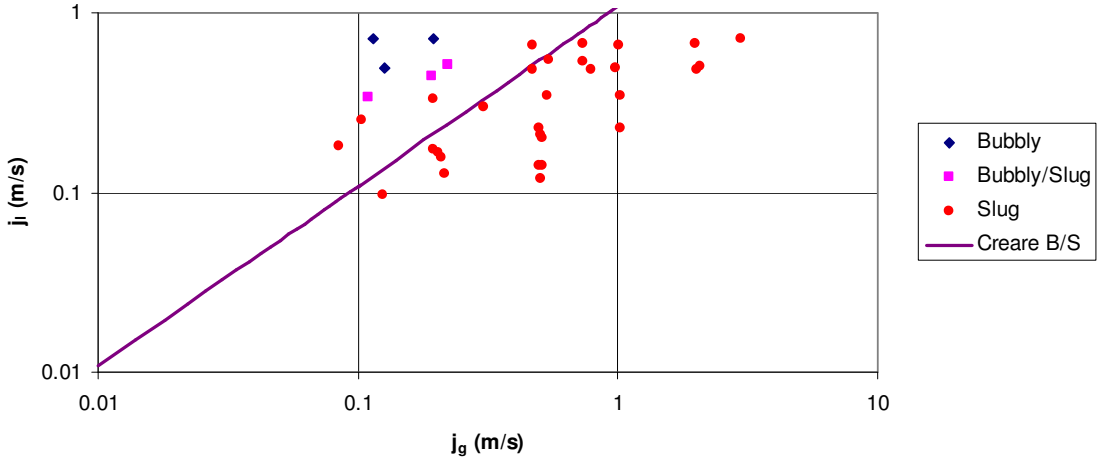

Figure 36: Creare Bubby-to-Slug Model with Data ID=25.4 mm

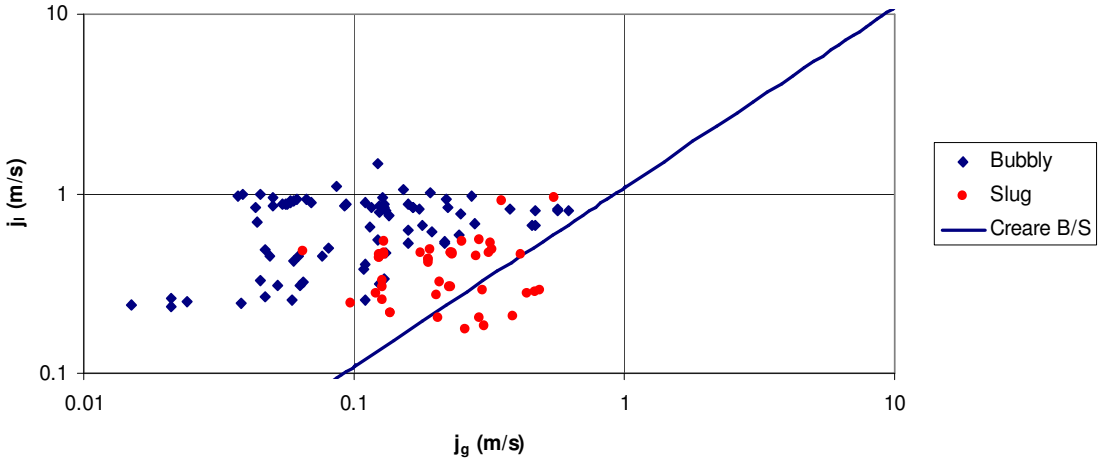

Figure 37: Creare Bubby-to-Slug Model with Data ID=40mm

5.3 Slug-to-Annular Transition Models

Four slug-to-annular transition models are presented in this section. These include Lee, Reinarts, Bousman, and Creare.

5.3.1 Lee Slug-to-Annular Model

Lee developed a microgravity two-phase flow regime transition model for slug-to-annular flow using a force balance between the two governing forces in the flow regime transition, inertial force and surface tension force (Ref 12). He postulated that at the transition, the inertial force keeps the vapor core continuous while the surface tension force forms the vapor core into a bubble (Ref 12). Therefore at the transition, the axial surface tension force encouraging slug flow is equivalent to the axial vapor inertial force encouraging annular flow. The Equation that Lee uses for the slug-to-annular flow regime transition is shown below in Equation 50 where r is the inner radius, ρ_g is the density of the gas phase, σ is the surface tension, and v_g is the velocity of the gas phase.

$$\frac{1}{2}\rho_g v_g^2 = \frac{2\sigma}{r}$$

Equation 50

$$v_g = \frac{j_g}{\alpha}$$

Equation 51

The superficial vapor velocity can be calculated through Equation 52 and the vapor velocity defined in Equation 51 if a void fraction is assumed. The liquid superficial velocity is found by first calculating the Martinelli parameter as shown in Equation 52 and then using Equation 53 below. The transition curve is produced by repeating the calculations for a range of void fractions.

$$X^2 = \frac{\left(U_g^* D_g^*\right)^{-m}\left(U_g^*\right)^2\left[\frac{S_g^*}{A_g^*} + \left[\frac{f_i}{f_g}\right]\left[\frac{S_i^*}{A_l^*} + \frac{S_i^*}{A_g^*}\right]\right]}{\left(U_l^* D_l^*\right)^{-n}\left(U_l^*\right)^2 \frac{S_l^*}{A_l^*}}$$

Equation 52

$$X^2 = \frac{C_l\left[\frac{\rho_l j_l D}{\mu_l}\right]^{-m}\frac{\rho_l j_l^2}{2}}{C_g\left[\frac{\rho_g j_g D}{\mu_g}\right]^{-n}\frac{\rho_g j_g^2}{2}}$$

Equation 53

Where h_l is the equilibrium liquid level, and h^* is the dimensionless liquid level given by Equation 54.

$$h^* = \frac{h_l}{D}$$

Equation 54

A_l^* and A_g^* are the dimensionless equilibrium cross sectional areas of the liquid and gas calculated through Equation 55 and Equation 56.

$$A_l^* = \frac{1}{4}\left[\pi - \cos^{-1}\left(2h^* - 1\right) + \left(2h^* - 1\right)\sqrt{1 - \left(2h^* - 1\right)^2}\right]$$

Equation 55

$$A_g^* = \frac{1}{4}\left[\cos^{-1}\left(2h^* - 1\right) + \left(2h^* - 1\right)\sqrt{1 - \left(2h^* - 1\right)^2}\right]$$

Equation 56

S_l^* and S_g^* are the dimensionless equilibrium cross sectional perimeters of the liquid wall contact and gas wall contact. S_i^* is the cross sectional perimeter of the gas and liquid interface. These cross sectional perimeters are defined in Equation 57 through Equation 59.

$$S_l^* = \pi - \cos^{-1}\left(2h^* - 1\right)$$

Equation 57

$$S_g^* = \cos^{-1}\left(2h^* - 1\right)$$

Equation 58

$$S_i^* = \sqrt{1-\left(2h^* - 1\right)^2}$$

Equation 59

D_g^* and D_l^* are dimensionless hydraulic diameters of the liquid and gas defined below in Equation 60 and Equation 61.

$$D_g^* = \frac{4A_g^*}{S_g^* + S_i^*}$$

Equation 60

$$D_l^* = \frac{4A_l^*}{S_l^*}$$

Equation 61

U_l^* and U_g^* are the dimensionless liquid and vapor velocities calculated through Equation 62 and Equation 63.

$$U_g^* = \frac{\pi}{4A_g^*} = \frac{1}{\alpha}$$

Equation 62

$$U_l^* = \frac{\pi}{4A_l^*} = \frac{1}{1-\alpha}$$

Equation 63

Figure 38 through Figure 40 show Lee's slug-to-annular transition model with the experimental flow regime data already presented.

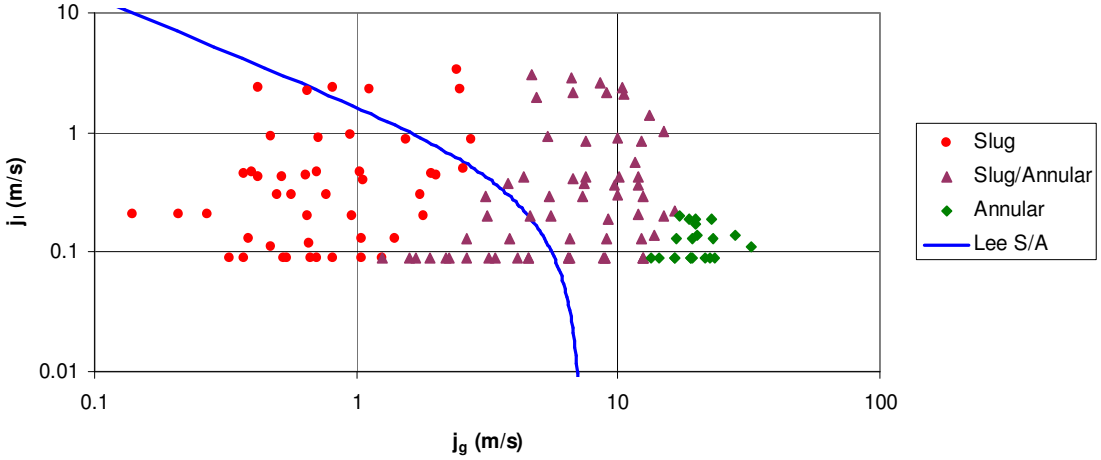

Figure 38: Lee Model with Data ID=9.525mm

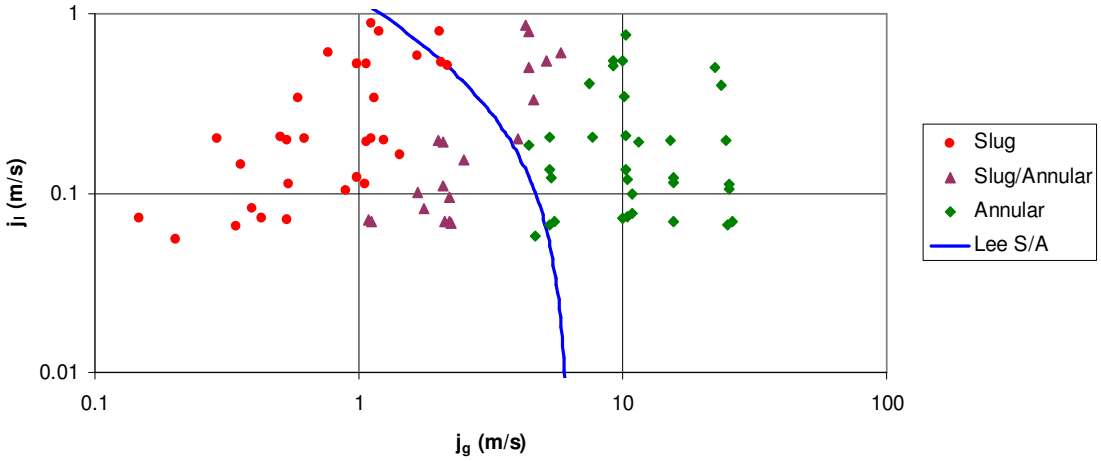

Figure 39: Lee model with Data ID=12.7mm

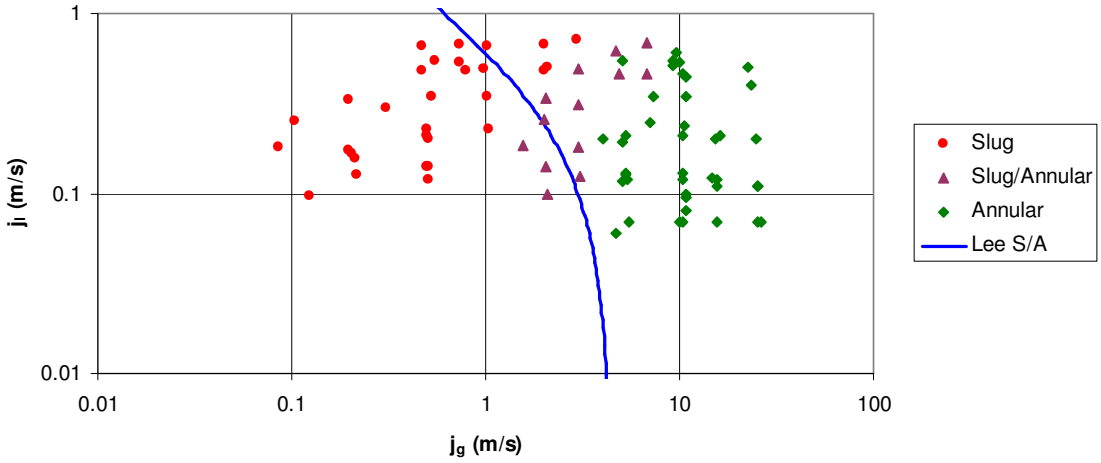

Figure 40: Lee Model with Data ID=25.4mm

5.3.2 Reinarts' Slug-to-Annular Flow Regime Transition

Reinarts expanded on Lee's slug-to-annular flow transition model by incorporating the changing bubble nose radius (Ref 12). Reinarts' analysis shows that the radius of the bubble decreases as liquid velocity increases (Ref 12). In the Lee model, the bubble radius is assumed to be the inner tube radius. For lower liquid velocities, Lee's assumption is valid. However as velocities increase, the bubble nose radius decreases. Reinarts developed a model for the changing bubble radius for use in Lee's model. The new transition Equation for slug-to-annular flow is shown below in Equation 64 where r_b is the radius of the bubble and the expression $\frac{2\sigma}{r_b}$ represents the surface tension force acting on the elongated bubble nose (Ref 12).

$$\frac{2\sigma}{r_b} = \frac{\rho_g v_g^2}{2}$$

Equation 64

Rearranging Equation 64 to solve for the vapor velocity v_g at the transition gives Equation 65 . In this Equation, $v_{g-sl/a}$ represents the vapor velocity at the transition which occurs when the inertia force is equal to the surface tension force (Ref 12).

$$v_{g-sl/a} = \sqrt{\frac{4\sigma}{r_b \rho_g}}$$

Equation 65

The radius of the bubble nose changes as a function of vapor to liquid flow (Ref 12). For lower liquid velocities the bubble nose radius is approximately equal to the radius of the tube. Then as liquid velocity increases, the bubble nose radius will decrease (Ref 12). Reinarts proposes that the radius of the bubble can be approximated by the radius of the

tube minus the film thickness if the flow was arranged in annular form. Since the location of interest is the transition, an annular shear balance is used to predict the film thickness (Ref 12). Equation 66 shows the liquid momentum balance and Equation 67 shows the vapor momentum balance.

$$-A_L\left(\frac{dP}{dx}\right)_{liquid} = -\tau_i S_i + \tau_{wL} S_L$$

Equation 66

$$-A_G\left(\frac{dP}{dx}\right)_{vapor} = \tau_i S_i$$

Equation 67

Setting the axial pressure drops in the vapor and liquid spaces equal becomes the shear balance on annular flow which is shown in Equation 68. Equal axial pressure gradients is a valid assumption given that in annular flow if the pressure drops were not equal vapor would appear in the liquid and vice-versa (Ref 12).

$$0 = \frac{\tau_i S_i}{A_g} + \frac{\tau_i S_i}{A_L} - \frac{\tau_{wL} S_L}{A_L}$$

Equation 68

In the above Equations, A_L is the cross sectional area of the liquid, A_G is the cross sectional area of the vapor, τ_i is the interfacial shear, τ_{wL} is the liquid shear on the wall, S_i is the interface perimeter, S_L is the liquid/tube interface, and $\frac{dP}{dx}$ is the axial pressure gradient. The terms in the above Equations are calculated as shown below:

$$A_G = \pi\left(\frac{D}{2} - t\right)^2$$

Equation 69

$$A_L = \pi\left[\left(\frac{D}{2}\right)^2 - \left(\frac{D}{2} - t\right)^2\right]$$

Equation 70

$$S_i = 2\pi\left(\frac{D}{2} - t\right)$$

Equation 71

$$S_L = \pi D$$

Equation 72

$$\tau_i = f_i \frac{\rho_g V_g^2}{2}$$

Equation 73

$$\tau_{wL} = f_L \frac{\rho_L V_L^2}{2}$$

Equation 74

$$f_L = C_L\left(\frac{\rho_L D_L V_L}{\mu_L}\right)^{-m}$$

Equation 75

$$D_L = t$$

Equation 76

$$f_i(zero - G) = 0.0036 + 0.38\delta^*$$

$$where$$

$$\delta^* = \frac{t}{D}$$

Equation 77

In Equation 69 through Equation 77, D is the inner tube diameter, t is the annular flow film thickness, f_i is the interfacial friction factor, f_L is the liquid/smooth wall friction factor, ρ_g is the vapor density, ρ_L is the liquid density, V_G is the vapor velocity, V_L is the liquid velocity, μ_L is the liquid viscosity, D_L is the hydraulic diameter of the liquid,

C_L is a constant (0.046 if liquid film turbulent, 16 if laminar), and m is a constant (0.2 if liquid film turbulent, 1 if laminar). Reinarts' model assumes that the transition from laminar to turbulent flow in the liquid film occurs at a Reynolds number of 400 (Ref 12).

For a given pair of liquid and vapor velocities, Equation 68 is used to solve iteratively for a film thickness. A maximum vapor velocity is calculated from Equation 65 with the assumption that the film thickness is zero (Ref 12). This is done to create a transition curve. A liquid velocity is chosen so that the vapor velocity of the solution is higher than the liquid velocity (slip must be greater than or equal to 1), and a film thickness is calculated iteratively from Equation 68. With the film thickness value, a new radius of the bubble nose is calculated from Equation 78.

$$r_b = \left(\frac{D}{2} - t \right)$$

Equation 78

The next step in Reinarts method is to take the new value of r_b and the same liquid velocity and obtain an improved estimate of the maximum vapor velocity for the transition using Equation 65. This process is repeated until the velocity calculated for the transition no longer changes (Ref 12). A void fraction can then be calculated from Equation 79 and superficial velocities, j_l and j_g, calculated from Equation 80.

$$\alpha = \frac{A_G}{A_G + A_L}$$

Equation 79

$$j_l = V_g \alpha$$
$$j_g = V_L (1 - \alpha)$$

Equation 80

This process is repeated for a range of liquid velocities less than or equal to the vapor velocity, and the slug-to-annular transition line is formed.

Figure 41 through Figure 43 shows Reinarts' transition lines plotted with the data for the inner diameters of 9.525mm, 12.7mm, and 24.5mm respectively.

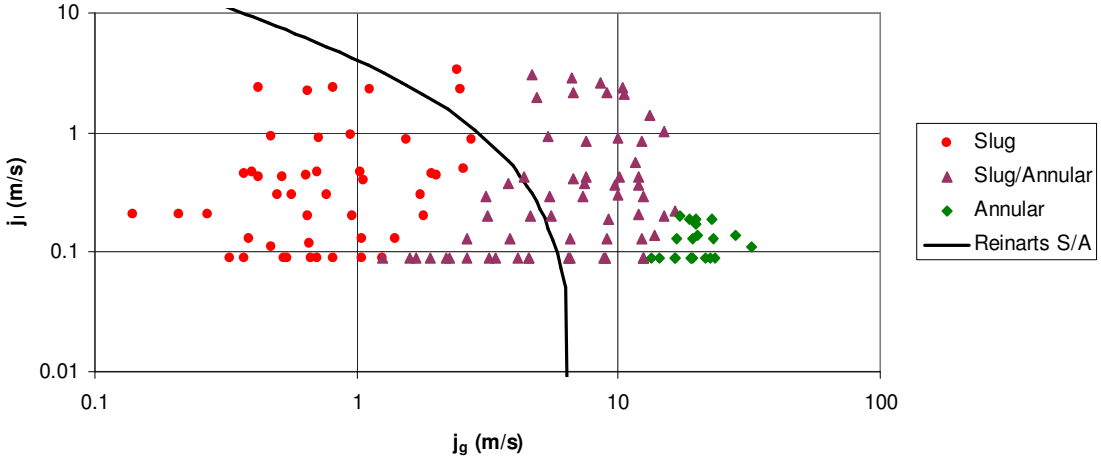

Figure 41: Reinarts' model with Data ID=9.525mm

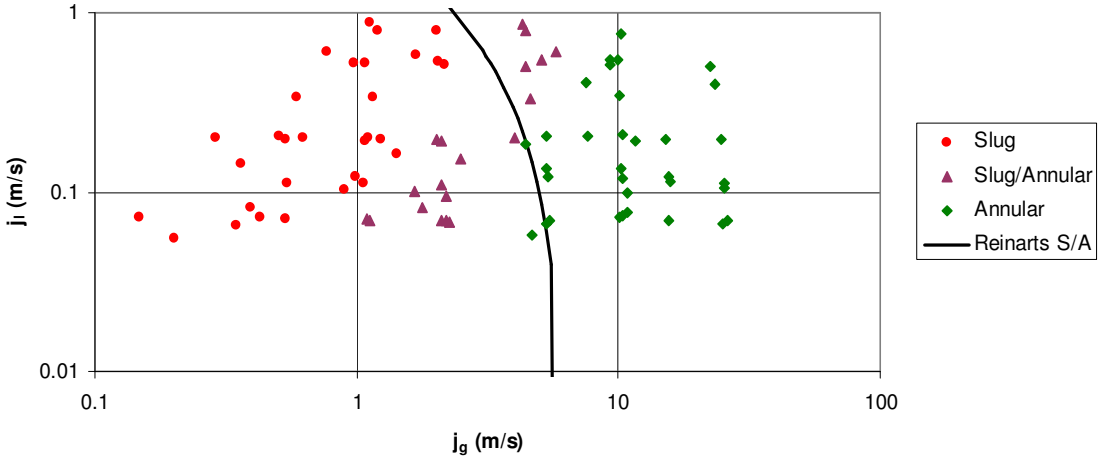

Figure 42: Reinarts' model with Data ID=12.7mm

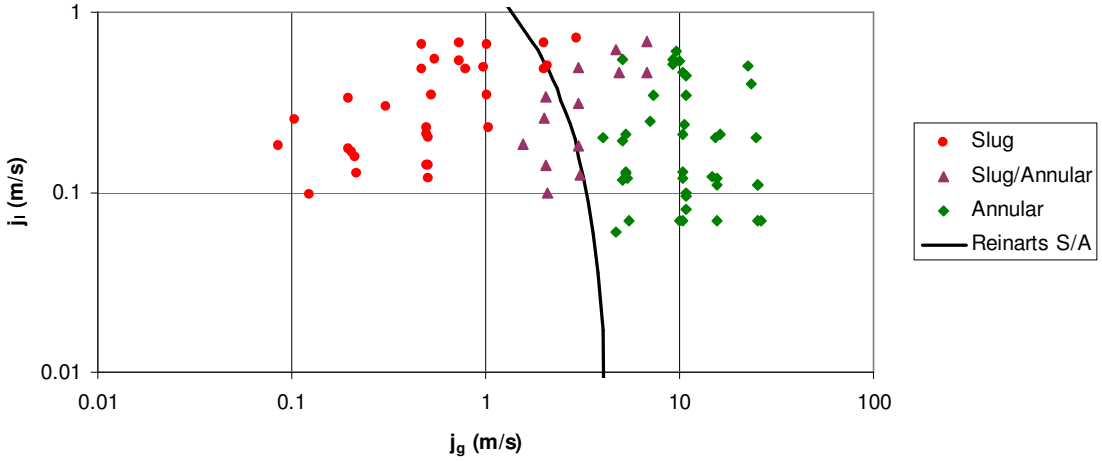

Figure 43: Reinarts' model with Data ID=25.4mm

5.3.3 Bousman Slug-to-Annular

Bousman's slug-to-annular flow regime transition model uses the void fraction calculated from the Drift Flux model for slug flow and compares it with the void fraction calculated from a force balance for annular flow (Ref 13). The region where the void fractions are equal to each other is the region Bousman identifies as the slug-to-annular transition. The mechanistic model of the void fraction of microgravity annular flow identified by Bousman is shown in Equation 81 and is a force balance on the control volume bounded by the tube walls and planes perpendicular to the flow (Ref 13).

$$\tau_i = \tau_w \alpha^{1/2}$$

Equation 81

The sheer stress at the interface, τ_i, is related to the sheer stress at the wall, τ_w and the void fraction. The sheer stresses are next expressed in terms of friction factors in Equation 82 and Equation 83 shown below.

$$\tau_i = \frac{f_i \rho_g \left\langle v_g \right\rangle^2}{2} = \frac{f_i \rho_g \left\langle j_g \right\rangle^2}{2\left\langle \alpha \right\rangle^2}$$

Equation 82

$$\tau_w = \frac{f_w \rho_l \left\langle v_l \right\rangle^2}{2} = \frac{f_w \rho_l \left\langle j_l \right\rangle^2}{2\left(1-\left\langle \alpha \right\rangle\right)^2}$$

Equation 83

These definitions are then substituted into Equation 81 to get Equation 84.

$$\frac{\left\langle \alpha \right\rangle^{5/2}}{\left(1-\left\langle \alpha \right\rangle\right)^2} = \frac{f_i}{f_w}\frac{\rho_g}{\rho_l}\left[\frac{j_g}{j_l}\right]^2$$

Equation 84

The interfacial friction factor term is defined in Equation 85 where f_g is the friction factor of the gas flowing alone (Ref 13).

$$f_i = \phi\left(\left\langle \alpha \right\rangle\right) f_g$$

Equation 85

Substituting the relationship for the interfacial friction factor in Equation Equation 85 into Equation 83 yields Equation 86.

$$\frac{\left\langle \alpha \right\rangle^{5/2}}{\left(1-\left\langle \alpha \right\rangle\right)^2} = \phi\left(\left\langle \alpha \right\rangle\right)\frac{f_g}{f_w}\frac{\rho_g}{\rho_l}\left[\frac{j_g}{j_l}\right]^2$$

Equation 86

The single phase vapor and liquid friction factors are calculated through the Blasius relation in Equation 87.

$$f = \frac{C}{\mathrm{Re}^n}$$

Equation 87

The Reynolds numbers for the vapor and liquid phases implemented in Equation 87 are shown in Equation 88 and Equation 89.

$$\mathrm{Re}_g = \frac{D j_g \rho_g}{\mu_g \langle \alpha \rangle^{1/2}}$$

Equation 88

$$\mathrm{Re}_l = \frac{D j_l \rho_l}{\mu_l}$$

Equation 89

The model developed will be different if the flow is laminar than if the flow is turbulent. If the flow is turbulent, C = 0.046, n = 0.2 and if the flow is laminar C = 16, n = 1. The Equation for turbulent flow using the correct Blasius constants yields Equation 90.

$$j_l = j_g \left[\frac{\left(1 - \langle \alpha \rangle\right)^2 \phi\left(\langle \alpha \rangle\right)}{\langle \alpha \rangle^{2.4} B} \right]^{1/1.8}$$

Equation 90

Where B is a physical property grouping for void fraction models and is defined in Equation 91 and ν_l represents the kinematic viscosity of the liquid phase and ν_g represents the kinematic viscosity of the vapor phase. The value of B is 481.5 for air/water systems (Ref 13).

$$B = \left[\frac{\nu_l}{\nu_g}\right]^{0.2}\left[\frac{\rho_l}{\rho_g}\right]$$

Equation 91

The appropriate Blasius constants for turbulent gas flow with laminar liquid flow results in the laminar annular flow Equation shown in Equation 92.

$$j_l = \frac{0.00288 D^{0.8} \nu_g^{0.2} \rho_g j_g^{1.8} \phi\left(\langle\alpha\rangle\right)\left(1-\langle\alpha\rangle\right)^2}{\mu_l \langle\alpha\rangle^{2.4}}$$

Equation 92

The void fraction model for microgravity annular flow is now developed as Equation 90 and Equation 92. The Drift Flux model for slug flow was discussed earlier and is shown in Equation 93.

$$\frac{j_g}{j} = C_0 \langle\alpha\rangle$$

Equation 93

Bousman's model determines the conditions where the void fraction produced by either Equation 90 or Equation 92 depending on flow conditions and Equation 93 are equal. Equating the turbulent annular void fraction model with the drift flux model results in the turbulent void matching slug-annular transition model shown in Equation 94.

$$\langle\alpha\rangle = \frac{1}{C_0} - \langle\alpha\rangle\left[\frac{\left(1-\langle\alpha\rangle\right)^2 \phi\left(\langle\alpha\rangle\right)}{\langle\alpha\rangle^{2.4} B}\right]^{5/9}$$

Equation 94

The distribution coefficient Co is a constant and ϕ is a function of void fraction only. This implies that the transition between slug and annular flow for turbulent flow will be along a line of constant void fraction (Ref 13). This Equation can be solved numerically by successive substitution.

Equating the laminar annular void fraction model with the drift flux model results in the laminar void matching slug-annular transition model shown in Equation 95.

$$j_g\left[\frac{1-C_0\langle\alpha\rangle}{C_0\langle\alpha\rangle}\right]=\frac{0.00288D^{0.8}v_g^{0.2}\rho_g j_g^{1.8}\left(1-\langle\alpha\rangle\right)^2\phi\left(\langle\alpha\rangle\right)}{\mu_l\langle\alpha\rangle^{2.4}}$$

Equation 95

The laminar flow transition model does not lie along a line of constant void fraction as the turbulent model does. It is a function of superficial gas velocity, diameter, and physical properties of the phases such as density, viscosity, and kinematic viscosity. The friction factor enhancement function ϕ is determined using the Wallis model shown in Equation 96 (Ref 13).

$$\phi\left(\langle\alpha\rangle\right)=1+150\left(1-\alpha^{1/2}\right)$$

Equation 96

The results of Bousman's modeling efforts for slug-to-annular transition are shown in Figure 44 through Figure 46 for inner diameters of 9.525 mm, 12.7 mm, and 25.4 mm shown with data.

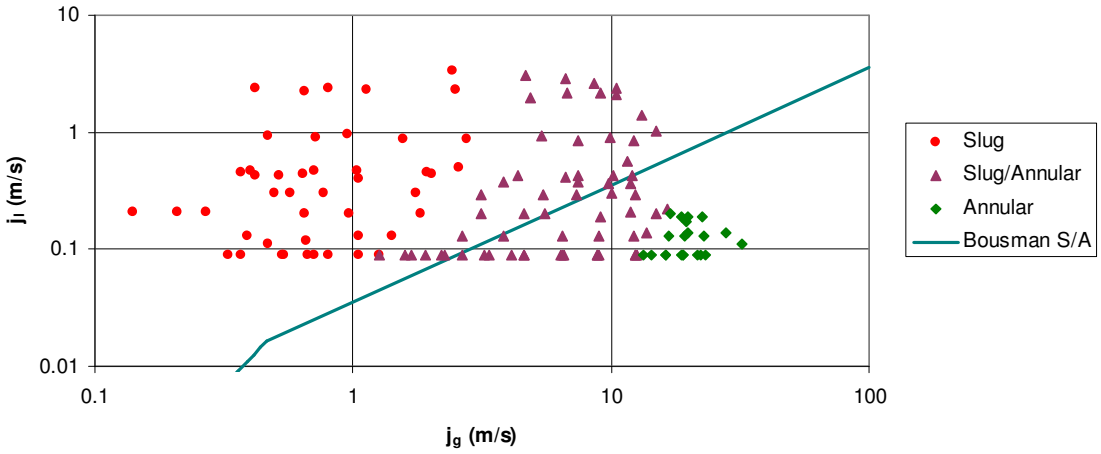

Figure 44: Bousman Model with Data ID=9.525mm

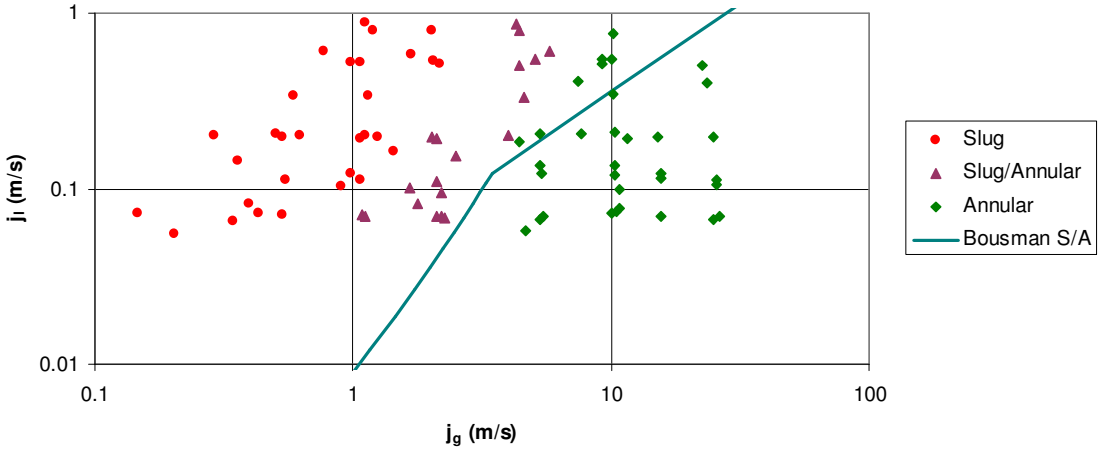

Figure 45: Bousman Model with Data ID=12.7mm

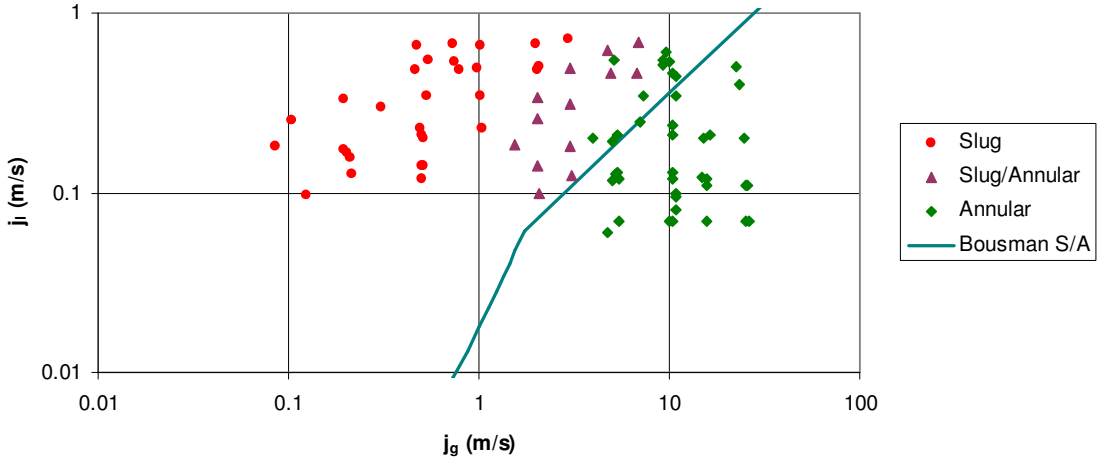

Figure 46: Bousman Model with Data ID=25.4mm

5.3.4 Creare Slug-to-Annular Model

The Creare slug-to-annular flow regime transition is based on two parameters, the Martinelli Parameter X and the dimensionless pipe inclination parameter Y shown in Equation 97 and Equation 98 below.

$$X = \left[\frac{\left[\frac{4C_l}{D}\right]\left[\frac{\rho_l D j_l}{\mu_l}\right]^{-n}\left[\frac{\rho_l j_l^2}{2}\right]}{\left[\frac{4C_g}{D}\right]\left[\frac{\rho_g D j_g}{\mu_g}\right]^{-n}\left[\frac{\rho_g j_g^2}{2}\right]} \right]^{0.5}$$

Equation 97

$$Y = -\left[\frac{a\left(\rho_l - \rho_g\right)\cos\theta}{\left[\frac{4C_g}{D}\right]\left[\frac{\rho_g D j_g}{\mu_g}\right]^{-n}\left[\frac{\rho_g j_g^2}{2}\right]} \right]$$

Equation 98

The first part of the transition involves simultaneously solving two Equations. These Equations are shown below in Equation 99 and Equation 100 which are the two-phase void fraction Equation for the annular flow regime and the second Equation is the transition criterion derived by Barnea (Ref 14). The parameter $\left(f_i / f_{wg} \right)$ in Equation 101 below represents the interfacial friction factor between the gas and liquid phases. The value used came from Wallis in 1969 and is shown in Equation 101 (Creare Manual).

$$Y = \left[\frac{\left(f_i / f_{wg} \right)}{\alpha^{2.5}\left(1-\alpha\right)} \right] - \left[\frac{1}{\left(1-\alpha\right)^3} \right] X^2$$

Equation 99

$$Y = \frac{\left[2 - 1.5(1-\alpha)\right]}{\left(1-\alpha^3\left[1-1.5\right](1-\alpha)\right)} X^2$$

Equation 100

$$\left(f_i / f_{wg}\right) = \left[1 + 75(1-\alpha)\right]$$

Equation 101

The coordinates (X,Y) are then located on the plot in Figure 47. If the location of (X,Y) is below the curve then the flow regime is annular (Ref 14). If the location is above the curve then the flow regime is slug flow. The shaded region represents an uncertainty region between the values for interfacial friction of 1.0 and Equation 101 above.

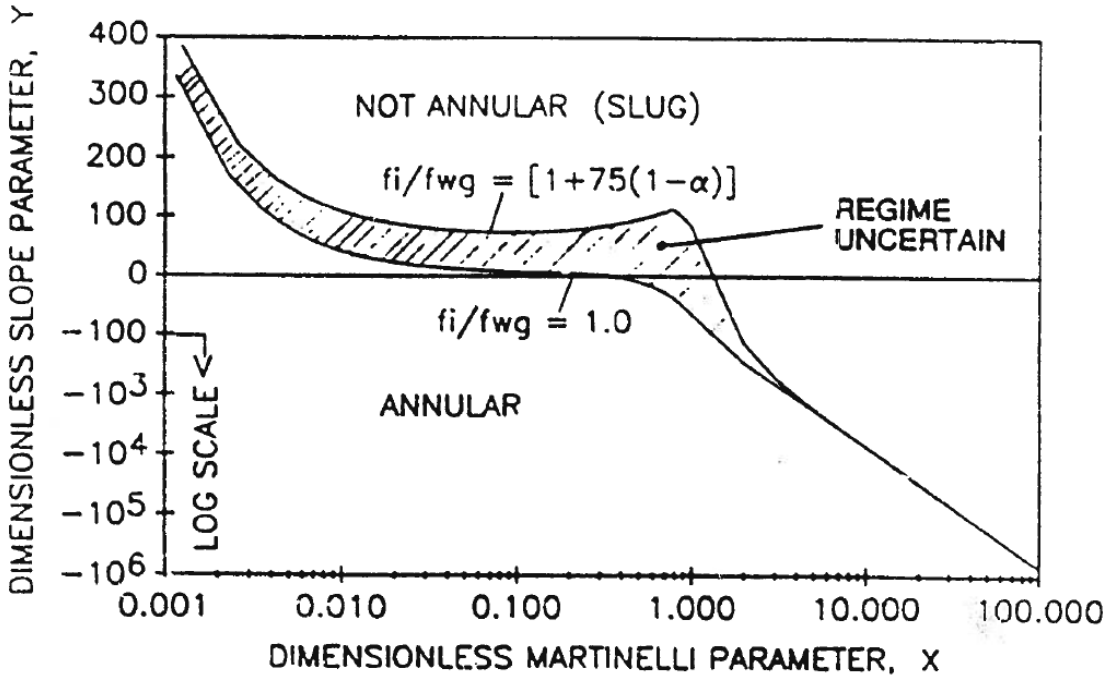

Figure 47: Dimensionless Design Map for Slug to Annular Transition (Ref 14)

The Creare model is plotted with data in Figure 48 through Figure 50 for inner diameters of 9.525mm, 12.7mm and 24.5 mm respectively.

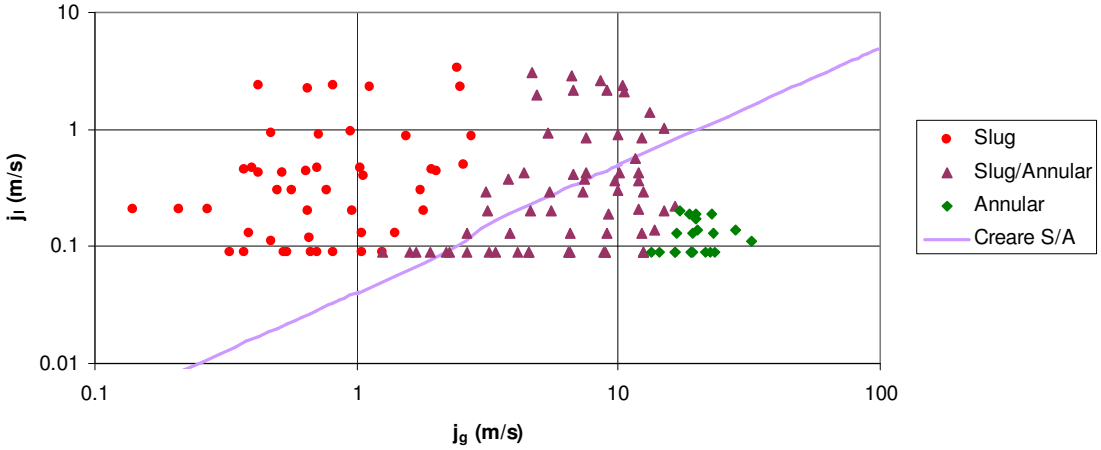

Figure 48: Creare Model with Data ID=9.525mm

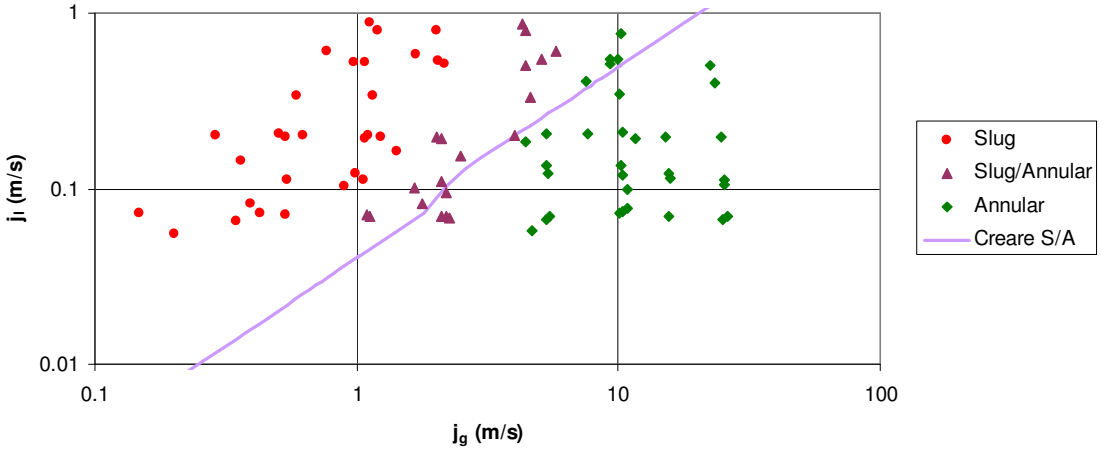

Figure 49: Creare Model with Data ID=12.7mm

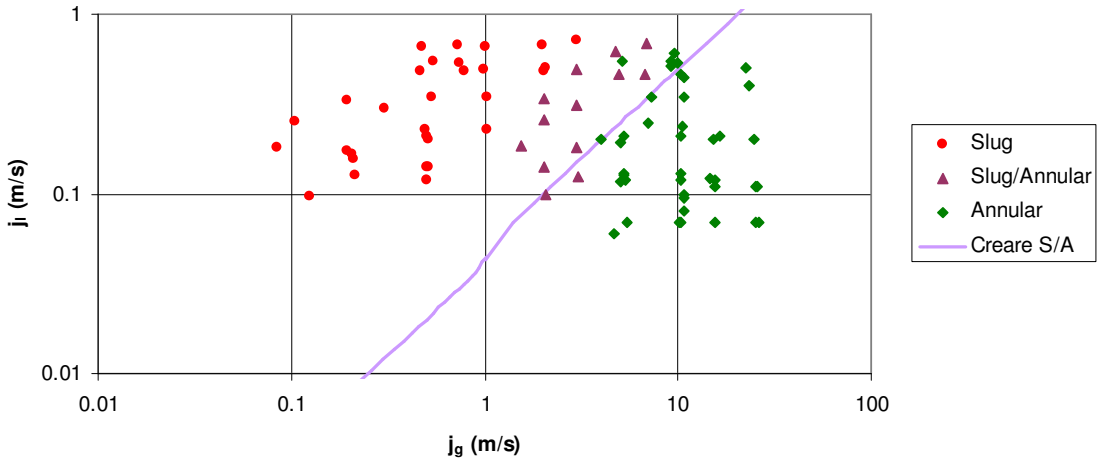

Figure 50: Creare Model with Data ID=25.4mm

5.4 Summary

Now that each of the models has been discussed in some depth, a summary is provided in a form that makes comparing them with each other a little simpler. Table 7 and Table 8 list each model, the approach taken by the model, the key parameter or Equation, and a baseline value of the parameter or assumptions made by each model. Table 7 shows the models for the bubbly-to-slug transition and Table 8 shows the models for the slug-to-annular transition. There are a lot of similarities with the bubbly-to-slug transition models. All three models use a void fraction based criterion to some degree. Creare utilizes a two-step approach which results in either using a turbulence model or a critical void fraction.

Table 7: Zero Gravity Model Comparisons for Bubbly to Slug

Model	Approach	Key Parameter	Baseline Value of key parameter
Creare 1)Turbulence 2) Max Void Fraction	1)Inertia/buoyancy 2) max packing of vapor bubbles	1) turbulence coefficient (k) 2) Critical void fraction (α_c) --Bubble distribution (Co)	1) k=1.14 2)α_c =0.45 Co=1.2
Dukler	Max packing density	Critical void fraction (α_c)	α_c =0.45
Drift Flux	Max void fraction	Centerpoint void fraction for transition (α_c)	α=0.40

Table 8: Zero Gravity Model comparisons for Slug to Annular

Model	Approach	Key Parameter/Equation	Assumptions
Lee	Inertial forces vs surface tension forces	$\frac{1}{2}\rho_g v_g^2 = \frac{2\sigma}{r}$	Taylor bubble nose diameter = inner tube diameter
Reinarts	Inertial forces vs surface tension forces with varying bubble nose radius	$\frac{\rho_g v_g^2}{2} = \frac{2\sigma}{r_b}$	Radius of the bubble nose changes as a function of vapor liquid flow
Creare	Neutral stability or physical blockage	Interfacial shear $\left[f_i / f_{wg} \right]$	(1+75(1-α))
Bousman	Void fraction from drift flux model compared with void fraction from force balance for annular flow	$\frac{j_g}{j} = C_0 \langle \alpha \rangle$ from mechanistic force balance $j_l = j_g \left[\frac{\left(1-\langle\alpha\rangle\right)^2 \phi\left(\langle\alpha\rangle\right)}{\langle\alpha\rangle^{2.4} B} \right]^{1/1.8}$ for turbulent liquid flow $j_l = \frac{0.00288 D^{0.8} \nu_g^{0.2} \rho_g j_g^{1.8} \phi\left(\langle\alpha\rangle\right)\left(1-\langle\alpha\rangle\right)^2}{\mu_l \langle\alpha\rangle^{2.4}}$ for laminar liquid flow	Co=1.2

CHAPTER VI

COMPARISON OF MODELS WITH DATA

6.1 Introduction

This chapter will begin a comparison of the various models discussed in the previous chapter in order to validate the recommendations that will be made. Each individual model was shown plotted with the data in the previous chapter. Now the models will be compared to each other in relation to the data. A mathematical method for comparing the models to the data are developed using a squared difference approach. This method quantifies how well each model matches the data and provides another validation for the best suited model. An equal distribution is then applied to the data so that the number of data points is equal in each flow regime being compared. Lastly, a transition region is developed for the models that are recommended for use in the RELAP5-3D code.

6.2 Bubbly-to-Slug Transition Model Comparison

In the following figures, the models are plotted together for a visual inspection. Figure 51 through Figure 54 show the three bubbly-to-slug transition models and the data for the corresponding diameter.

Figure 51 shows the 9.525 mm diameter tubing results. In this figure, all three models show a linear correlation on the log-log plot for the bubbly-to-slug flow regime transition. All models correctly predict the bubbly data points collected during the experiment. However, by visual inspection the drift flux model incorrectly identifies

more of the slug data points. The Dukler and Creare models are similar in location. A statistical method will have to differentiate the better prediction model for this diameter.

Figure 52 shows the results for the 12.7 mm diameter tubing. In this figure, the Creare model and the Drift Flux model overlap entirely. As explained in the previous chapter, under certain conditions the Creare model is based on the Drift Flux model. From a visual inspection, all three models correctly predict all bubbly and slug data points for the 12.7 mm diameter tube. The transition points fall very close to the models' predicted transition. The Creare and Drift Flux model correctly predict one transition point. There are three transition points that the models predict incorrectly as bubbly flow and three transition points that the models predict incorrectly as slug flows. The Dukler model predicts incorrectly 3 transition points as bubbly flow and 4 transition points as slug flow.

Figure 53 shows the three bubbly-to-slug transition models compared with the data for an inner diameter of 25.4 mm. From a visual inspection only, the drift flux model appears to more correctly identify the transition for this diameter. Although there is a slug point that falls on the drift flux transition line, the transition points are much closer to the drift flux model than the other two models. There are only three data points for bubbly flow and three data points for bubbly/slug transition flow. More data in this region would be helpful for the determination of best suited model.

Figure 54 shows the data for an inner diameter of 40 mm along with the corresponding transition models. As discussed previously in chapter III, the data collected in the 40 mm test section may not all be correct due to the effects of the arrangement of the experiment in the plane. From a visual inspection, it appears that

overall the models do not match the data as well as in the smaller diameter test sections. This may be due to the acceleration effects. Both the Dukler and Creare transition models predict a transition at a vapor superficial velocity that is too high compared with the apparent transition in the data. The drift flux model seems to predict the transition at a more appropriate superficial vapor velocity, but this model incorrectly predicts several identified bubbly data points.

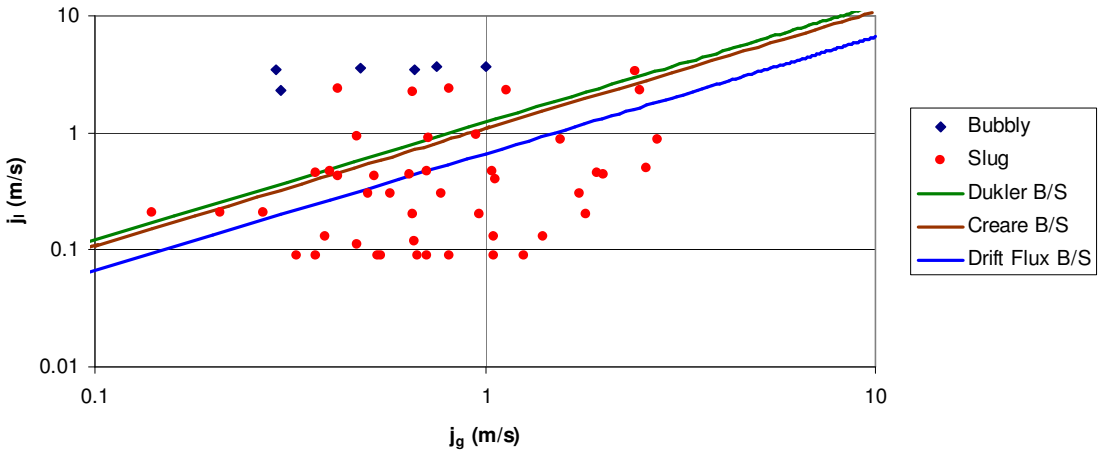

Figure 51: Bubbly/Slug Models with Data ID=9.525mm

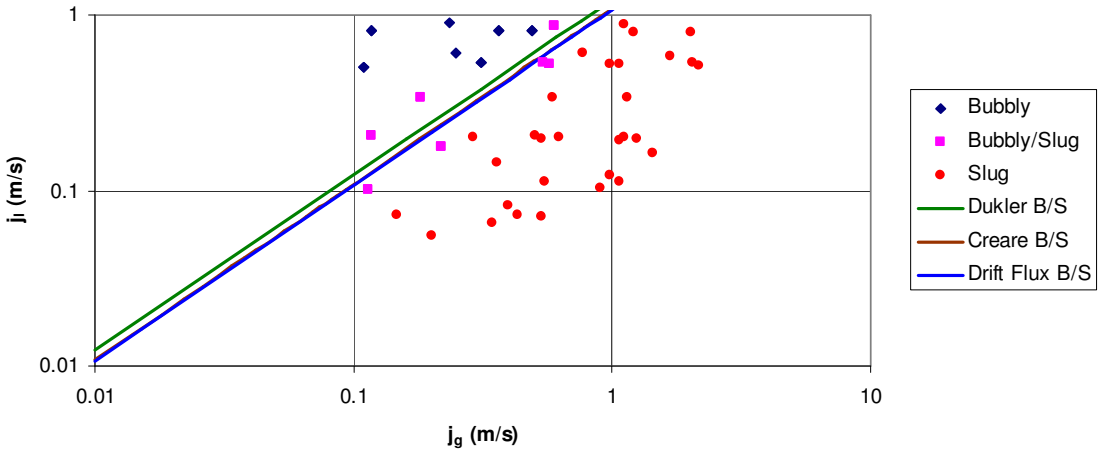

Figure 52: Bubbly/Slug Models with Data ID=12.7mm

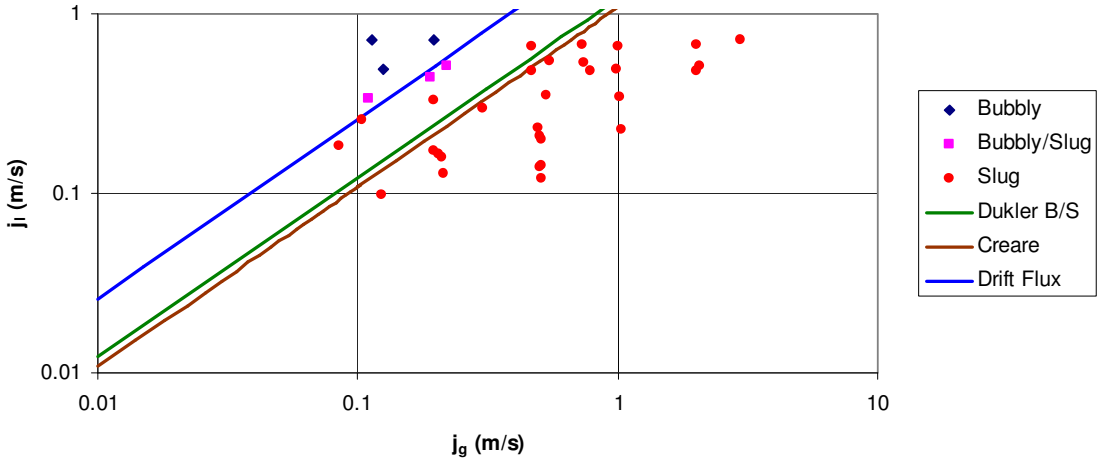

Figure 53: Bubbly Slug Models with Data ID=25.4mm

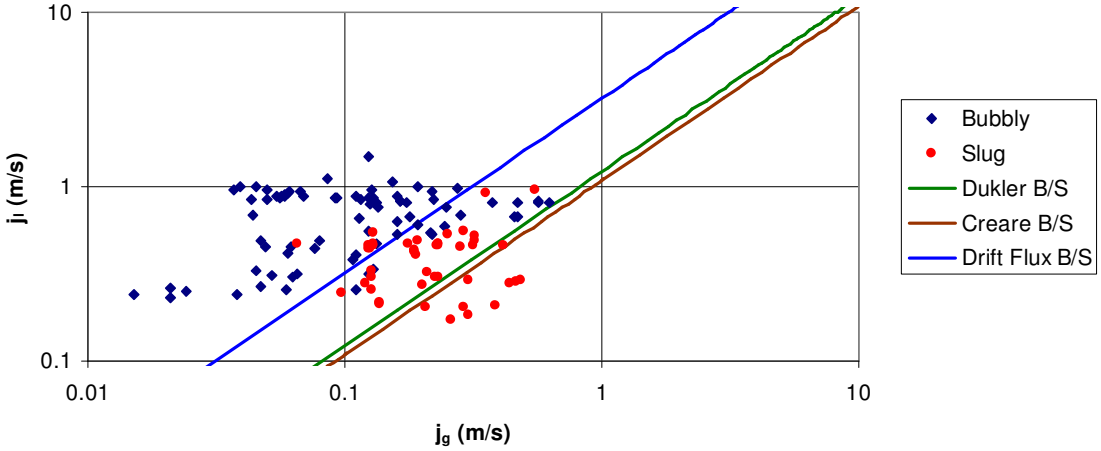

Figure 54: Bubbly/Slug Models with Data ID=40mm

6.3 Slug-to-Annular Transition Model Comparison

The slug-to-annular transition models and data are compared in Figure 55 through Figure 57 for tube inner diameters of 9.525 mm, 12.7 mm, and 25.4 mm. There

are no data points for the slug-to-annular transition for the 40 mm diameter experiment so that diameter is omitted from this comparison.

The slug-to-annular transition models for an inner diameter of 9.525 mm are shown in Figure 55. The models follow two different patterns. Lee's model and Reinarts' model show a similar pattern as does Bousman's and the Creare model. Both the Bousman model and the Creare model correctly predict all of the slug and annular data points while the Lee and Reinarts' models incorrectly predict several slug points. The transition region as shown by the data covers a large area in the plot. The next section of this chapter will mathematically differentiate which model more correctly models the data for this diameter.

The model comparison for an inner diameter of 12.7 mm is shown in Figure 56. All models except for the Lee model correctly predict the slug region. The Lee and Reinarts' models very closely predict the annular flow regime by incorrectly predicting only 1 and 2 data points respectively. The Bousman and Creare models mislabel several annular data points and predict the transition from slug-to-annular at a vapor superficial velocity that is higher than the transition region shown in the data.

The transition models for an inner diameter of 25.4 mm are shown in Figure 57. On this flow regime map, the Creare and Bousman transitions correctly predict the slug data points while the Lee and Reinarts' models correctly predict the annular data points. Again, the Creare and Bousman models seem to predict the transition at a higher vapor superficial velocity than the experimental transition does.

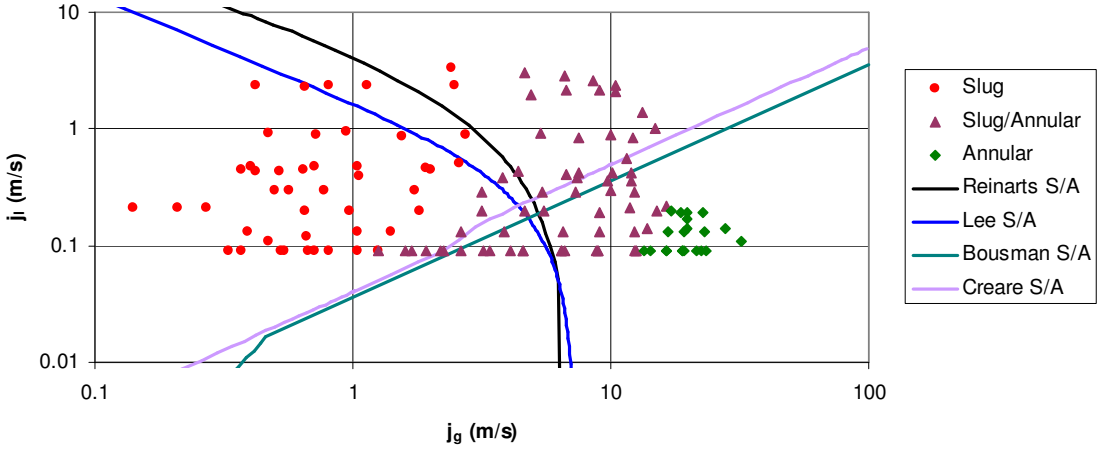

Figure 55: Slug/Annular Models with Data ID=9.525mm

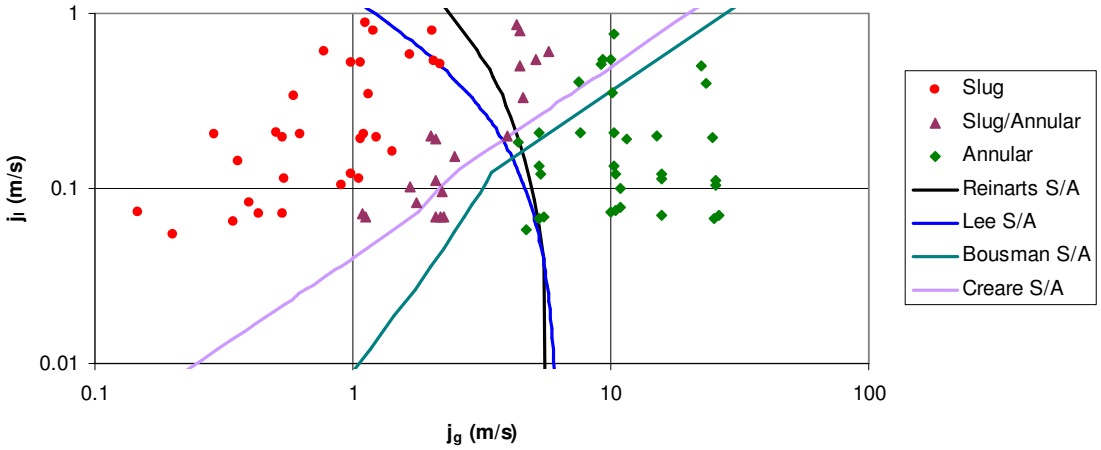

Figure 56: Slug/Annular Models with Data ID=12.7mm

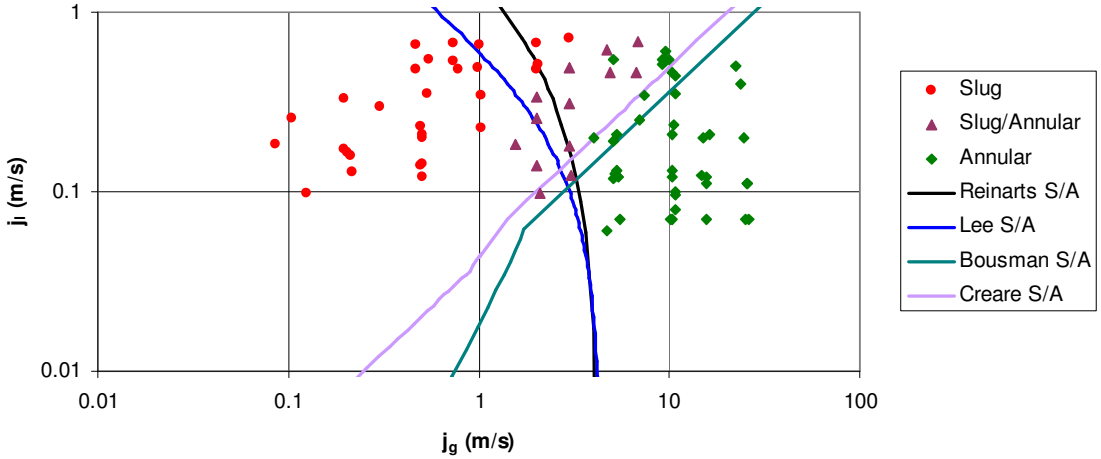

Figure 57: Slug/Annular Models with Data ID=25.4mm

6.4 Squared Difference Comparison Method

A method was developed to determine how well the different models matched the data. This information will aid in the recommendation since the recommendation will be the model best validated by the data. The approach used is an absolute value of the squared difference between what the model predicts and what was visually observed on the experiment itself. Each data point was assigned a numerical value based on the visual flow regime identification. The transition data were not used for this comparison. Table 9 shows the corresponding values.

Table 9: Numerical Values for Flow Regime Identification

Flow Regime	**Numerical Assignment**
Bubbly	1
Slug	2
Annular	3

Once each data point has an assigned value, this value is compared to the models predictions through Equation 102 where R is the squared difference value, E is the numerical value from Table 9 corresponding to the experimental results, and P is the numerical value from Table 9 corresponding to the model prediction results. For a perfect model, the squared difference value would be zero. The higher the squared difference value, the more the model deviates from the data. For example, if the model predicts the point to be in the slug flow regime but the experimental observation shows the point to be a bubbly point, the squared difference value would have a value of 3.

$$R = \left\| \left[(\mathrm{E})^2 - (\mathrm{P})^2 \right] \right\|$$

Equation 102

A squared difference value for each experimental point is calculated and plotted on a superficial velocity map with the corresponding model. If an data point landed directly on the transition line, the point was counted as having transitioned according to the model. For example, if a bubbly data point lies on top of the bubbly-to-slug transition line, the model has predicted it to be slug flow for this comparison. Each squared difference value for each flow regime will be represented by a unique shape/color. These plots will provide a visual indication of where the models fail to predict the data.

6.4.1 Bubbly to Slug Squared Difference Results

The first squared difference plot is the Creare bubbly-to-slug transition model for an inner diameter of 9.525 mm shown in Figure 58. In this data comparison, the majority of the squared differences are zeros represented by the color black (square for

bubbly and triangle for slug flow). There are several points with a squared difference value of 3 for slug flow. Some of these misidentified data points are very close to the transition line while others are further away. The data points that are further away are the data points that are of the most concern since the model does not predict them very well. All of these higher squared differences are located above the transition line indicating that the Creare model predicted the transition at too low a liquid superficial velocity.

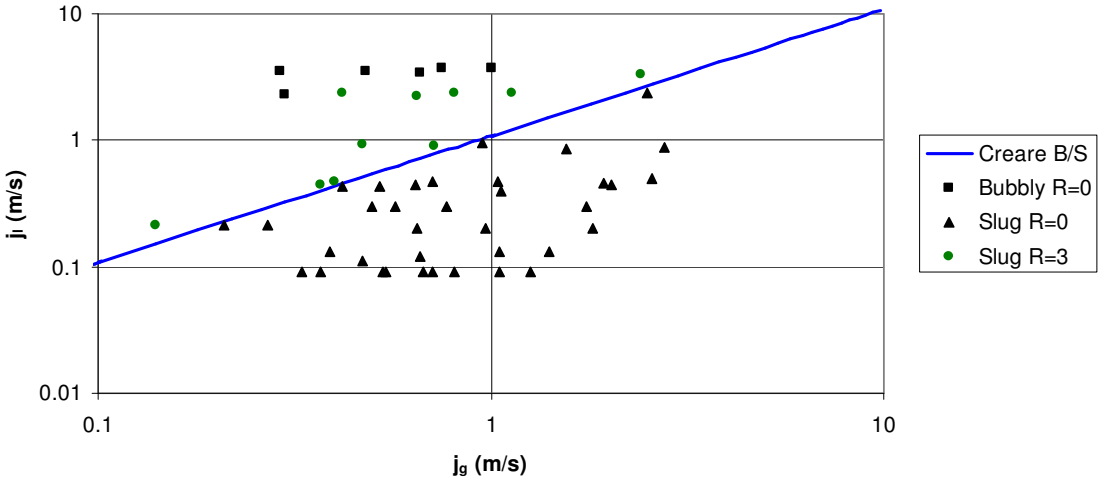

Figure 58: Squared Difference Comparison with ID=9.525mm and Creare Model

Figure 59 shows Dukler's model compared with data for an inner diameter of 9.525 mm. Similar to the Creare model, all of the higher squared differences are above the predicted transition line indicating that the Dukler model also slightly under predicts the actual transition for this smaller diameter. There are 3 points that fall on the transition line itself that were actually slug flow and 7 slug points that were incorrectly predicted to be bubbly flow. The misidentified slug flow data points are many of the same data points also misidentified by the Creare model. This could possibly point to a

misidentified flow regime in the experiment. This will be discussed further in the recommendations section.

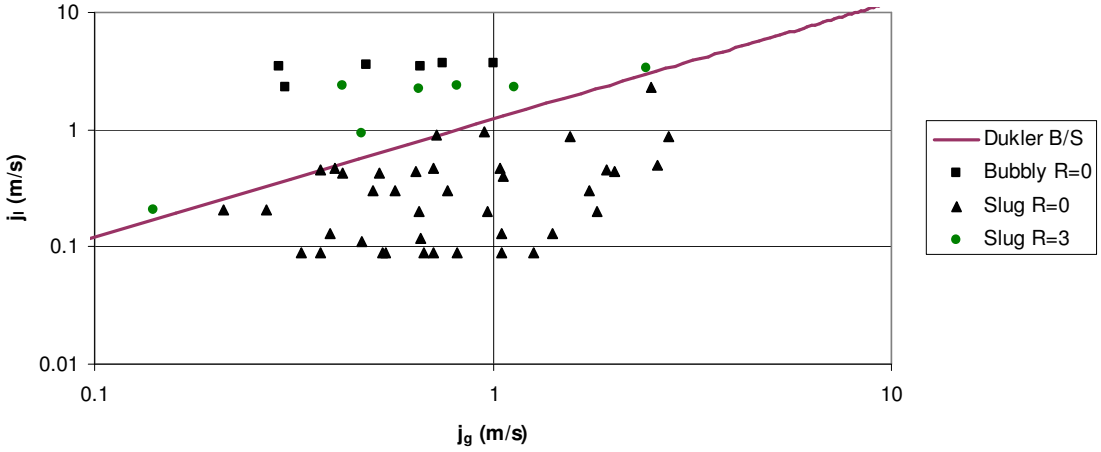

Figure 59: Squared Difference Comparison with ID=9.525mm and Dukler's Model

The drift flux model for 9.525 mm inner diameter shown in Figure 60 clearly has a higher quantity of nonzero squared differences than the previous two models. There are far more slug points that were incorrectly predicted by the Drift Flux model to be bubbly flow. This model predicts the transition to slug flow at a lower liquid superficial velocity than the previous two models. The drift flux model under predicts the liquid superficial velocity at which the transition occurs for this diameter.

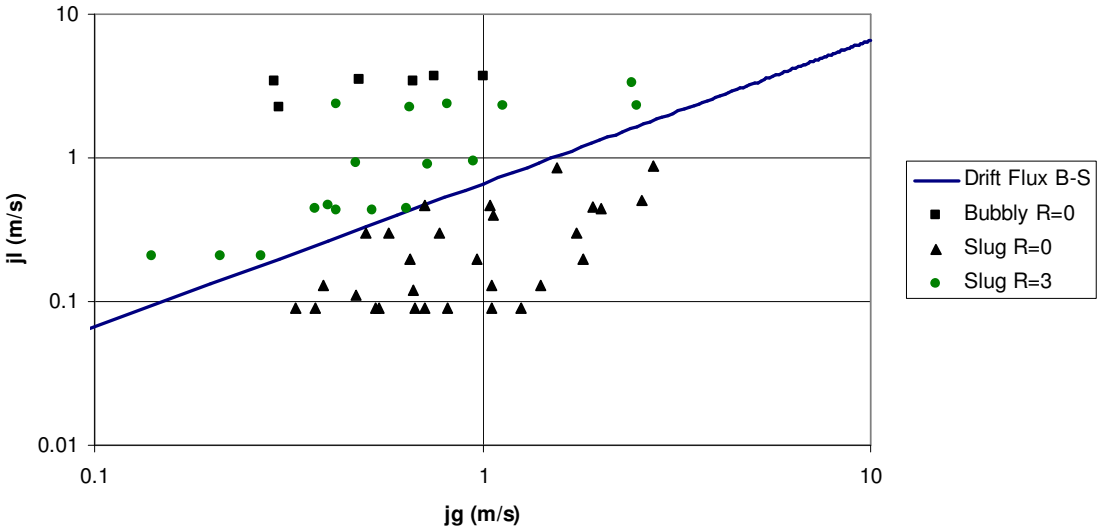

Figure 60: Squared Difference Comparison with ID=9.525mm and Drift Flux Model

The next comparison will be with the Creare, Dukler, and Drift Flux bubbly-to-slug models with an inner diameter of 12.7 mm. The Creare model is shown in Figure 61, the Dukler model in Figure 62, and the Drift Flux model in Figure 63. These models all predict the data for the 12.7 mm diameter very well. There are no bubbly flow or slug flow points that are incorrectly identified. Looking at the figures, all three models are very similar. The Creare and Drift Flux models are exactly the same line, and the Dukler model is very close to them.

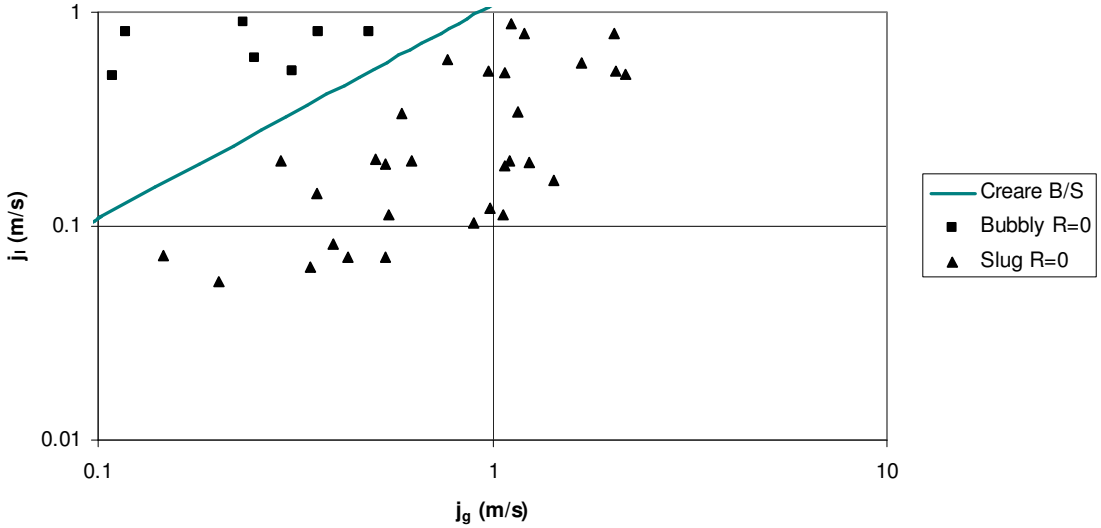

Figure 61: Squared Difference Comparison with ID=12.7mm and Creare Model

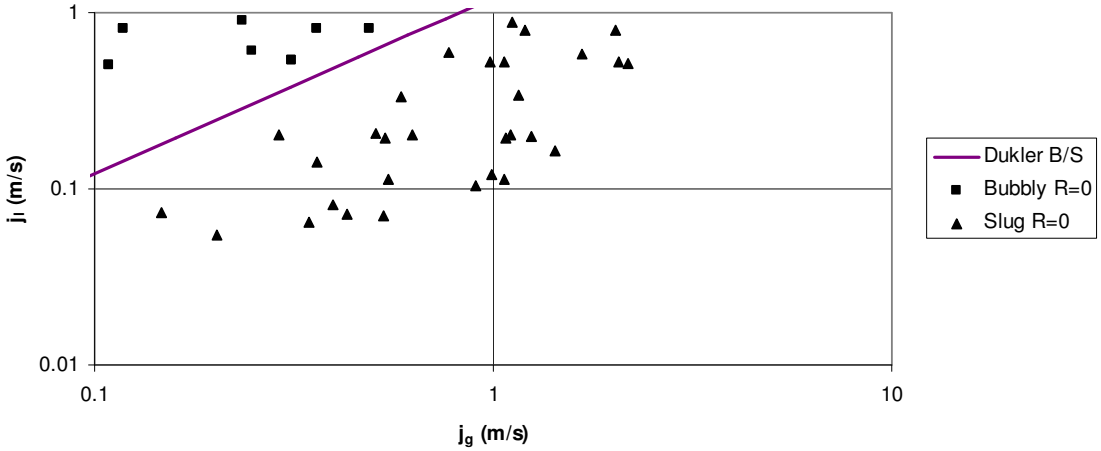

Figure 62: Squared Difference Comparison with ID=12.7mm and Dukler Model

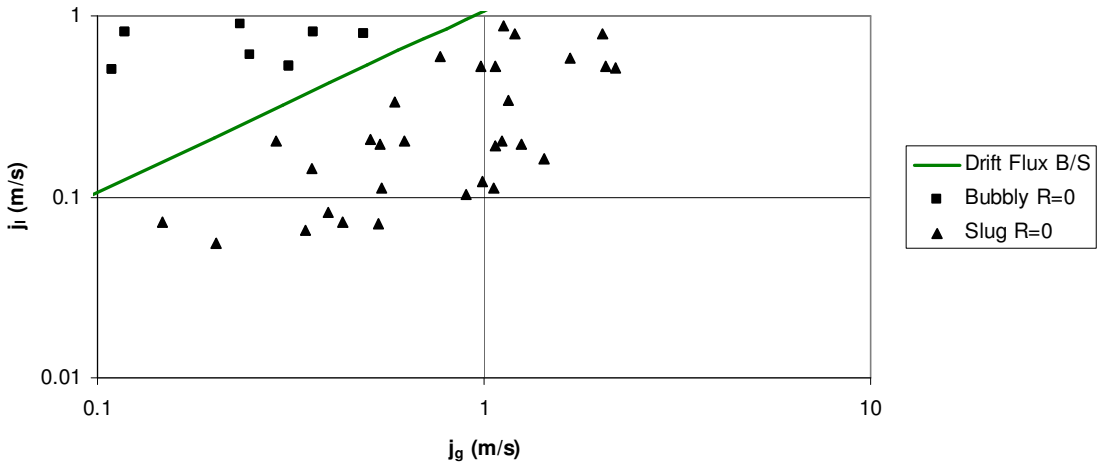

Figure 63: Squared Difference Comparison with ID=12.7mm and Drift Flux Model

The next bubbly-to-slug comparison made in this section will be for the inner diameter of 24.5 mm. The Creare model under predicts the bubbly-to-slug transition for the 25.4 mm diameter tube as shown in Figure 64. The higher squared differences appear above the predicted transition line. There are a total of four data points that were predicted to be bubbly flow by the Creare model when they were actually slug flow. There are not many data points in the bubbly flow regime for this diameter. More data points would be needed to definitively compare the models.

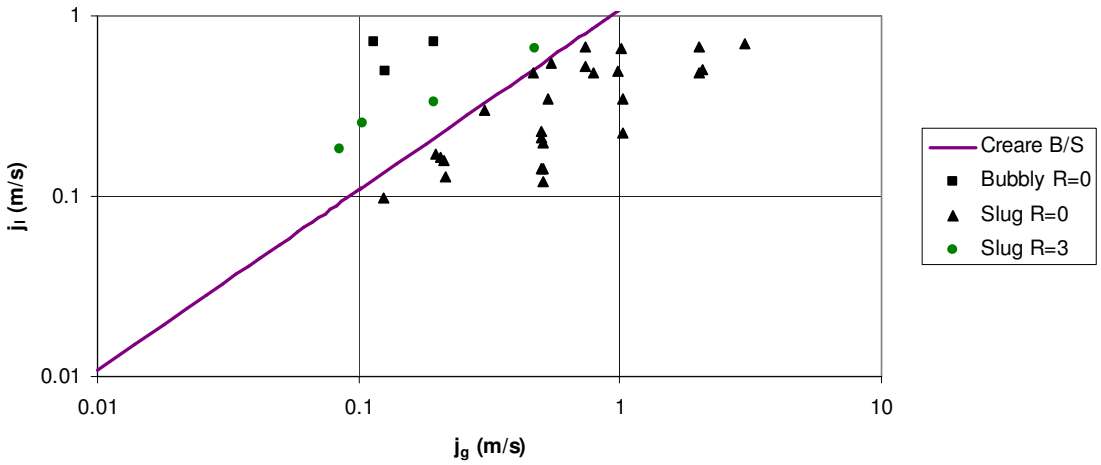

Figure 64: Squared Difference Comparison with ID=25.4mm and Creare Model

Figure 65 shows the squared difference comparison between Dukler's bubbly-to-slug model for 25.4 mm diameter and the 25.4 mm diameter data. From a visual inspection, there are four slug points that were incorrectly identified by the model to be bubbly flow. These four slug points were also misidentified in the Creare model discussed previously. More data points in this regime would be necessary to determine if the data points were misidentified in the experiment or if both models predict the transition too low.

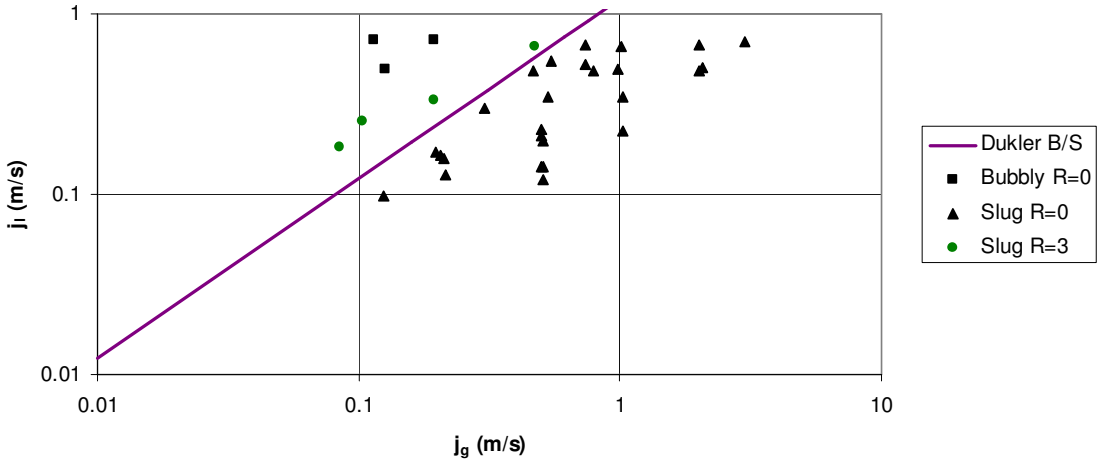

Figure 65: Squared Difference Comparison with ID=25.4 mm and Dukler Model

The Drift Flux model for an inner diameter of 25.4 mm matches the data very well. All bubbly flow and slug flow points are identified correctly by the Drift Flux model. The four data points incorrectly identified in the previous two models have been correctly identified by the Drift Flux model. Because all three models did not miss these data points, it is likely that the data points are correct and that the Creare and Dukler models predicted the transition incorrectly for this diameter tubing. This is shown in Figure 66.

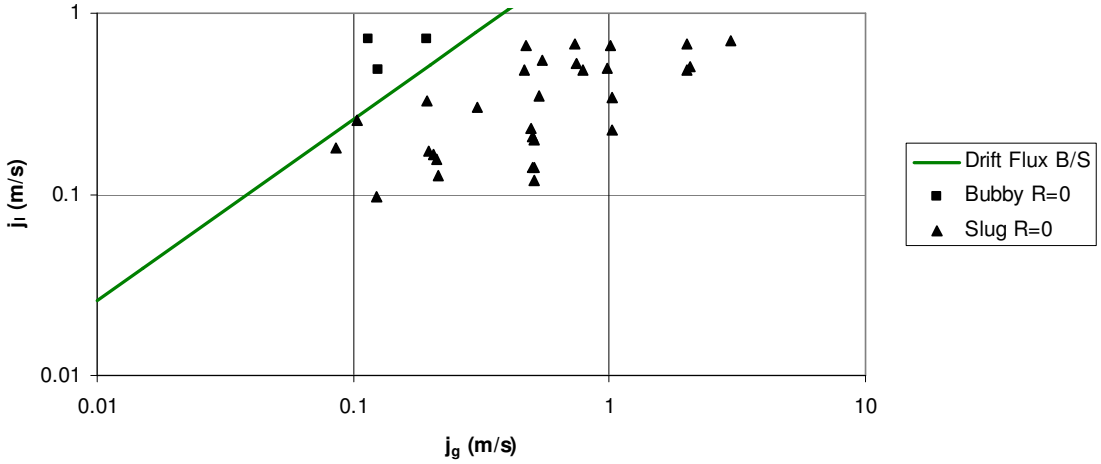

Figure 66: Squared Difference Comparison ID=25.4 mm and Drift Flux model

The comparison for the 40mm inner diameter tube will have uncertainty introduced into it because of the uncertainty in the data that was discussed in chapter III. The Creare model for bubbly-to-slug transition for the large 40 mm inner diameter test section again appears to under predict the actual transition. While some of the data in Figure 67 may be inaccurate due to acceleration effects, the overall picture from the data shows a fairly clear transition. The model correctly predicts the entire bubbly flow regime but incorrectly places the majority of the slug points.

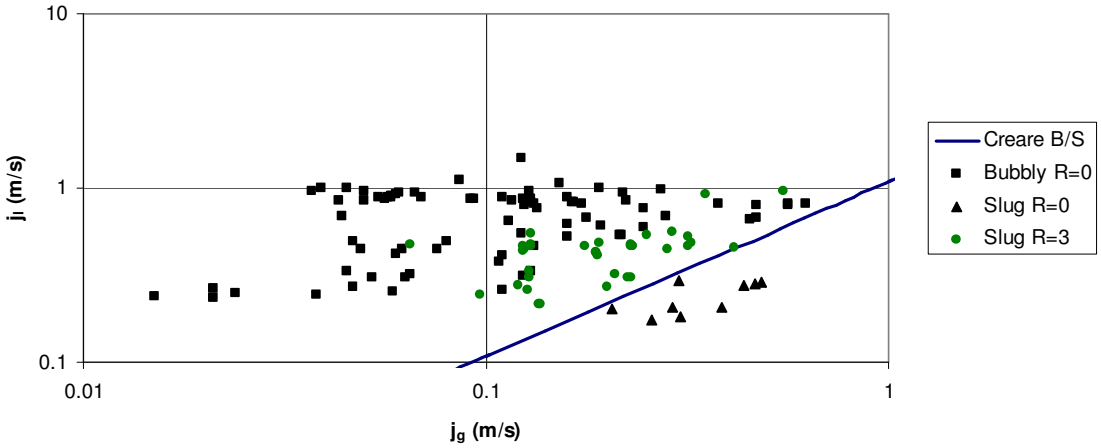

Figure 67: Squared Difference Comparison ID=40mm and Creare Model

The Dukler model for bubbly-to-slug flow transition shown in Figure 68 does not model the case of 40 mm diameter as well as it does with the smaller diameter tubes. There are numerous slug flow data points that the model predicts to be bubbly flow. However as mentioned previously, the data shows inconsistencies associated with acceleration effects. Taking those inconsistencies into account, the Dukler model may be more accurate than it appears visually.

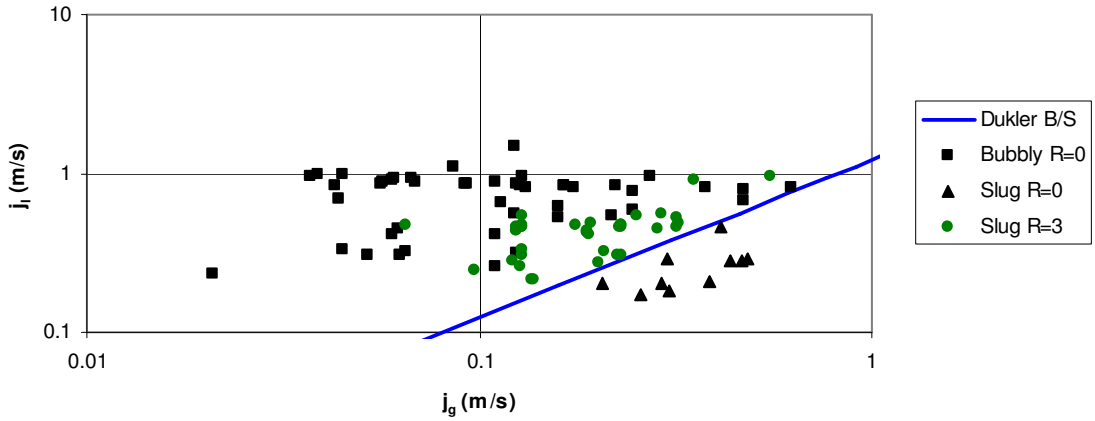

Figure 68: Squared Difference Comparison with ID=40mm and Dukler Model

The Drift Flux model shown in Figure 69 predicts the data points for the 40 mm diameter tube slightly better than the previous two models discussed. The transition occurs at a higher liquid superficial velocity than the others so many more of the slug data points are correctly identified. There are some misidentified bubbly flow data points with this model which did not appear in the previous two models, however there aren't as many overall squared difference values greater than zero as with the Drift Flux model.

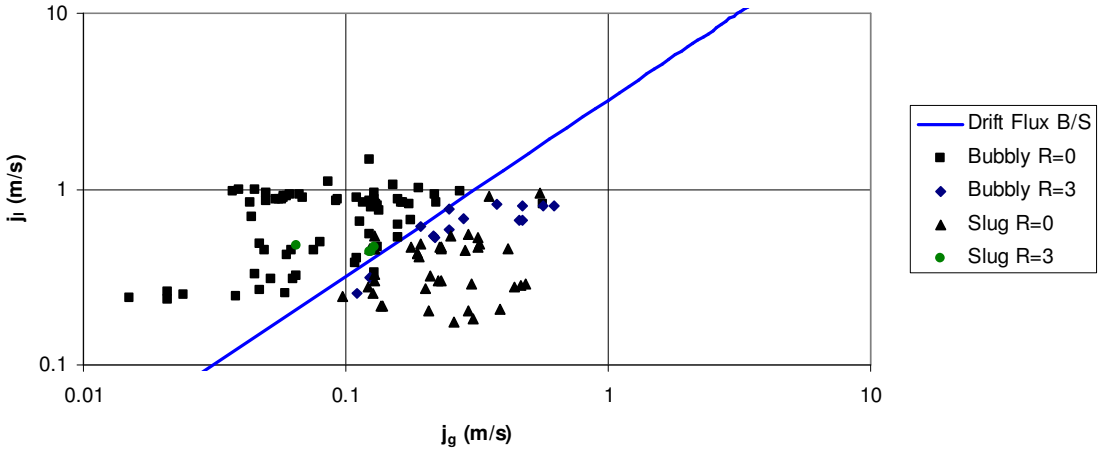

Figure 69: Squared Difference Comparison ID=40mm and Drift Flux model

6.4.2 Slug-to-Annular Squared Difference Results

The same approach is used for the slug-to-annular flow regime transition as in the previous section with the bubbly-to-slug flow regime transition. Figure 70 shows the squared difference results for Bousman's slug-to-annular transition compared with the data for the inner diameter of 9.525mm. Bousman's model correctly predicts all slug data points and all annular data points. There is a large gap present for the transition region which the Bousman model seems to split down the middle. The Creare Model shown in Figure 71 compares similarly to the Bousman model shown previously by predicting correctly all of the slug data points and all of the annular data points. These two models have a similar shape to them as an upward diagonal transition line from lower superficial velocity to high superficial velocity.

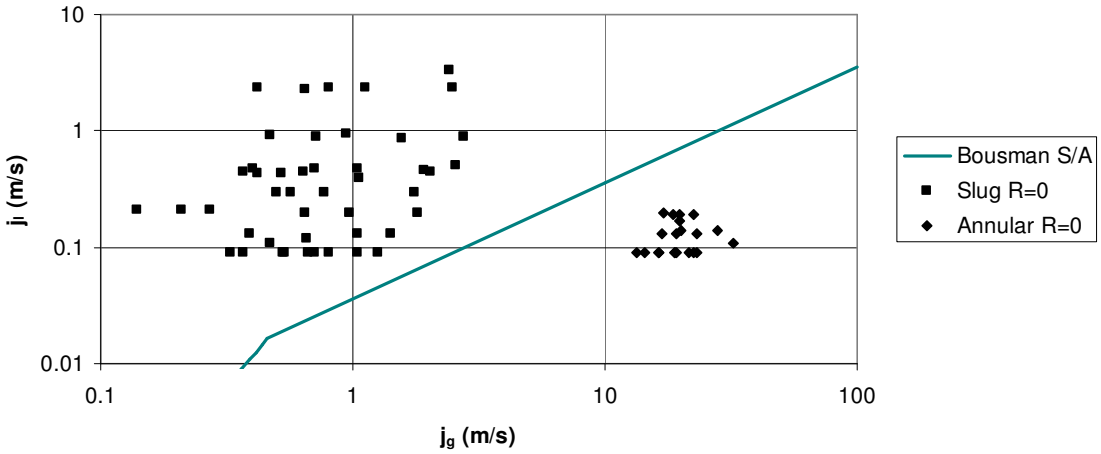

Figure 70: Squared Difference Comparison ID=9.525mm and Bousman Model

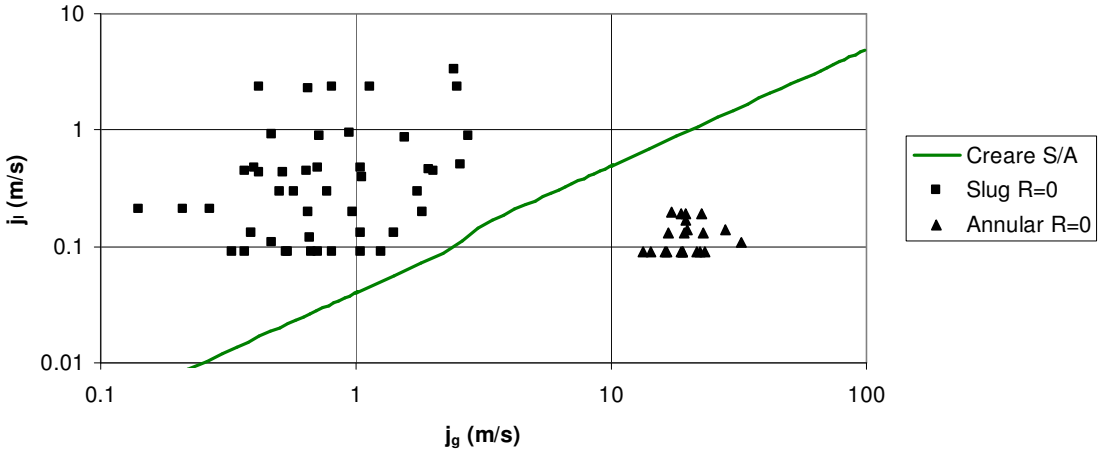

Figure 71: Squared Difference Comparison ID=9.525mm and Creare Model

The next two models are also similar to each other. Lee's transition model illustrated in Figure 72 and Reinarts transition model in Figure 73 have very similar shapes. This of course is expected because Reinarts' model is built from Lee's model. Furthermore, it would be expected for Reinarts' model to have fewer high squared difference data points than Lee's. In Lee's model for this diameter, there are five slug points that are identified to be annular flow. The location of these misidentified data

points are in a region distant to the identified annular points at higher liquid superficial velocities and lower gas superficial velocities. Reinarts' model is an improvement over Lee's model in that only 2 data points are mislabeled as annular points. These two data points are relatively close to the transition line but are again far away from the identified annular point cluster located at the higher gas superficial velocity and lower liquid superficial velocity.

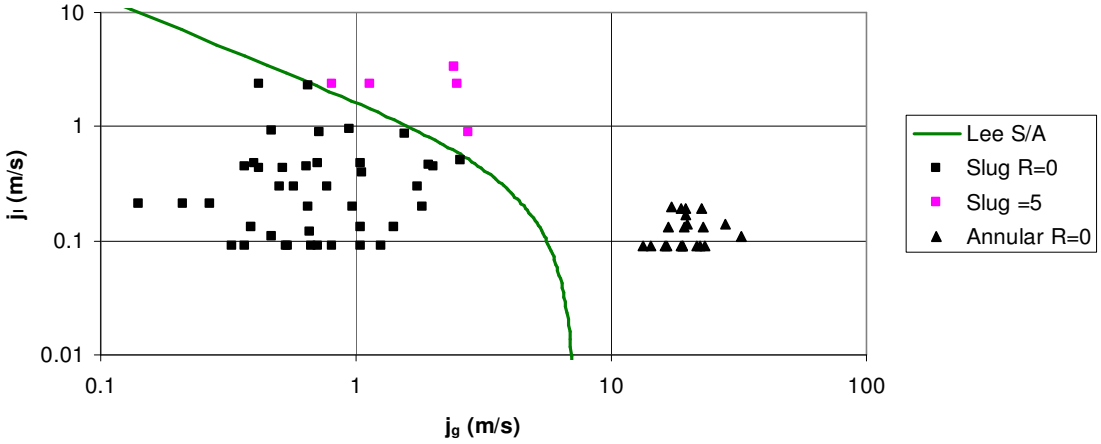

Figure 72: Squared Difference Comparison ID=9.525mm and Lee Model

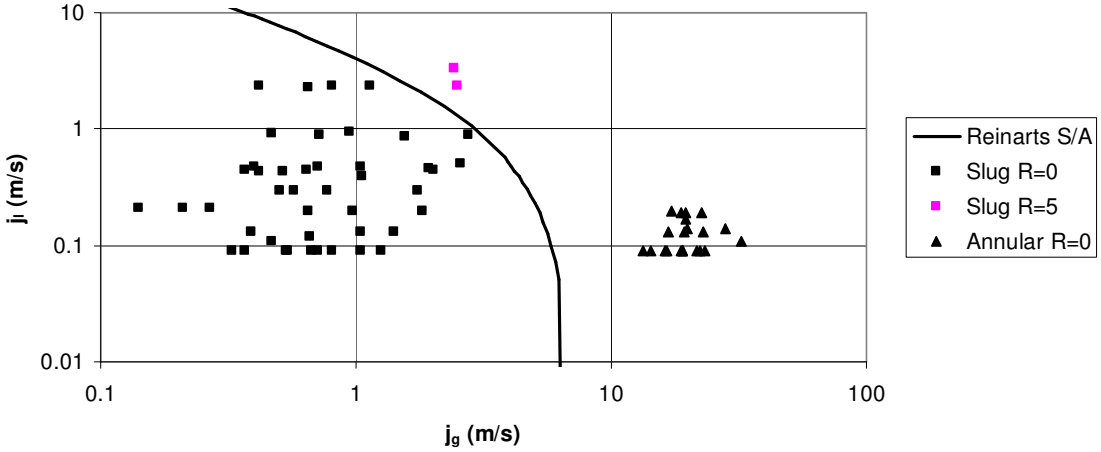

Figure 73: Squared Difference Comparison ID=9.525mm and Reinarts' Model

Figure 74 shows Bousman's model with the 12.7mm diameter data. The transition line seems to follow the general division between the slug regime data points and the annular regime data points but cuts off a group of annular points. There are seven points along the border of the annular flow data points that Bousman's model misidentifies as slug data points. Figure 75 shows a similar pattern for the Creare model with the 12.7mm diameter test data. However, the Creare model does not cut off as many data points. There are a total of five closely clustered annular data points that the model labels as slug flow.

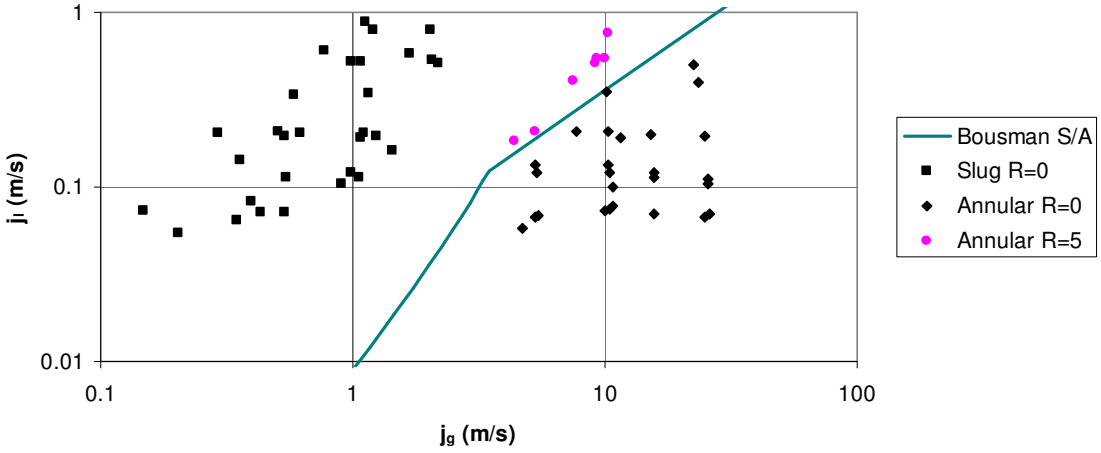

Figure 74: Squared Difference Comparison ID=12.7mm and Bousman Model

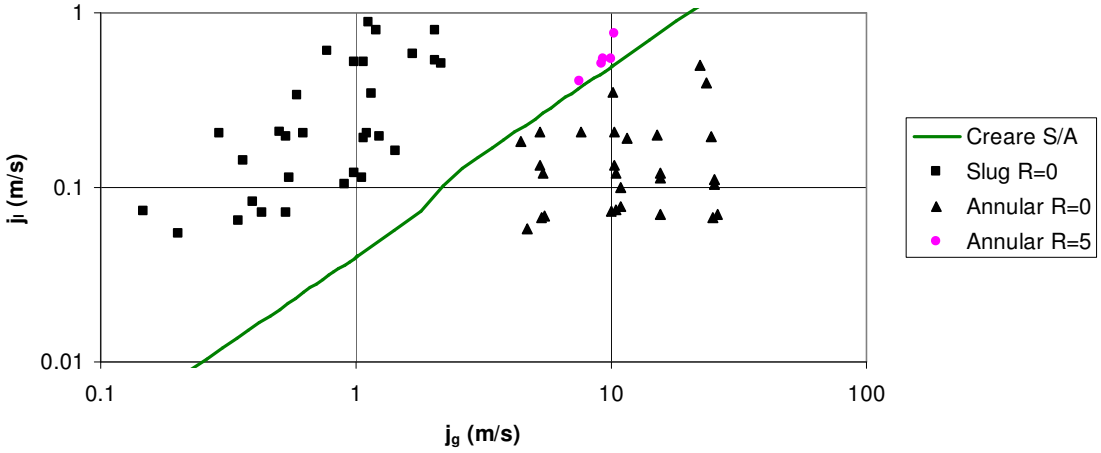

Figure 75: Squared Difference Comparison ID=12.7mm and Creare Model

Both Lee's and Reinarts' models for the 12.7 mm data are similar to each other. Figure 76 shows Lee's model for the slug-to-annular transition. There are three points in the upper right-hand corner of the slug regime that the transition line cuts off into the model's annular region. There is one annular point in the lower left-hand corner of the annular flow regime that is misidentified as a slug flow point. In Reinarts' model shown in Figure 77, the slug flow points are correctly identified. This is a result of varying the radius of the slug bubble nose. However, the same annular point is misidentified as a slug point.

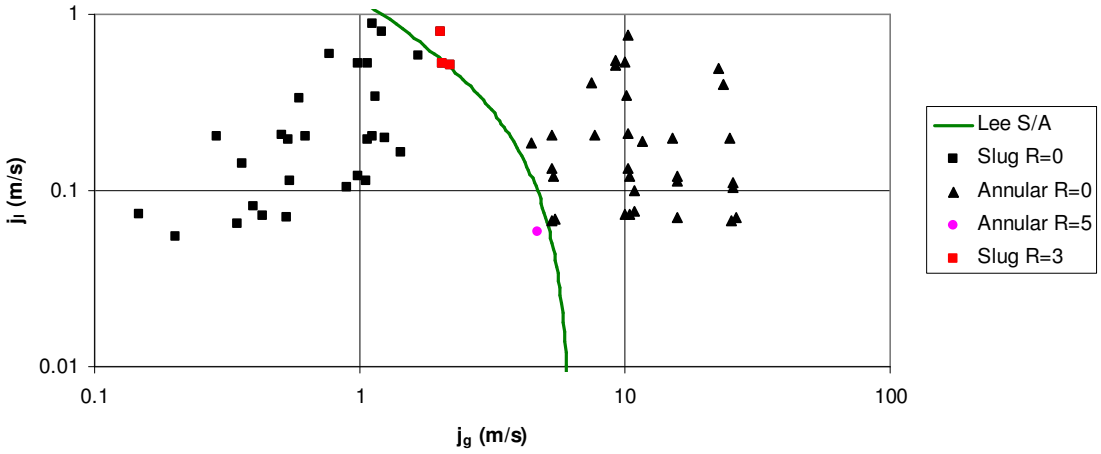

Figure 76: Squared Difference Comparison ID=12.7mm and Lee Model

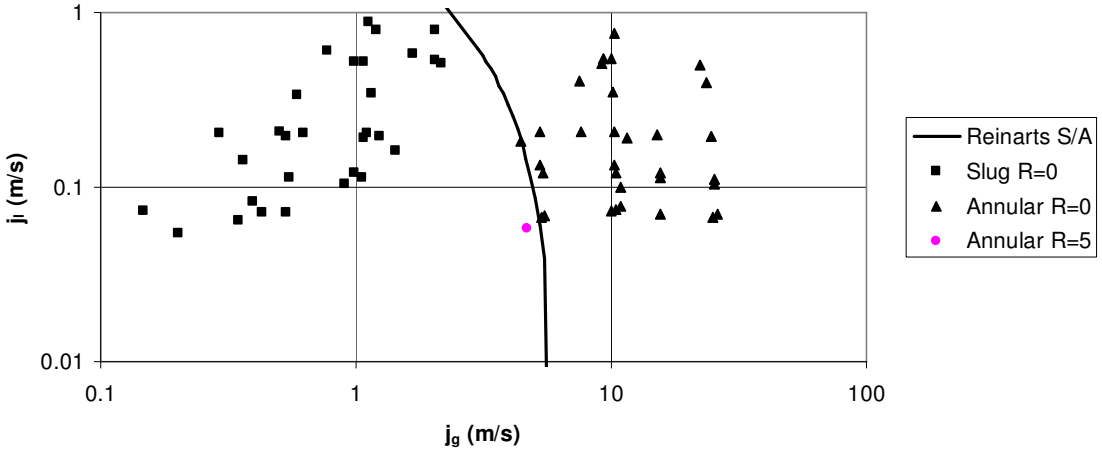

Figure 77: Squared Difference Comparison ID=12.7mm and Reinarts' Model

The last comparison made in this section is the four slug-to-annular transition models at 24.5 mm diameter. The Bousman model shown in Figure 78 seems to get worse as the diameter of the tube increases. The model was perfect in predicting all the slug and annular points in the 9.525 mm diameter, incorrectly identified 7 data points in the 12.7 mm diameter, and now has incorrectly identified 11 annular data points. The distance between the slug and annular regimes is much less in this instance than in the previous two diameters so more data would be needed to validate a conclusion on the accuracy of the data points. However, based on the data it appears that Bousman's model is more accurate at flow regime mapping in smaller diameter tubing. The Creare model shown in Figure 79 incorrectly identifies 5 annular data points in the same general region as the Bousman model.

Figure 80 shows Lee's model for the 24.5 mm diameter tubing. The model cuts through 5 slug points while Reinarts' model for the 24.5 mm shown in Figure 81 intersects two of the same points and incorrectly indentifies two of the same points.

Therefore Reinarts' model improved over Lee's model by one data point in this case. Reinarts' model has the least non zero squared difference values on this diameter.

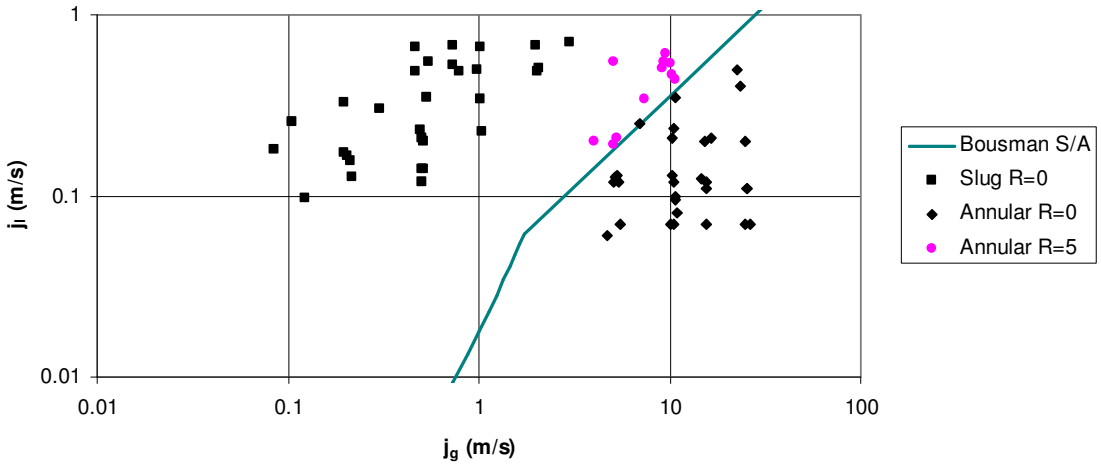

Figure 78: Squared Difference Comparison ID=25.4mm and Bousman Model

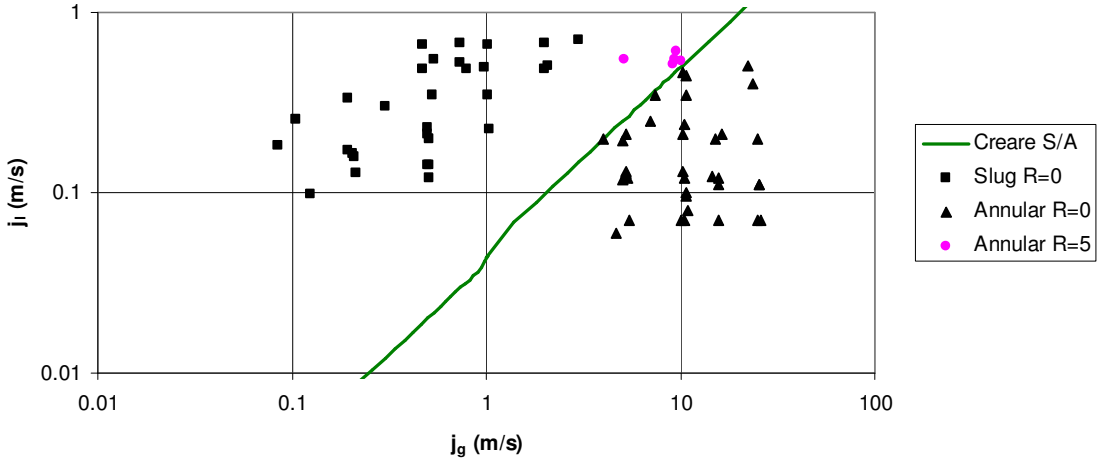

Figure 79: Squared Difference Comparison ID=25.4mm and Creare Model

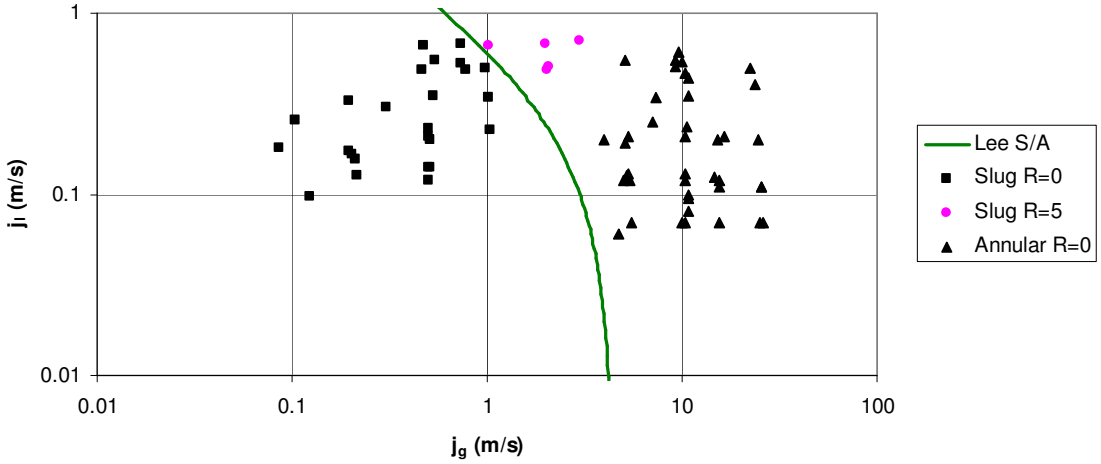

Figure 80: Squared Difference Comparison ID=25.4mm and Lee Model

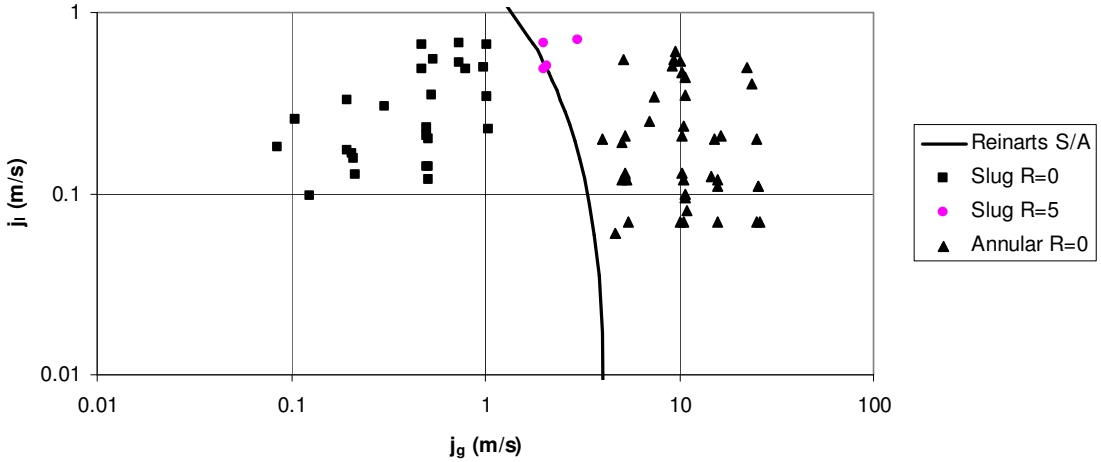

Figure 81: Squared Difference Comparison ID=25.4mm and Reinarts' Model

6.5 Bubbly-to-Slug Summary

Table 10 gives a summary of the quantities of each squared difference value for the Creare, Dukler, and Drift Flux models respectively. This table provides a quick reference for the previous section. The models can be compared by diameter by reading down each column directly underneath the diameter size.

Table 10: Bubbly-to-Slug Squared Difference Results

	Creare B/S							
R	**9.525**		**12.7**		**24.5**		**40**	
	B	**S**	**B**	**S**	**B**	**S**	**B**	**S**
0	6	36	12	30	3	26	82	9
3	0	10	0	0	0	4	0	37
	Dukler B/S							
	9.525		**12.7**		**25.4**		**40**	
	B	**S**	**B**	**S**	**B**	**S**	**B**	**S**
0	6	39	12	30	3	26	82	10
3	0	7	0	0	0	4	0	36
	Drift Flux B/S							
	9.525		**12.7**		**25.4**		**40**	
	B	**S**	**B**	**S**	**B**	**S**	**B**	**S**
0	6	29	12	30	3	30	68	42
3	0	17	0	0	0	0	14	4

Using the results from the above table, it is still unclear which model more accurately describes the data for each test section. For the 9.525 mm diameter it is clear that the drift flux model does not compare to the Creare model or the Dukler model for this diameter. However, the Creare and Dukler models are very similar. In order to compare the models with the results outlined in the table, a grade is given to each model. This grade is calculated through Equation 103 where the quantity of each squared difference result, $(N_1,N_2,\ldots N_n)$, is multiplied by the value of the squared difference, $(R_1,R_2,\ldots R_n)$ and then summed together. These results are shown in Table 11. The first number shown is the grade result from Equation 103 and the number in brackets is the percentage of data points correctly identified by the model. Therefore the model with the lowest grade and the highest percentage is the model that best fits the data.

$$\sigma_{SD} = \sum_{1}^{n} \left[R_1 N_1 + R_2 N_2 + ... R_n N_n \right]$$

Equation 103

Table 11: Bubbly to Slug Results

Model	9.525 mm	12.7 mm	24.5 mm	40 mm
Creare	30 [80.77]	0 [100]	12 [87.87]	111 [71.1]
Dukler	21 [86.5]	0 [100]	12 [87.87]	108 [71.8]
Drift Flux	51 [67.3]	0 [100]	0 [100]	54 [85.9]

For the 9.525mm diameter, the Dukler model has the lowest grade of the three models and correctly predicted 86.5% of the data points, therefore this is the model that best predicts the 9.525 mm data according to this grading system. The drift flux model is the worst at the smallest diameter but improves at the higher diameters. For the 12.7 mm diameter, all three models tie with a perfect score. The Drift Flux model again has a perfect score for the 24.5 mm diameter and also has the lowest score by at least 50% lower than the other two models and correctly identifies 14% more data points. The bubbly-to-slug results show that the larger diameter tubing is best modeled by the drift flux model. The lower diameter tubing is better modeled by the Dukler model.

6.6 Slug-to-Annular Summary

Table 12 shows the results for the slug-to-annular squared difference grading system. The numbers in the table are the quantities of each squared difference, R, value shown to the left of the table. This table is meant to provide a quick reference for a

previous section where these results were shown on plots. The models can be compared by diameter by comparing down the columns beneath the respective diameter size.

Table 12: Slug to Annular Squared Difference Results

	Creare S/A					
R	**9.525**		**12.7**		**25.4**	
	S	**A**	**S**	**A**	**S**	**A**
0	46	21	30	28	30	36
5	0	0	0	5	0	5
	Bousman S/A					
	9.525		**12.7**		**25.4**	
	S	**A**	**S**	**A**	**S**	**A**
0	46	21	30	26	30	30
5	0	0	0	7	0	11
	Lee S/A					
	9.525		**12.7**		**25.4**	
	S	**A**	**S**	**A**	**S**	**A**
0	41	21	27	32	25	41
5	5	0	3	1	5	0
	Reinarts S/A					
	9.525		**12.7**		**25.4**	
	S	**A**	**S**	**A**	**S**	**A**
0	44	21	30	32	26	41
5	2	0	0	1	4	0

Just as in the previous section, the grading scheme will be applied to the slug-to-annular results as well. In Table 13, the results of the grading system are outlined. The first number shown is the grade from Equation 103 followed by the percentage of correctly identified points in brackets. Therefore, the model with the lowest grade and the highest percentage is the model that is best suited for that diameter. The Creare and Bousman models both have a perfect score identifying correctly all of the data points followed closely by Reinarts' model with a score of 10 and identifying 97.01% of the

data points correctly. Reinarts' model best fits the data for both the 12.7mm and the 24.5 mm diameters as evidenced by the lowest scores and highest percentages.

Table 13: Slug to Annular Results

Model	9.525 mm	12.7 mm	24.5 mm
Creare	0 [100]	25 [92.06]	25 [92.95]
Bousman	0 [100]	35 [88.88]	55 [84.5]
Lee	25 [92.53]	20 [93.65]	25 [92.95]
Reinarts	10 [97.01]	5 [98.41]	20 [94.36]

6.7 Random Even Point Distribution

The previous section compared the different models with each other using a grading system based on squared differences. This section takes a closer look at each model highlighting its strengths and weaknesses. Previously the grading system was applied to all data points for each respective tube diameter. In each experiment the data points are not equally distributed between flow regimes. Some experiments contain more points of a certain flow regime or at higher or lower superficial velocities. This makes analyzing the models a little more difficult due to the bias introduced. Due to experimental or flight restrictions, certain flow rates may be easier for the researcher to collect. For example, in larger tube diameters, the steady state flow rates required for annular flow are difficult to produce in limited airplane space. The minimum length to diameter ratio for steady state should be 20. Larger tube diameters would require more space than is available on a typical airplane. In the 12.7 mm diameter data points there are only a few bubbly points.

Most of the data collected was in the slug or annular flow regimes. When analyzing the bubbly-to-slug flow regime transition models, a bias is introduced by having many more slug points than bubbly points. This bias in data also results in a bias in the modeling efforts. An efficient flow regime model must be validated at a large range of flow velocities. If the majority of data points used in the validation occur in one small area while other areas are empty, the model cannot be fully validated at these empty regions. Therefore in an attempt to improve on this problem, an equal distribution is applied to each tube diameter so that the number of data points in each flow regime is equal. The points are chosen randomly by assigning each data point in the underrepresented flow regime 500 random numbers, taking an average of the 500 random numbers, sorting the random numbers, and then choosing the lowest number of data points needed. The lowest number of data points is determined by the available data points in each flow regime. For example, if there are 30 bubbly points and only 5 slug points, all 5 slug points will be used and 5 randomly selected bubbly points will be used. Once the data points are chosen, the same grading scheme outlined in the previous section is applied. While this does not fully correct the bias in the data, each flow regime is equally represented. Equally distributed points at flow rates throughout all regimes using a predetermined test matrix would be best for model validation and should be attained in future research.

6.7.1 Bubbly-to-Slug

The following section applies the even distribution to the bubbly and slug data points. For each model and each diameter, a plot is shown with the results of the even distribution. Logarithmic plots are commonly used for flow regime maps. However, a linear plot allows a different view of the data with the model and also allows for visual inspection of clumps of data points. Clumps of data points in one location show poor distribution of data and could skew the grading of the model. For this section, both types of plots will be shown to allow for further comparison.

6.7.1.1 Creare Bubbly-to-Slug

Figure 82 through Figure 89 show the Creare bubbly-to-slug transition models for the varying tube sizes. Because the data points are evenly distributed between flow regimes, the model can be graded by flow regime. In the 9.525 mm data shown in Figure 82, two slug points are misidentified while all of the bubbly data points are correct. The Creare model correctly identifies all of the data points for the 12.7 mm diameter shown in Figure 84, misses one slug point for the 24.5 mm diameter tube shown in Figure 86, and incorrectly identifies 37 slug points for the 40 mm diameter tube. The Creare model correctly identifies all of the bubbly data points for each case. This suggests that the model is not predicting the transition soon enough. The results from the model are similar for all diameters except for the 40mm data which is unreliable. This suggests that Creare has properly accounted for the effects of diameter in the model. Figure 83, Figure 85, Figure 87, and Figure 89 show each of the previous figures on a linear scale rather than a logarithmic scale. No clumping of data points is

apparent in these plots for the smaller diameter tubes. However due to the amount of slug points omitted during the even distribution, there could be clumping in this section. Figure 89 shows a clump of data points in the low superficial velocity region. The clumped region is circled. Because the data points are equal for each region (bubbly and slug), overlapping and clumped data points can skew the results when comparing the number of points the model incorrectly identifies.

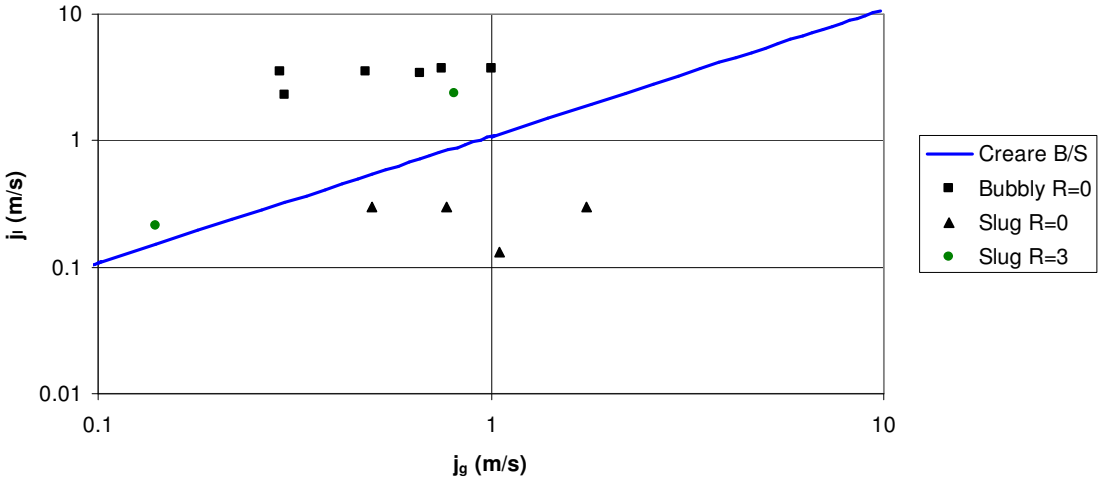

Figure 82: Creare Bubby-to-Slug 9.525mm

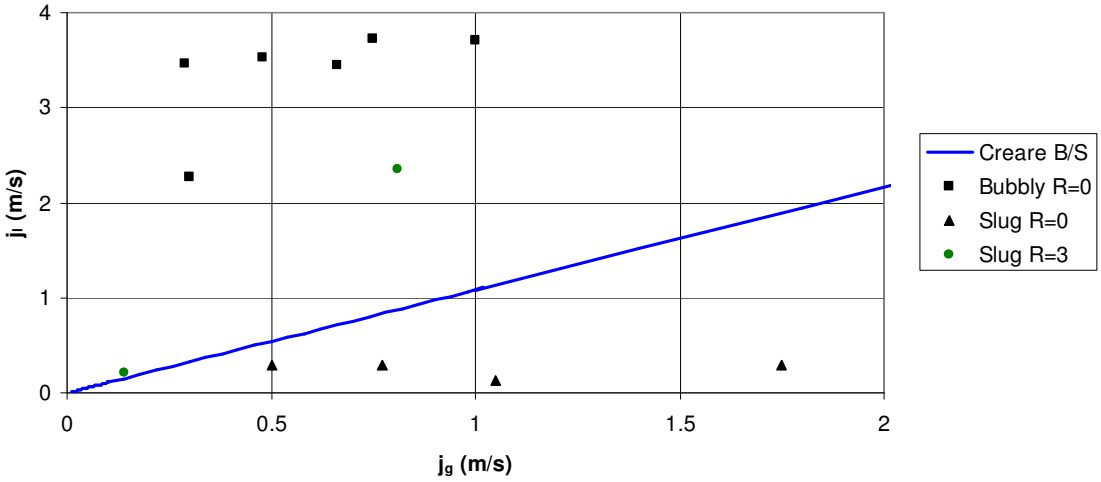

Figure 83: Creare Bubby-to-Slug 9.525mm linear

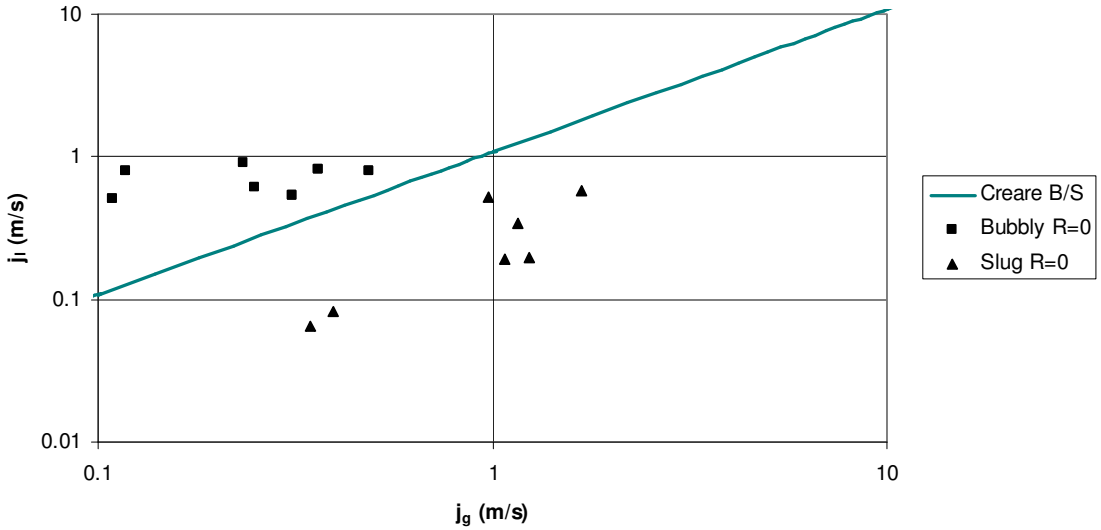

Figure 84: Creare Bubby-to-Slug 12.7mm

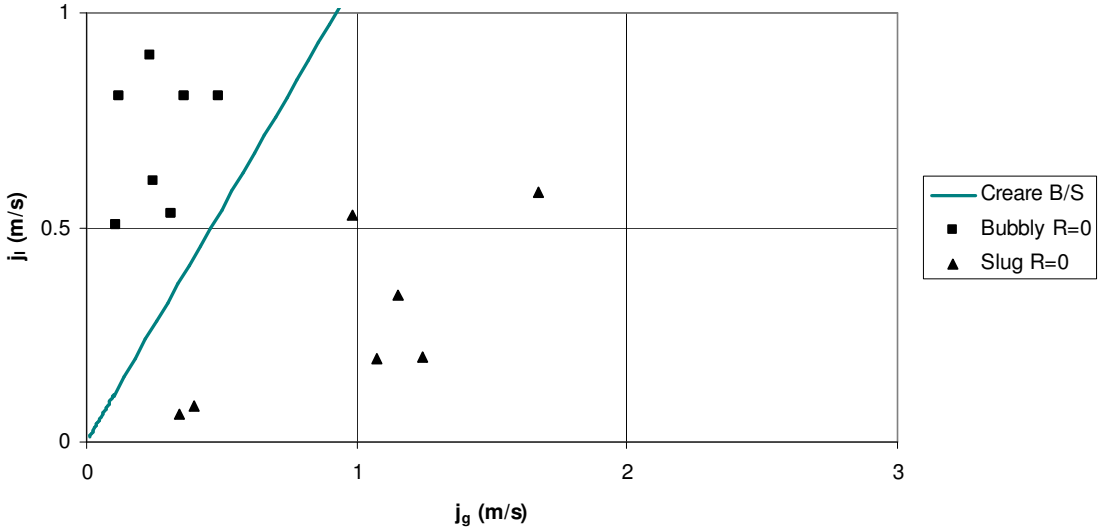

Figure 85: Creare Bubby-to-Slug 12.7mm Linear

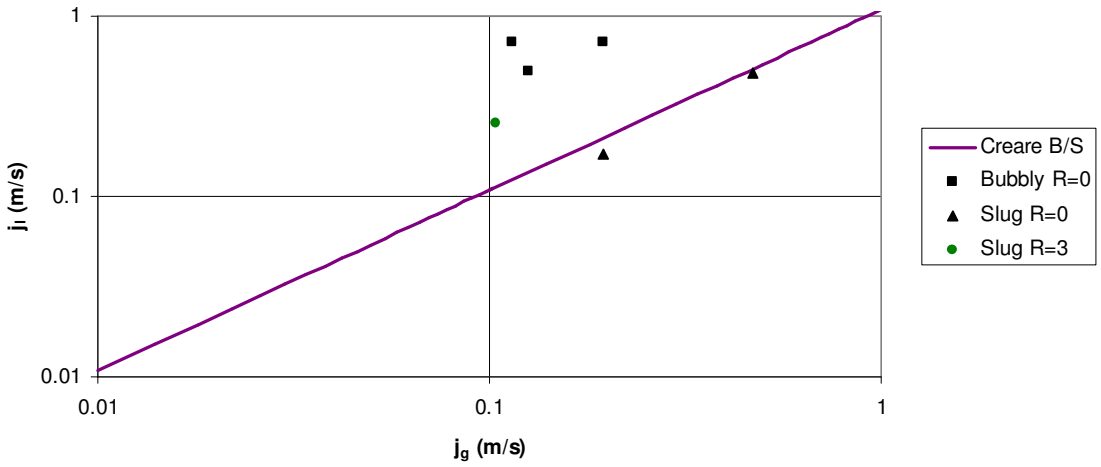

Figure 86: Creare Bubby-to-Slug 24.5mm

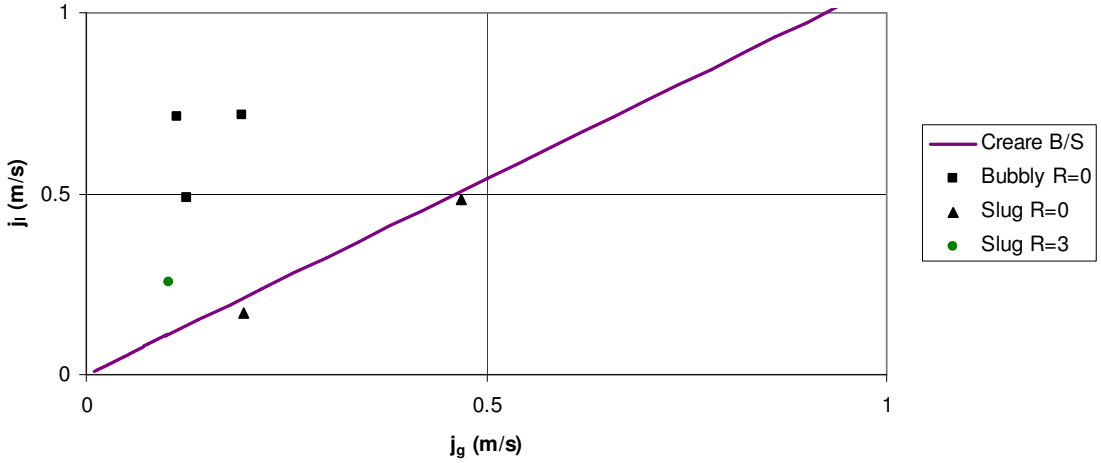

Figure 87: Creare Bubby-to-Slug 24.5 mm Linear

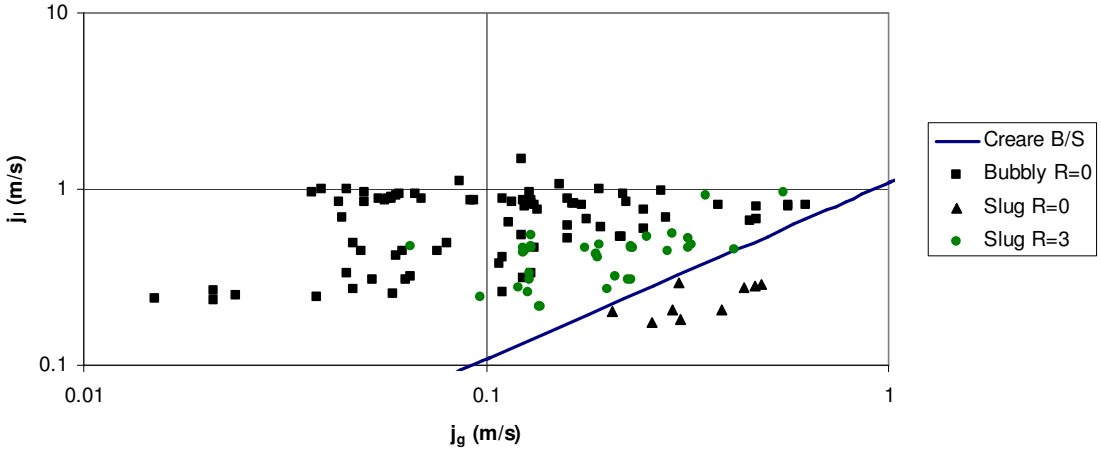

Figure 88: Creare Bubby-to-Slug 40mm

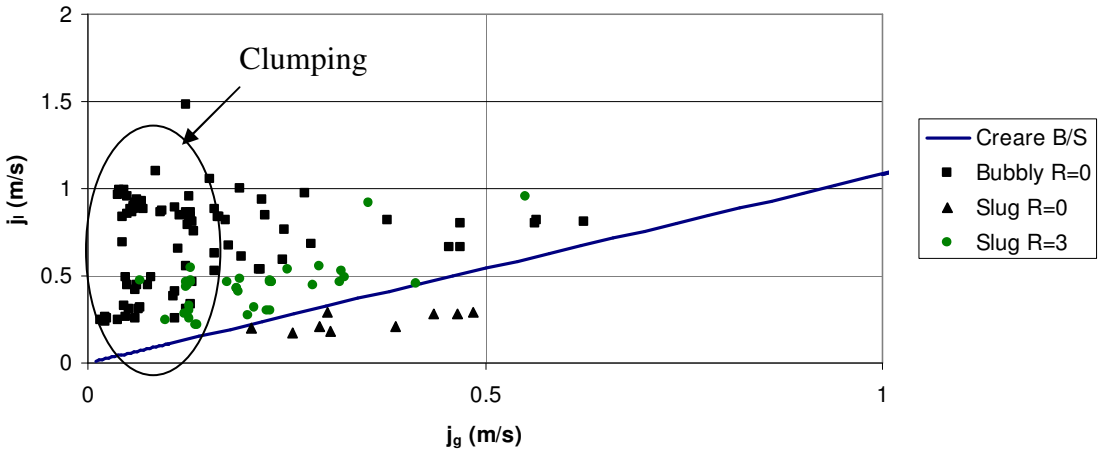

Figure 89: Creare Bubby-to-Slug 40mm Linear

6.7.1.2 Dukler Bubbly-to-Slug

Figure 90 through Figure 97 show the same data as the previous section compared with the Dukler bubbly-to-slug model. Dukler incorrectly identifies one slug data point in the 9.525 mm data and 36 slug points in the 40 mm data. The rest of the data points are correctly identified with the Dukler model. The same condition exists with the 40 mm clumped data shown in Figure 97. The data points that are incorrect according to the Dukler model are either inside the clumped region or fairly close to the

transition line. As pointed out previously, these data points were collected in non-ideal conditions and may not be as accurate as the smaller diameter data.

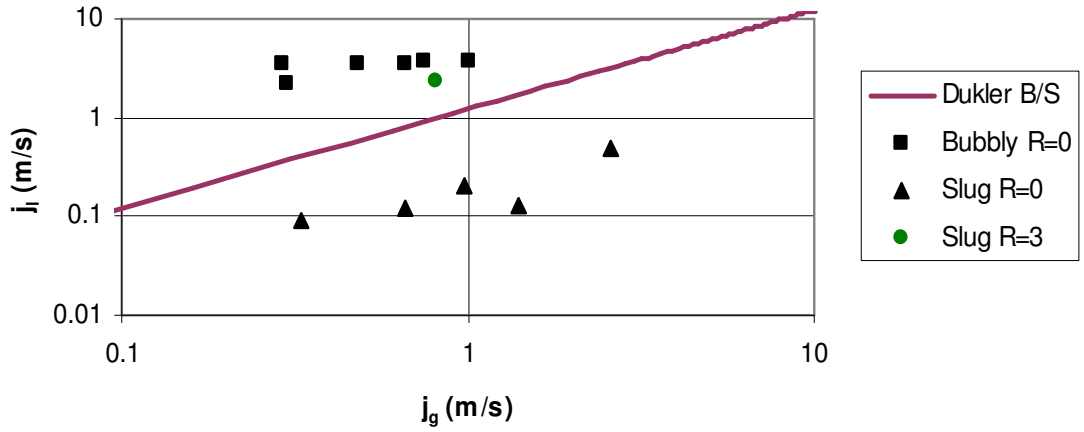

Figure 90: Dukler 9.525mm

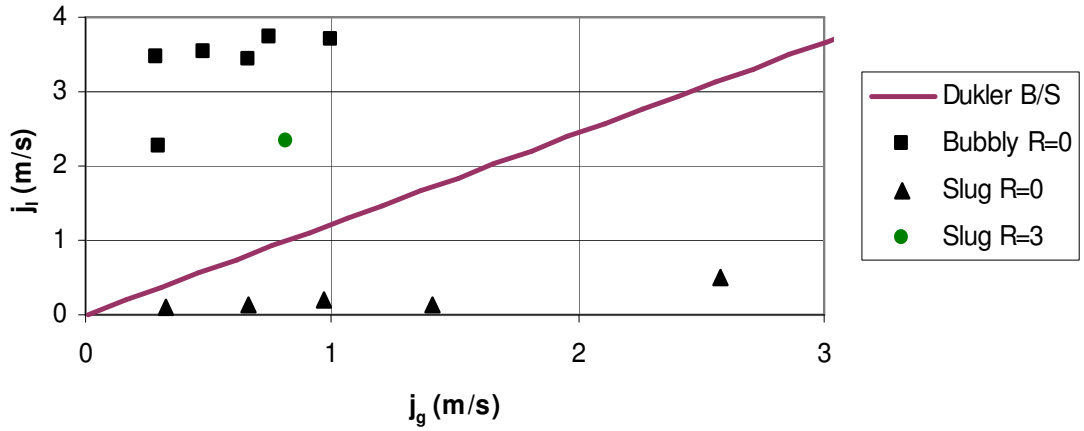

Figure 91: Dukler 9.525mm Linear

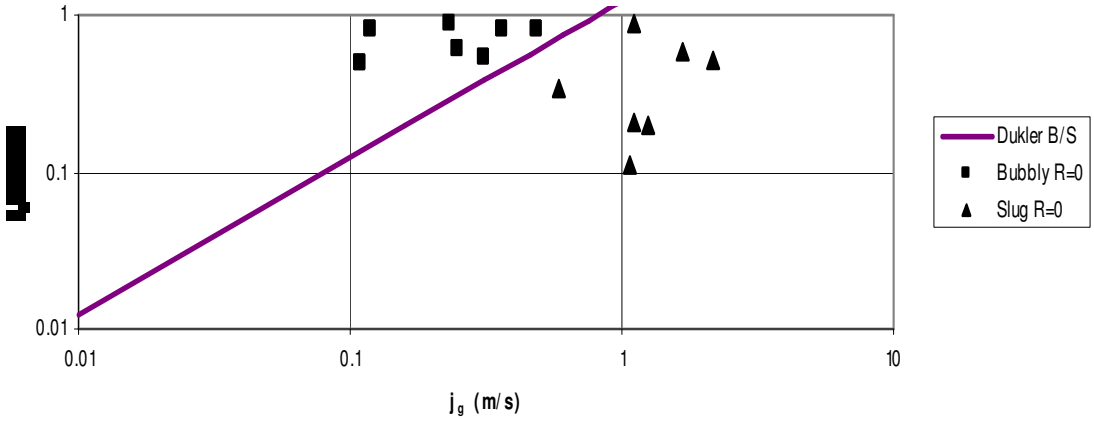

Figure 92: Dukler 12.7 mm

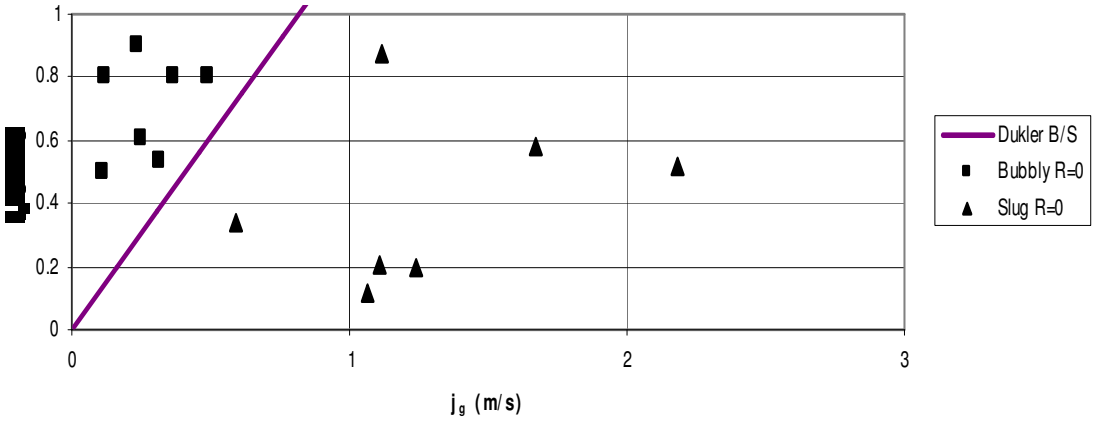

Figure 93: Dukler 12.7mm Linear

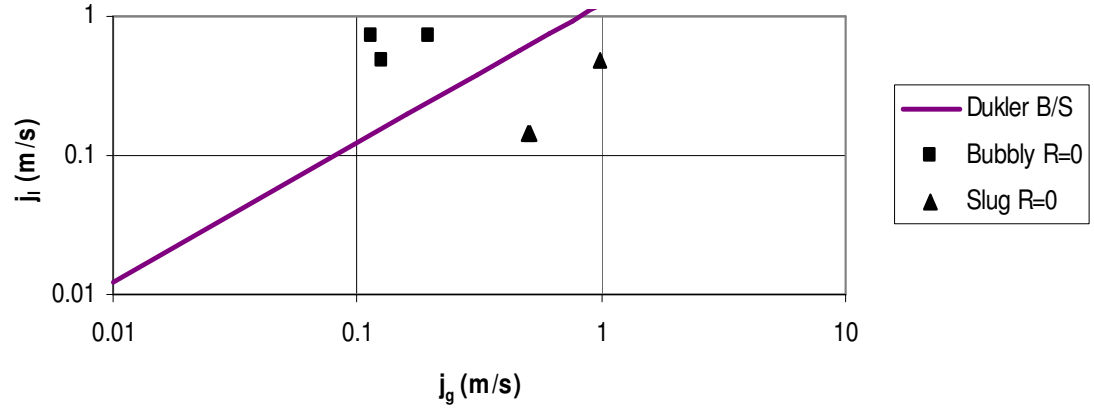

Figure 94: Dukler 24.5mm

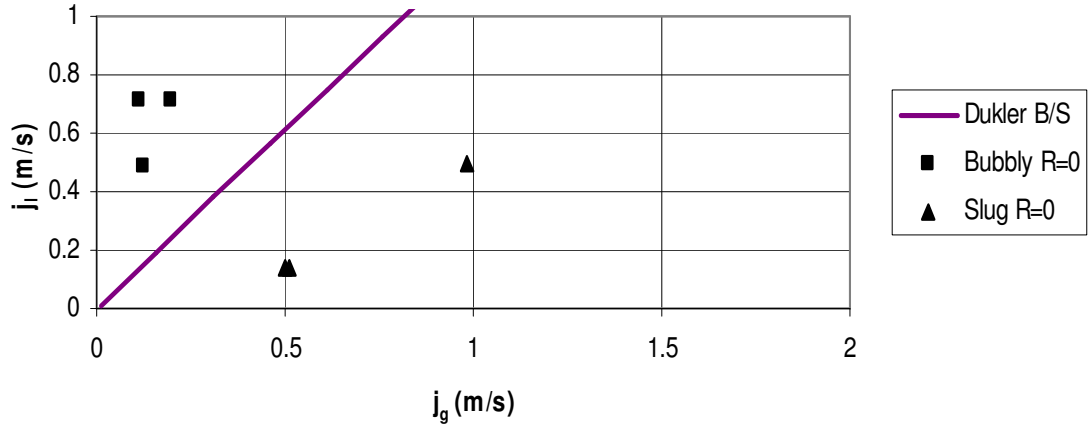

Figure 95: Dukler 24.5mm Linear

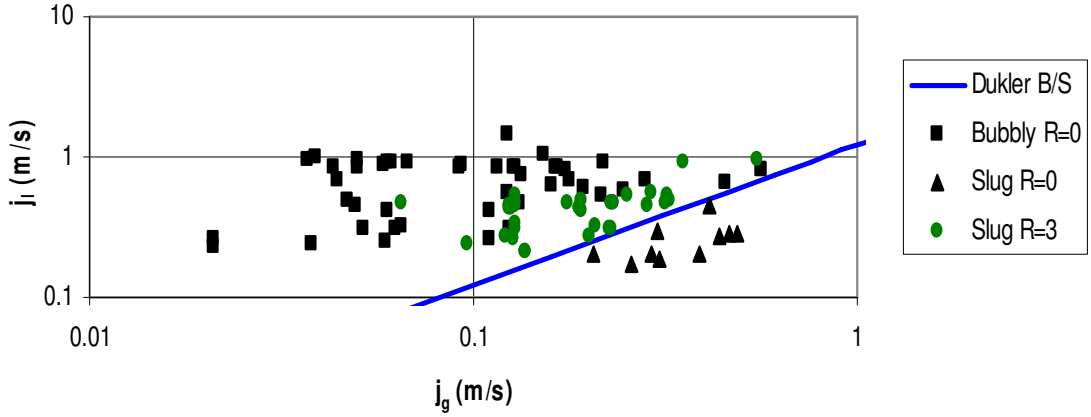

Figure 96: Dukler 40mm

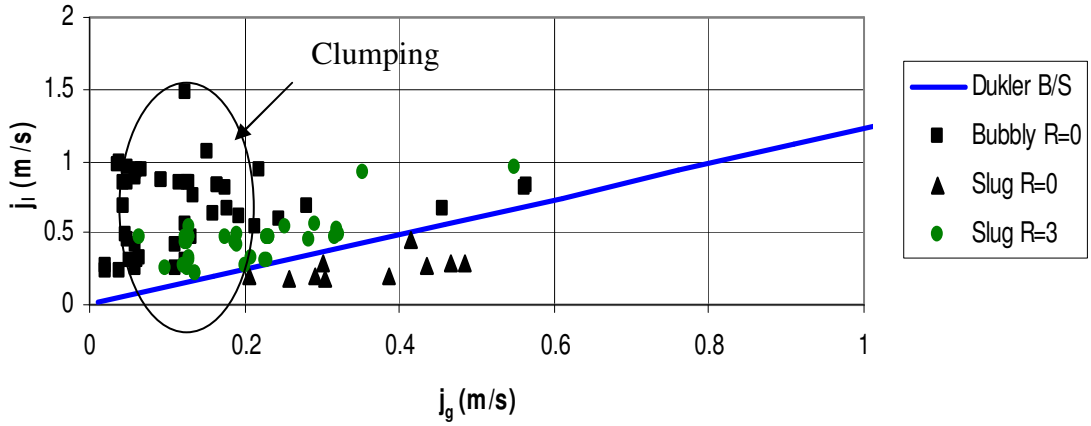

Figure 97: Dukler 40mm Linear

6.7.1.3 Drift Flux Bubbly-to-Slug

Figure 98 through Figure 105 show the Drift Flux model with evenly distributed flow regime data points for each diameter. The Drift Flux model misses two slug points in the 9.525 mm data and in the 40 mm data the model misses three slug points and eight bubbly points. This is the only model that is not affected much by the clumped data points in the 40 mm experiment. The Drift Flux model fits the larger diameter data better than the previous two models. The number of data points identified incorrectly by the drift flux model balance better between the bubbly and slug points than the previous two models. This suggests that the drift flux model more correctly predicts the transition from bubbly flow to slug flow than the other models. However because of the low confidence in the accuracy of the data, this statement cannot be said with much assurance. More data collection would be necessary to validate this assumption.

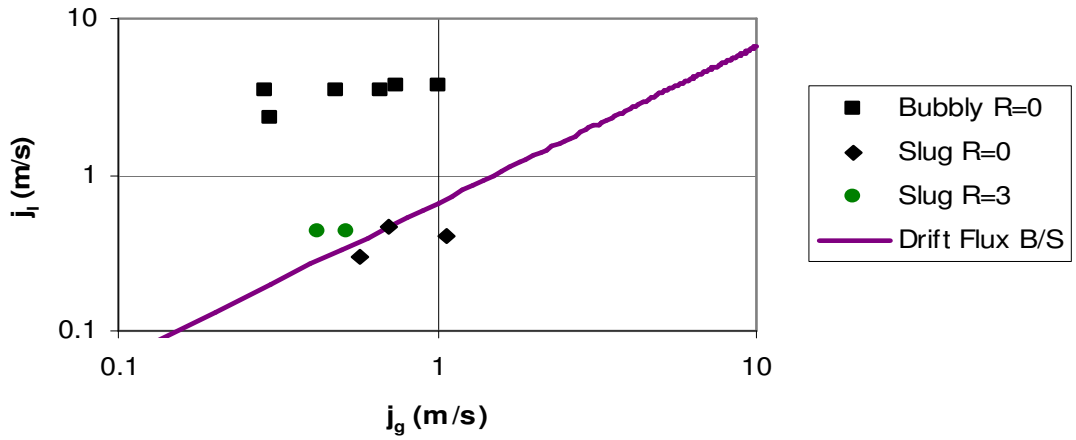

Figure 98: Drift Flux 9.525mm

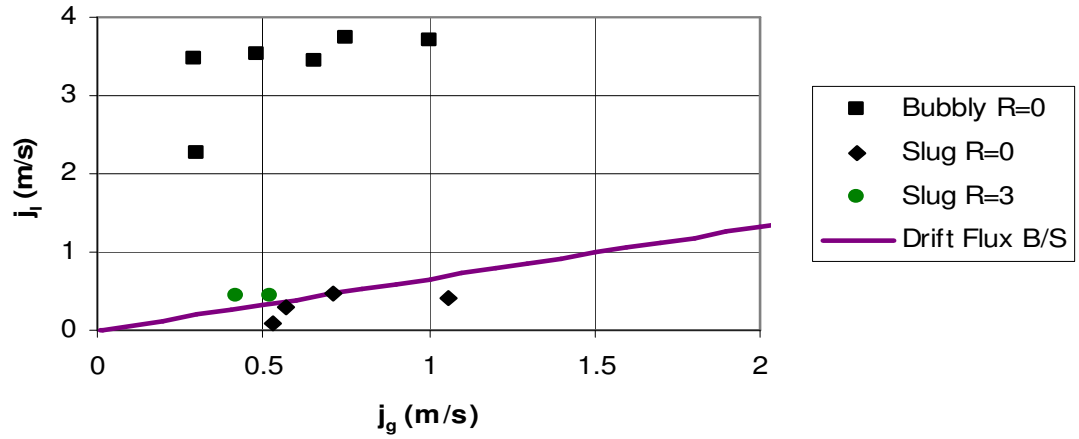

Figure 99: Drift Flux 9.525mm Linear

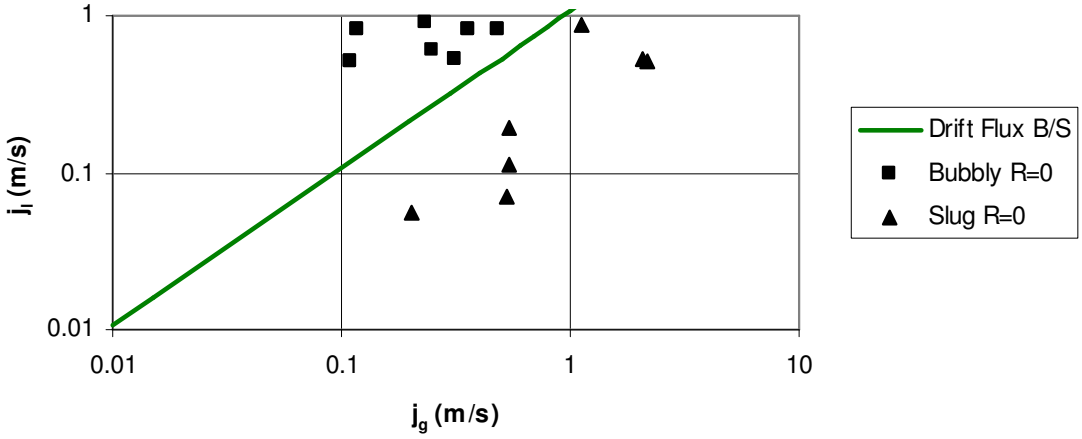

Figure 100: Drift Flux 12.7mm

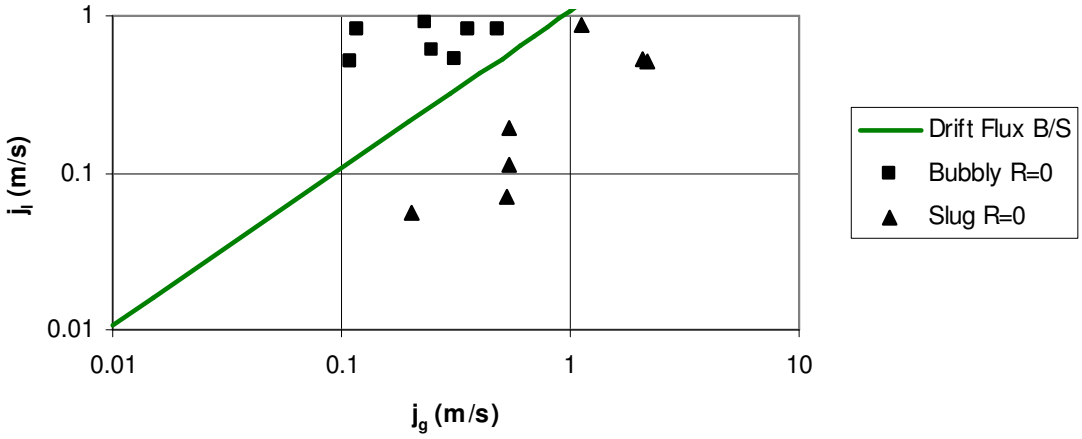

Figure 101: Drift Flux 12.7mm Linear

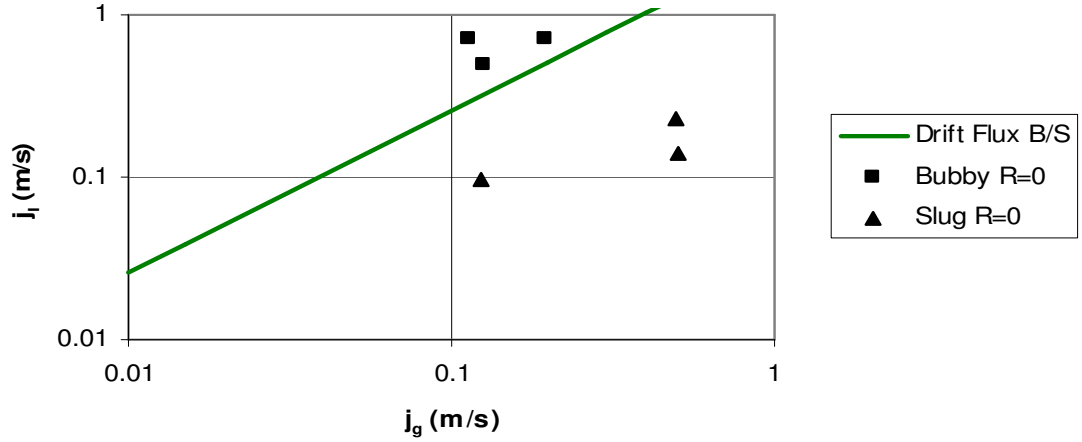

Figure 102: Drift Flux 24.5mm

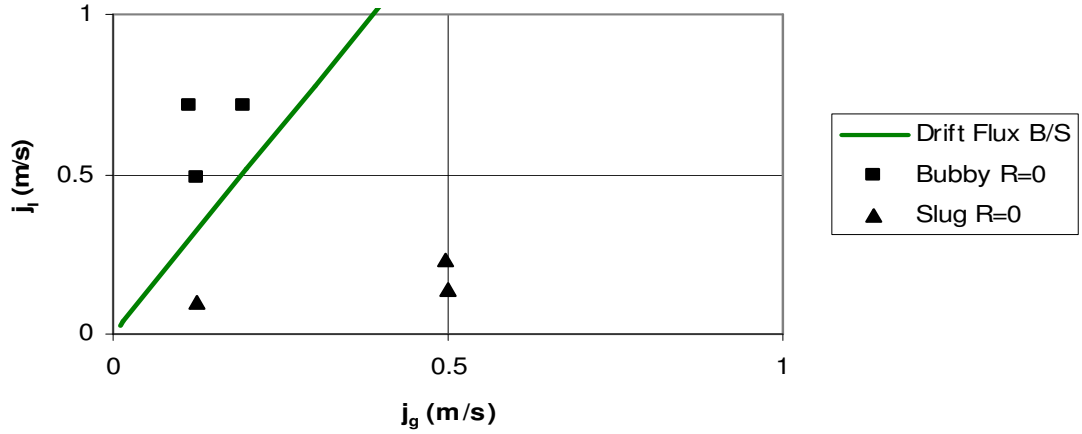

Figure 103: Drift Flux 24.5mm Linear

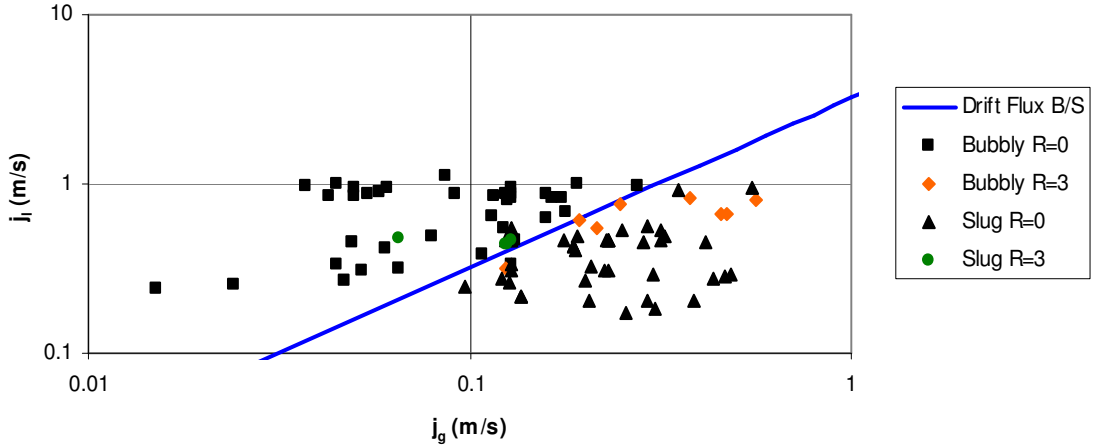

Figure 104: Drift Flux 40mm

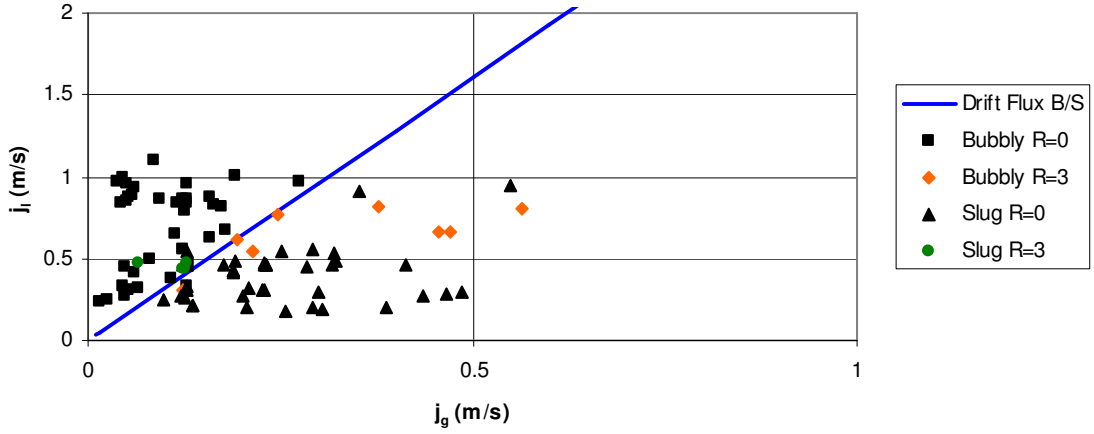

Figure 105: Drift Flux 40mm Linear

6.7.2 Slug-to-Annular

This section applies the flow regime even distribution to the slug and annular data points just as the previous section did with the bubbly and slug data. For each model and diameter, a plot is shown with the results of the even distribution. Logarithmic plots are shown again in this section for each diameter to reveal any clumping of data points.

6.7.2.1 Lee Slug-to-Annular

Figure 106 through Figure 111 show the Lee slug-to-annular transition model for the three diameter tubes. In the 9.525 mm diameter data, Lee's model incorrectly identifies two slug points. Two slug points and one annular point are incorrect for the 12.7 mm diameter data, and four slug points are incorrect in the 24.5 mm data. Visual inspection of the linear plots shows clumps of data present in the low superficial velocity regions of all three diameter experiments. The clumping of data is not affecting the Lee transition model.

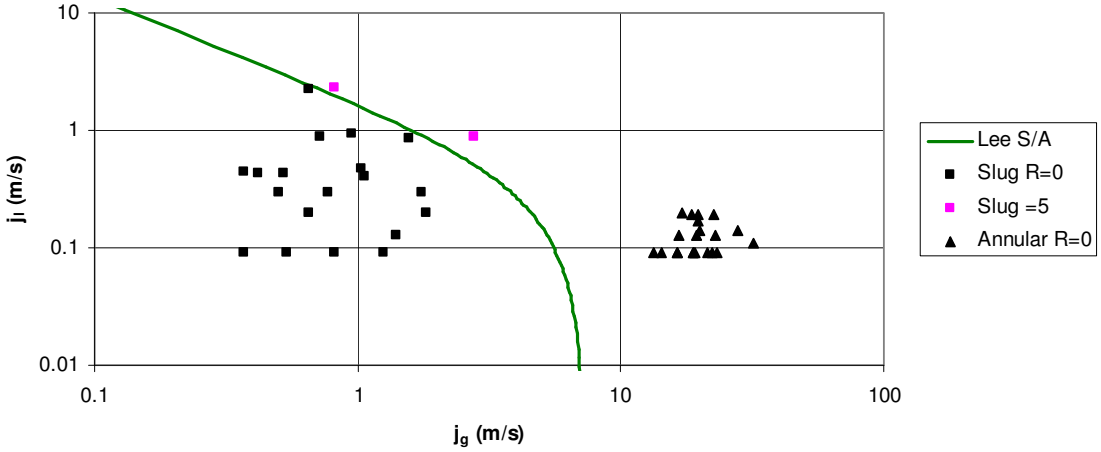

Figure 106: Lee 9.525mm

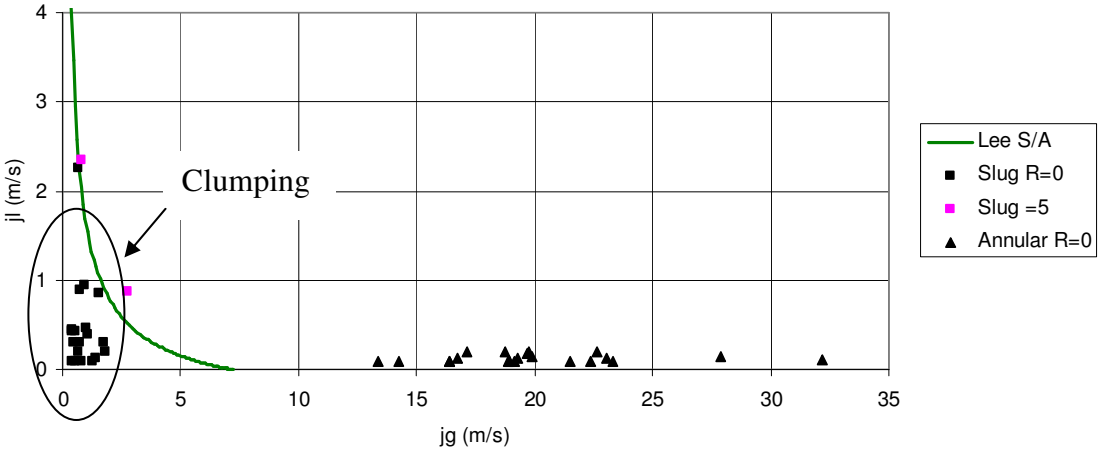

Figure 107: Lee 9.525mm Linear

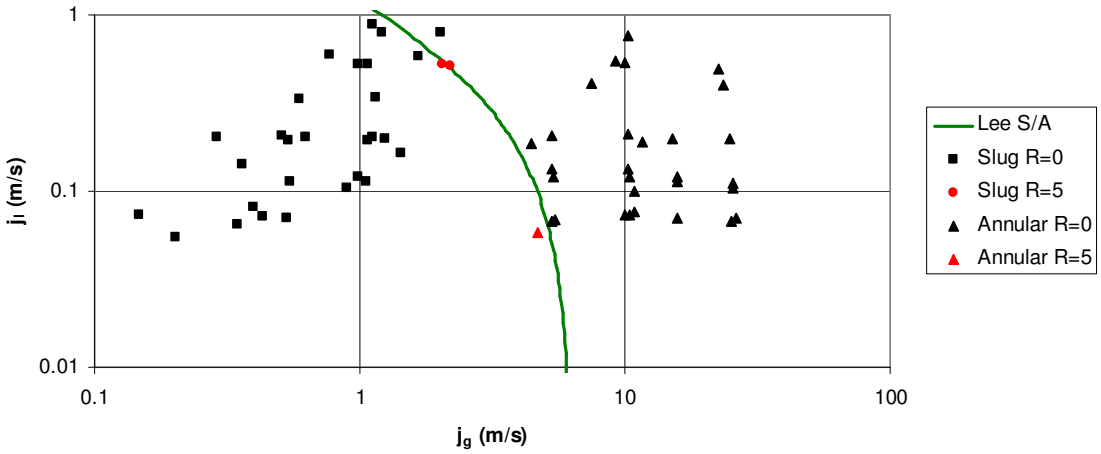

Figure 108: Lee 12.7mm

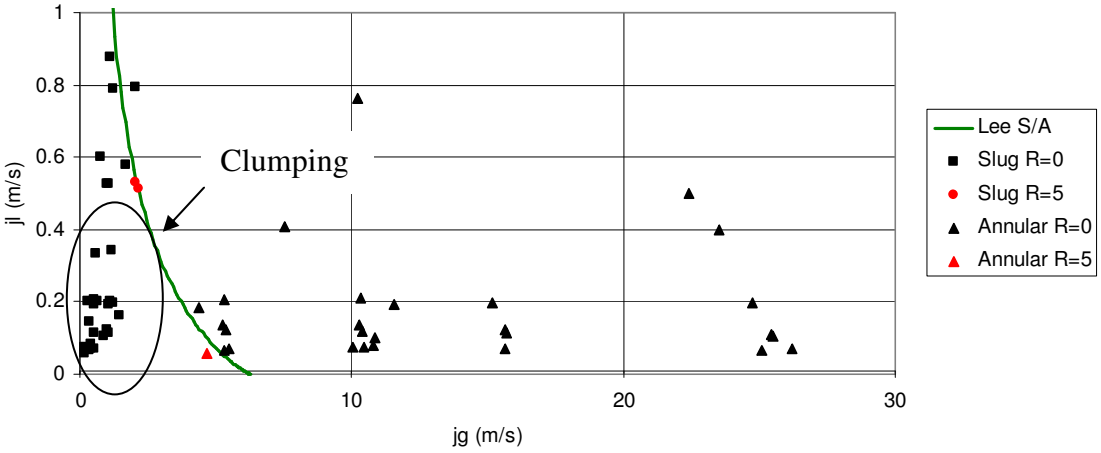

Figure 109: Lee 12.7mm Linear

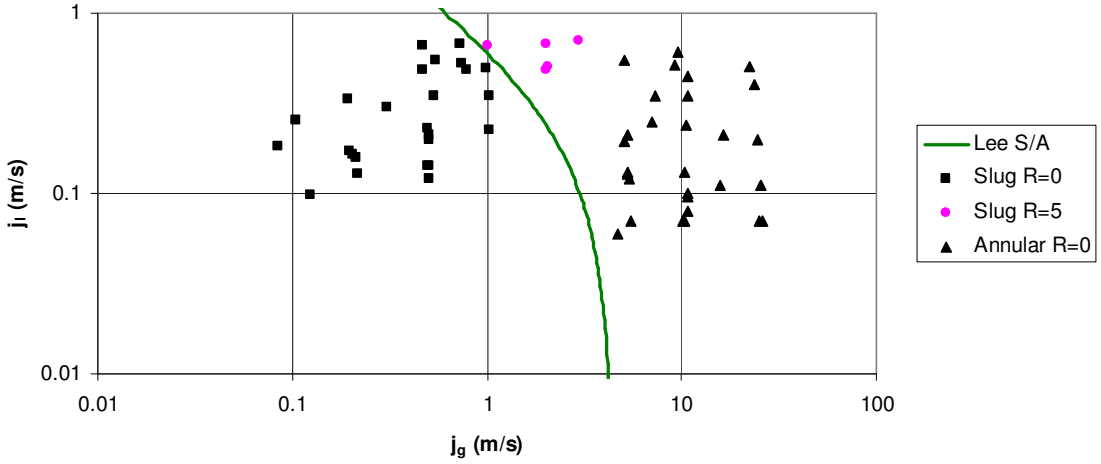

Figure 110: Lee 24.5 mm

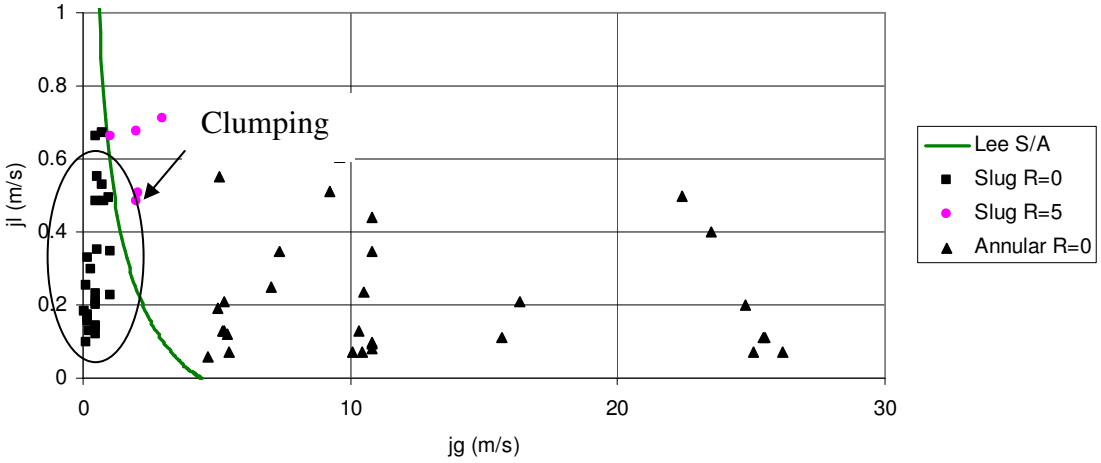

Figure 111: Lee 24.5mm Linear

6.7.2.2 Reinarts' Slug-to-Annular

Figure 112 through Figure 117 show Reinarts' slug-to-annular transition model results with the evenly distributed flow regime data points. This model is an improvement of Lee's slug-to-annular transition model so less incorrectly identified data points are expected. In the 9.525 and 12.7 mm data, one slug point is incorrect in each. The 24.5 mm data has four slug points that incorrect with two of those data points lying

directly on the transition line. As expected, Reinarts' transition line models the data better than Lee's transition line. The clumps of slug data points do not affect the grading of Reinarts' model.

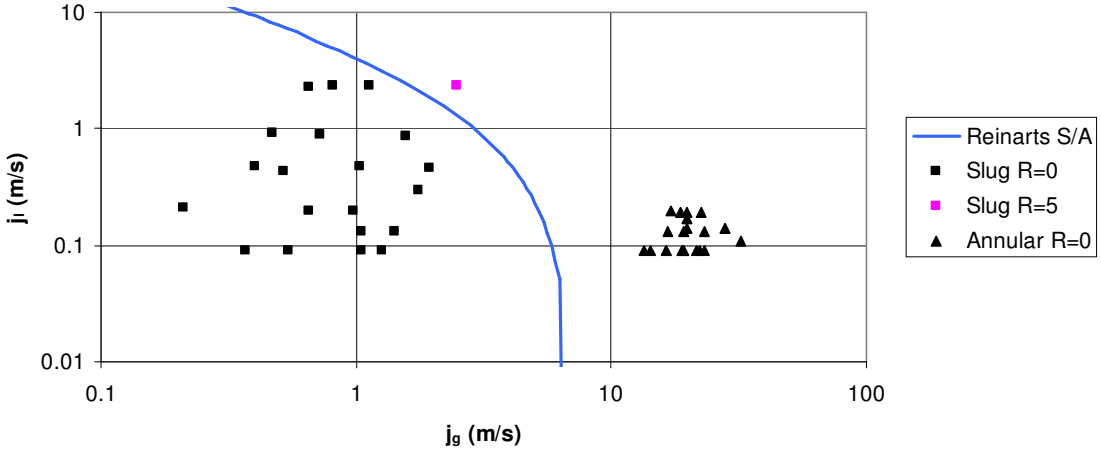

Figure 112: Reinarts 9.525mm

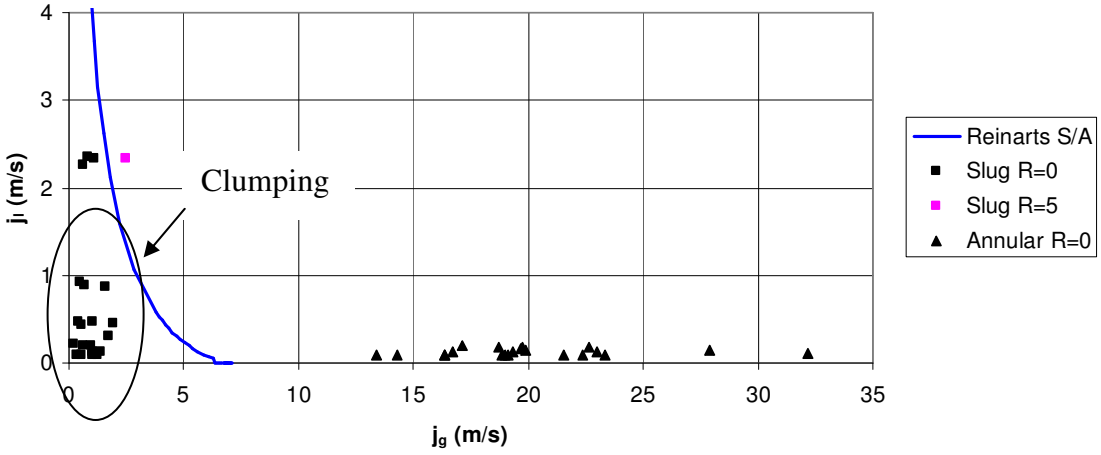

Figure 113: Reinarts 9.525mm Linear

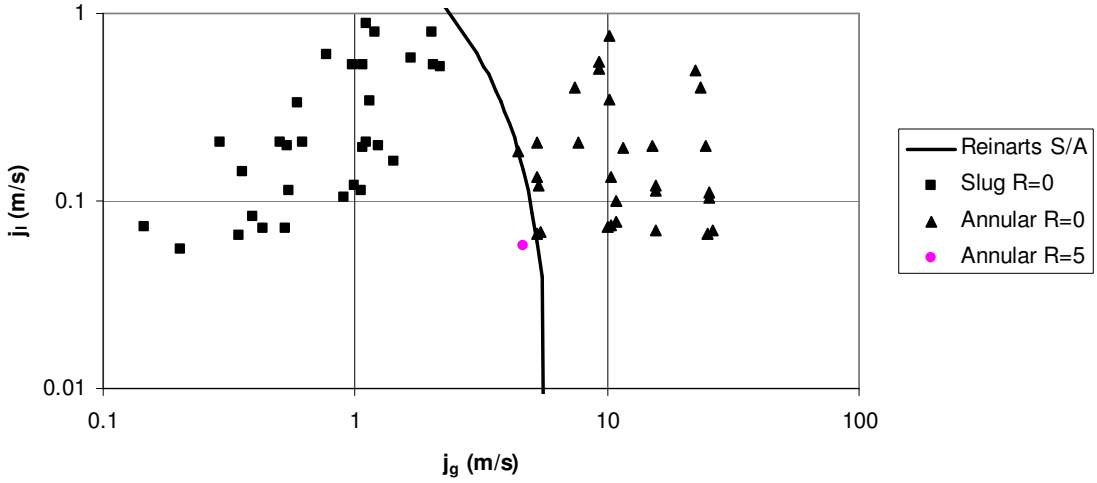

Figure 114: Reinarts 12.7mm

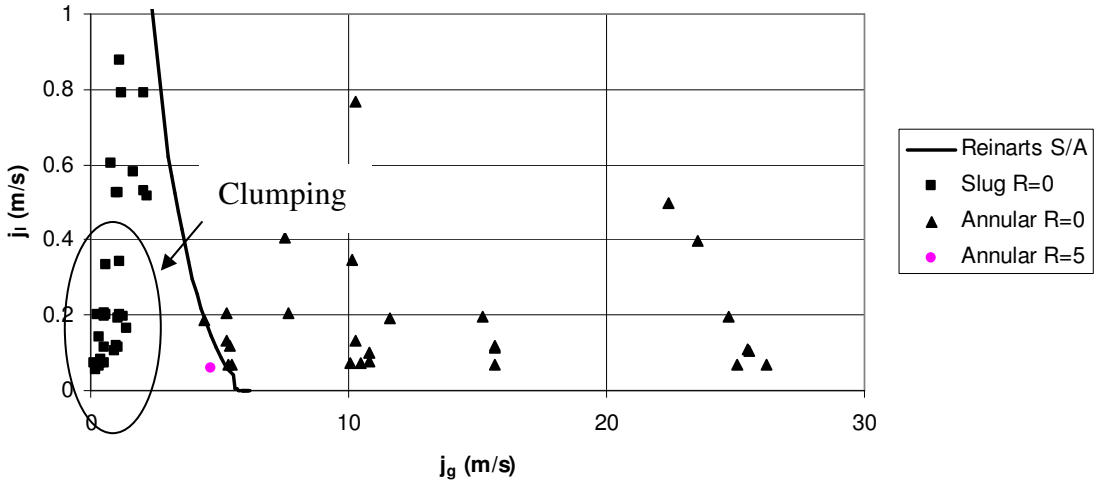

Figure 115: Reinarts 12.7mm Linear

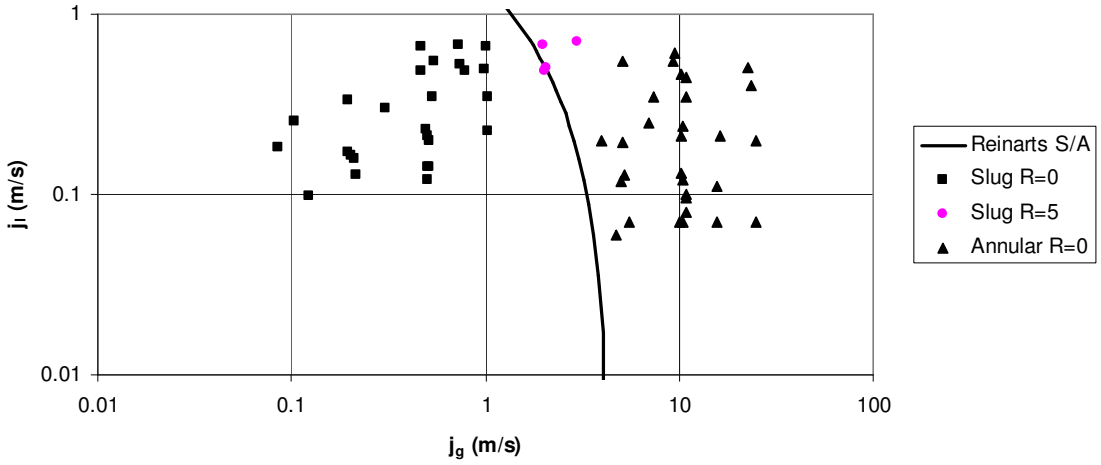

Figure 116: Reinarts 24.5mm

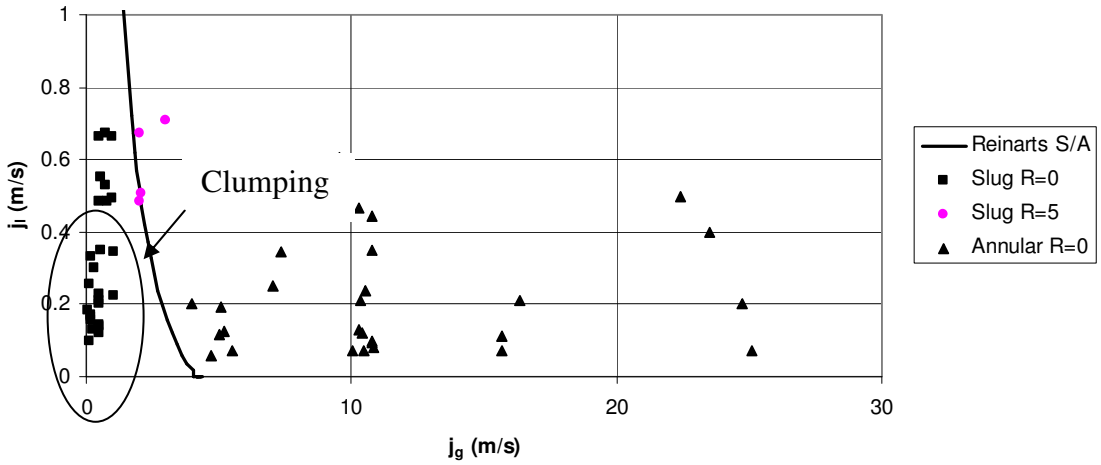

Figure 117: Reinarts 24.5mm Linear

6.7.2.3 Bousman Slug-to-Annular

Figure 118 through Figure 123 show Bousman's transition model even distribution results for each diameter tube. The model is completely correct for the 9.525 mm data, misplaces five annular points in the 12.7 mm data, and misplaces eight annular points in the 24.5 mm data. All of the incorrect points are in the annular region

suggesting that Bousman predicts the transition from slug to annular flow after the transition has already occurred.

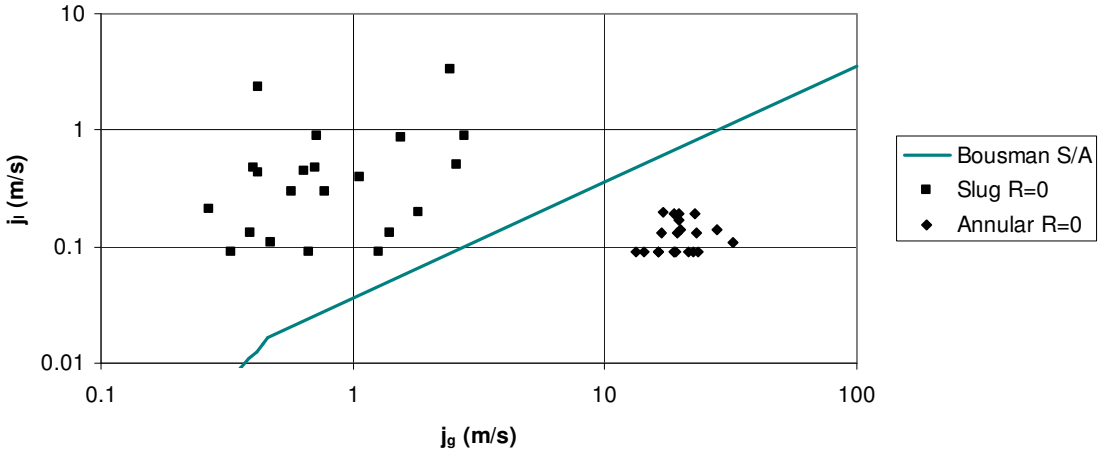

Figure 118: Bousman 9.525mm

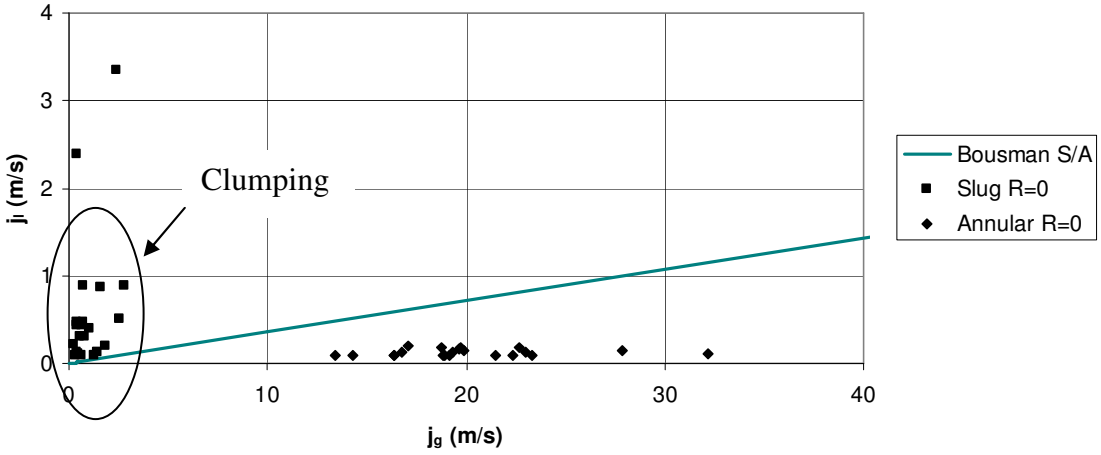

Figure 119: Bousman 9.525mm Linear

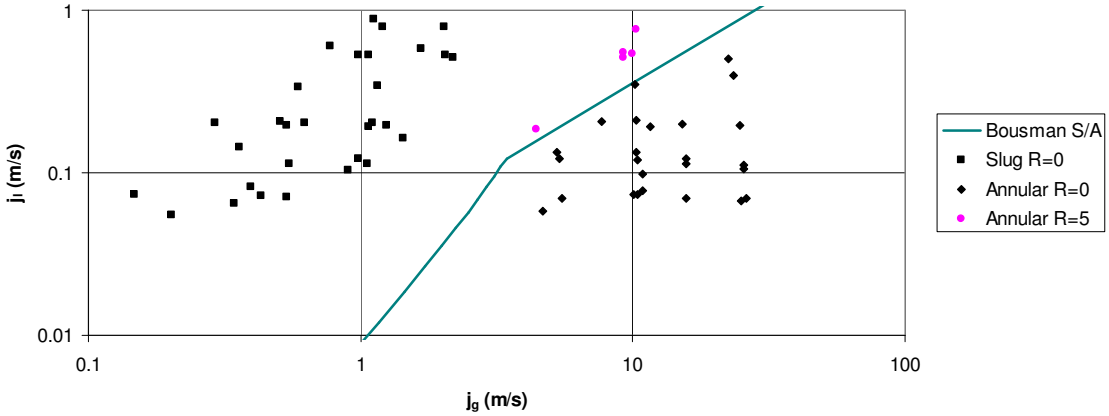

Figure 120: Bousman 12.7mm

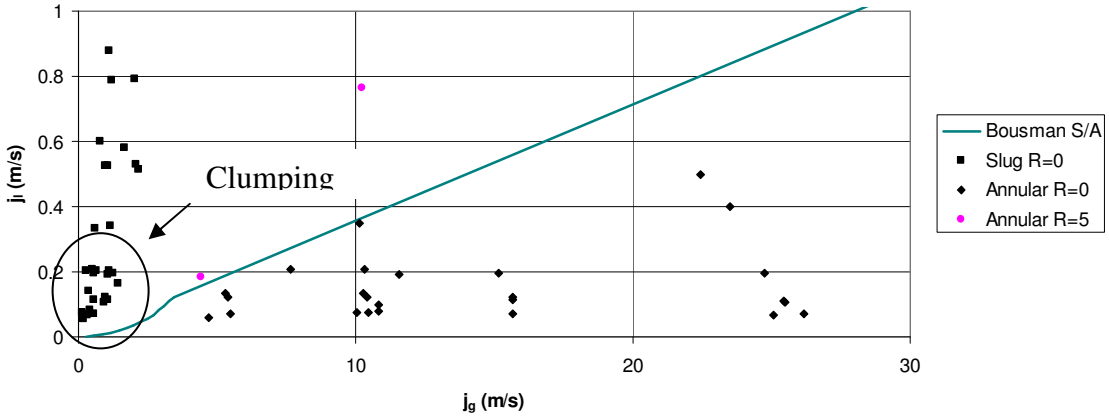

Figure 121: Bousman 12.7mm Linear

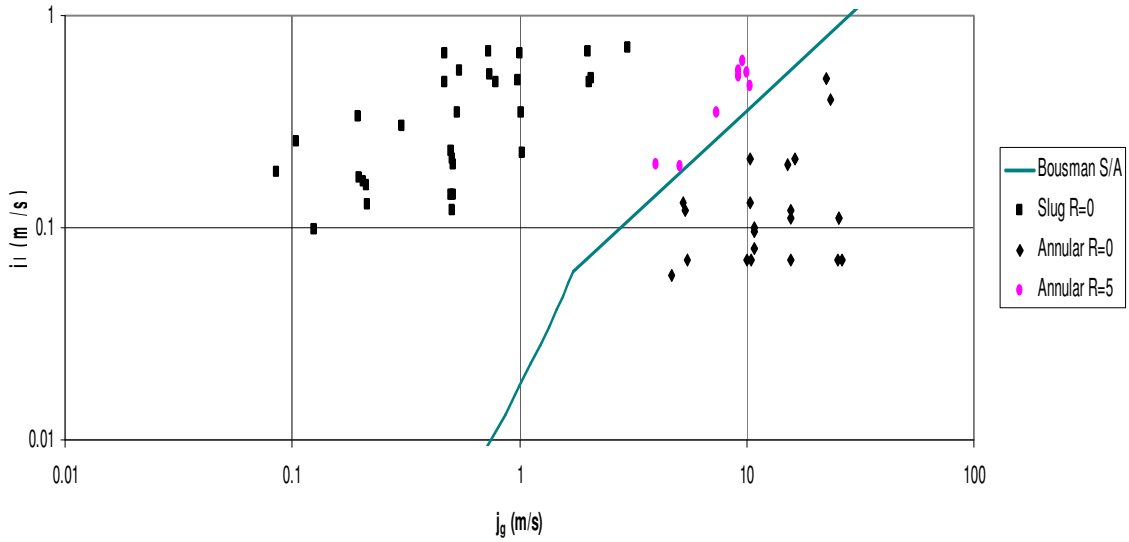

Figure 122: Bousman 24.5mm

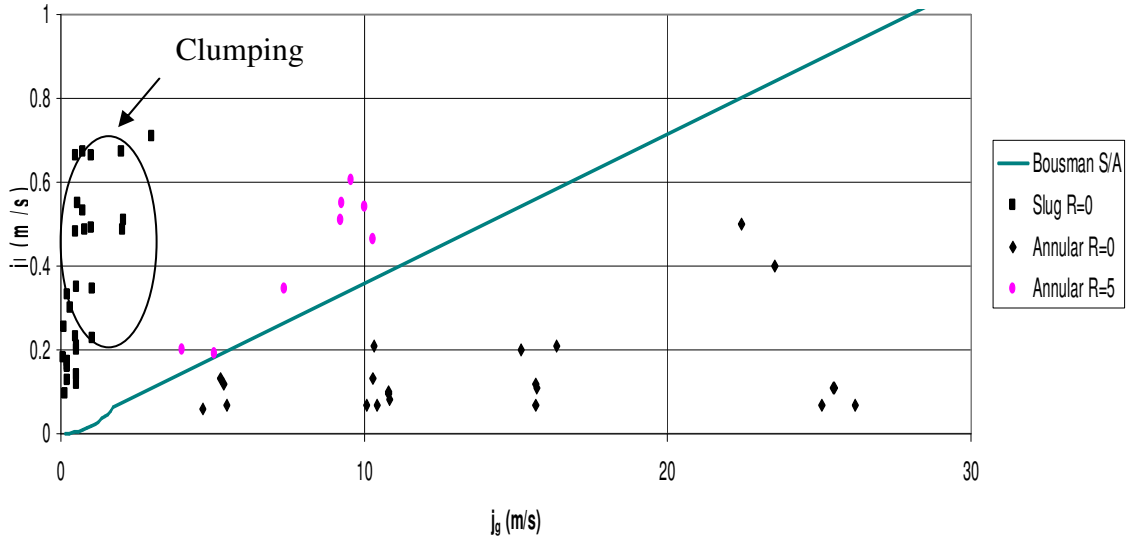

Figure 123: Bousman 24.5mm Linear

6.7.2.4 Creare Slug-to-Annular

Figure 124 through Figure 129 show the final slug-to-annular transition model, the Creare model. Creare correctly predicts all of the 9.525 mm data just as Bousman's model did. Four annular data points are incorrect in the 12.7 mm data, and five annular

data points are incorrect in the 24.5 mm data. Again all of the incorrect data points are in the annular region. The Creare model is also too late in predicting the transition from slug to annular flow.

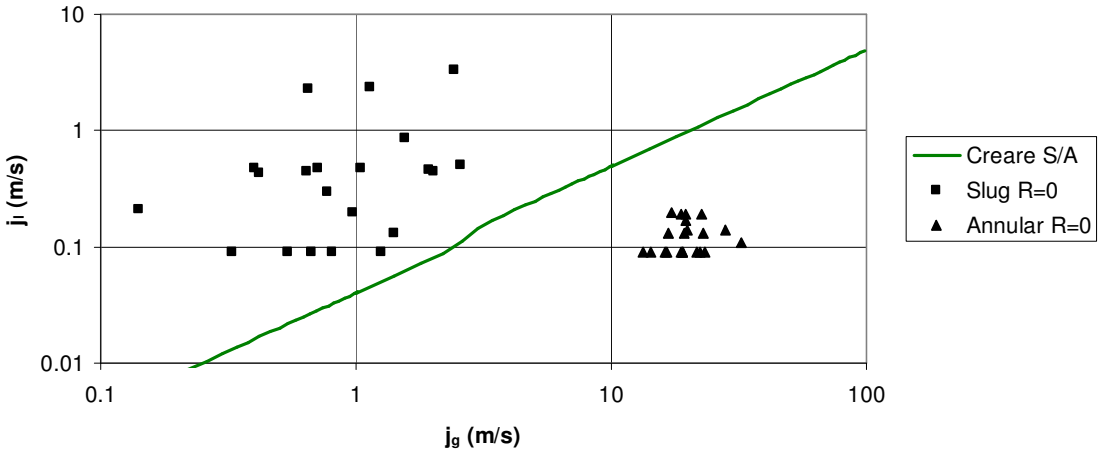

Figure 124: Creare 9.525mm

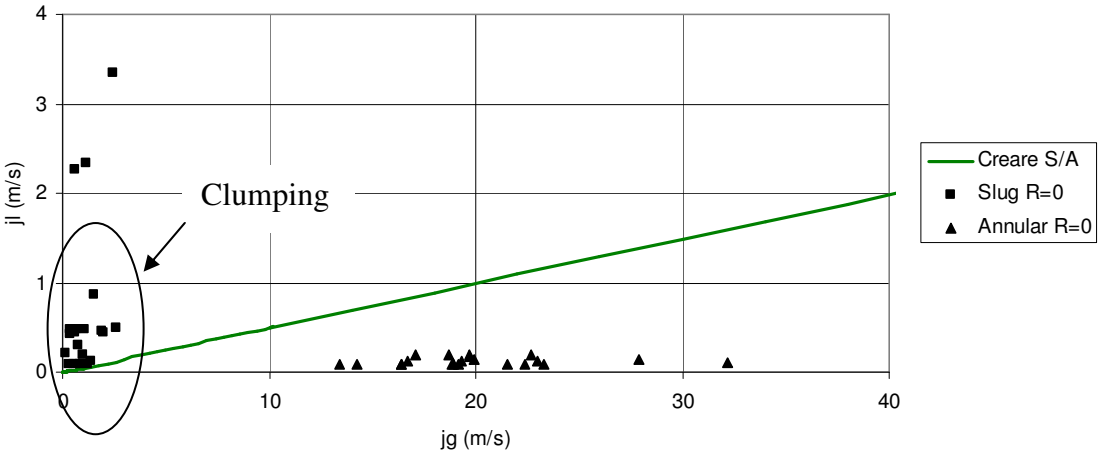

Figure 125: Creare 9.525mm Linear

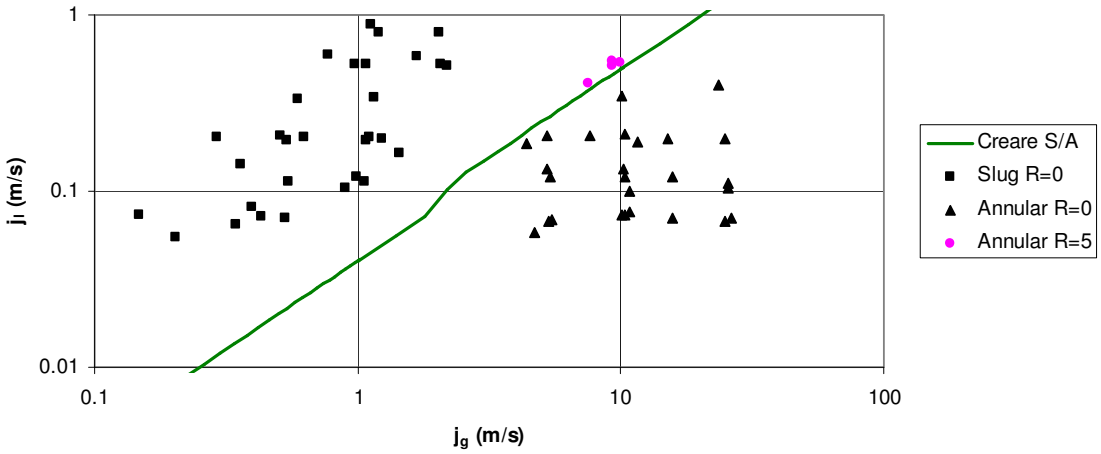

Figure 126: Creare 12.7mm

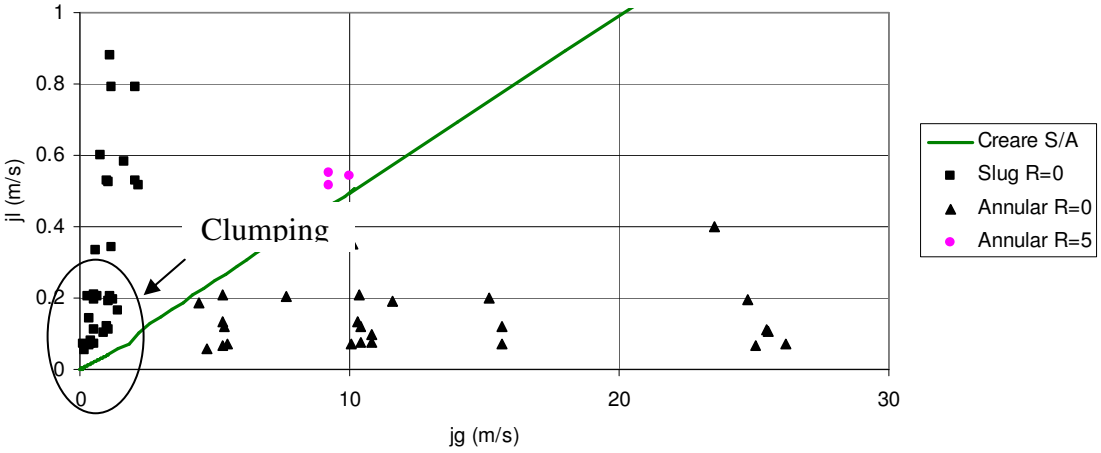

Figure 127: Creare 12.7mm Linear

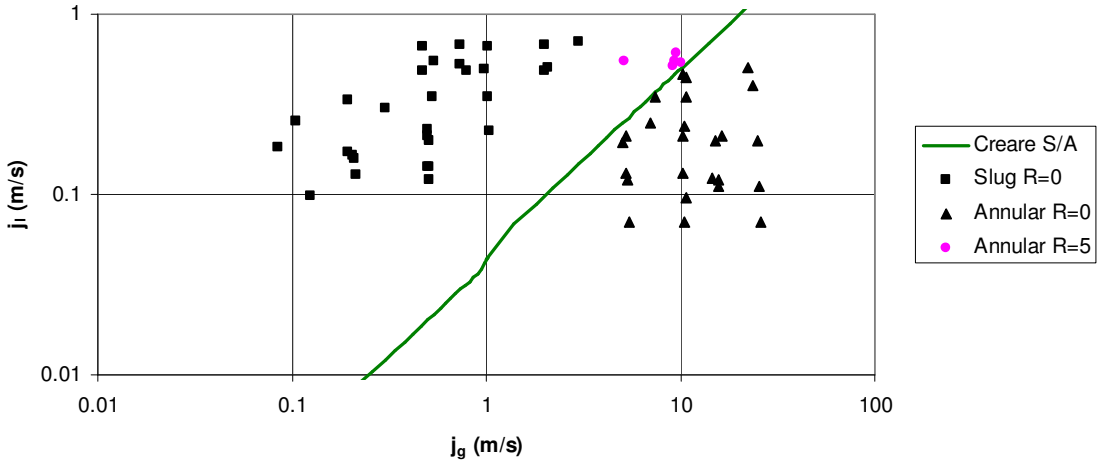

Figure 128: Creare 24.5mm

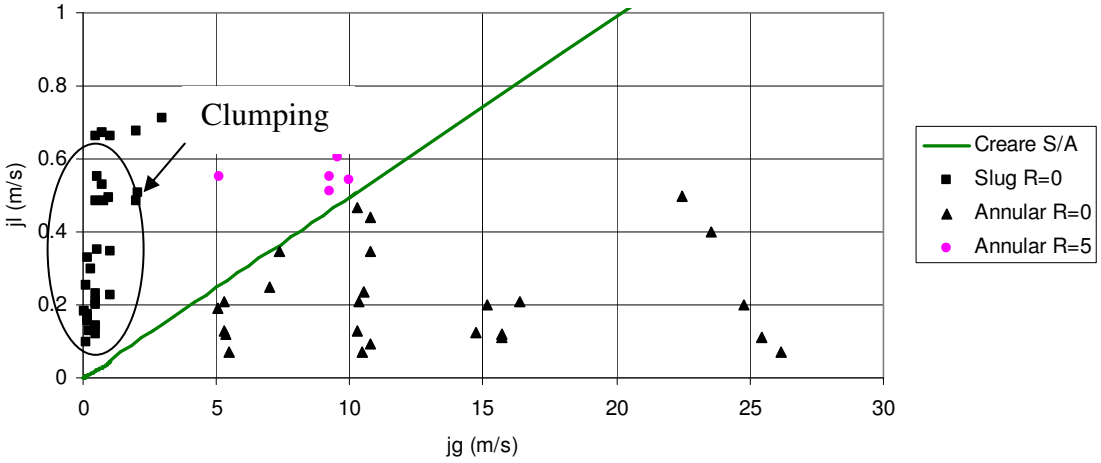

Figure 129: Creare 24.5mm Linear

6.8 Transition Region Development

The data collected from all the experiments shows that the transition from bubby to slug flow and slug to annular flow does not occur along a single line. In fact, there is a transition region where a mixed flow exists. The models all have a transition line so this section of the thesis will focus on developing a thickness study and determining how thick the transition line should be to encompass the transition region. Based on the

previous section results, the models focused in this section will be Dukler and Drift Flux for the bubbly-to-slug transition and Creare and Reinarts for the slug-to-annular transition.

6.8.1 Bubbly-to-Slug Transition Region

The 9.525 mm diameter experiment did not collect any bubbly/slug transition data so this diameter will not be studied in this section. The 12.7 mm data was perfectly modeled by all three models (Creare, Drift Flux, and Dukler) when analyzed earlier in the chapter while omitting the transition points. Now the models will be analyzed using the transition points. The Creare model utilizes the drift flux methods for bubbly-to-slug transitions in the 12.7 mm diameter tubing so Creare's model will yield the same results as the Drift Flux. The purpose of this comparison is to determine which model most efficiently captures the transition region by expanding the thickness of the transition line. Error bars of 35% are added to the transition lines of the Drift Flux and Dukler models. The results are shown below in Figure 130 and Figure 131 respectively. The Drift Flux model transition region captures all except for two transition points. Three bubbly points fall inside the transition region. The Dukler model transition region captures all but one transition point. While two bubbly data points fall on the transition boundary line, no other bubbly or slug data points fall into the transition region. Therefore the Dukler model is slightly more accurate in this comparison.

The 24.5 mm data were clearly best modeled by the Drift Flux model. A 25% error bar adjustment provides an adequate transition region as shown below in Figure 132. The transition data points either fall into the transition region or are touched by the

boundary lines. Two slug point falls within the boundary region. More data points collected in this predicted transition region would be necessary to validate the transition region.

There were no transition data points available for the 40mm diameter tube, but it is reasonable to assume that many of the data points in the region where the bubbly and slug points overlap where actually transition points. More experimentation and data collection is needed in the larger diameter tubing.

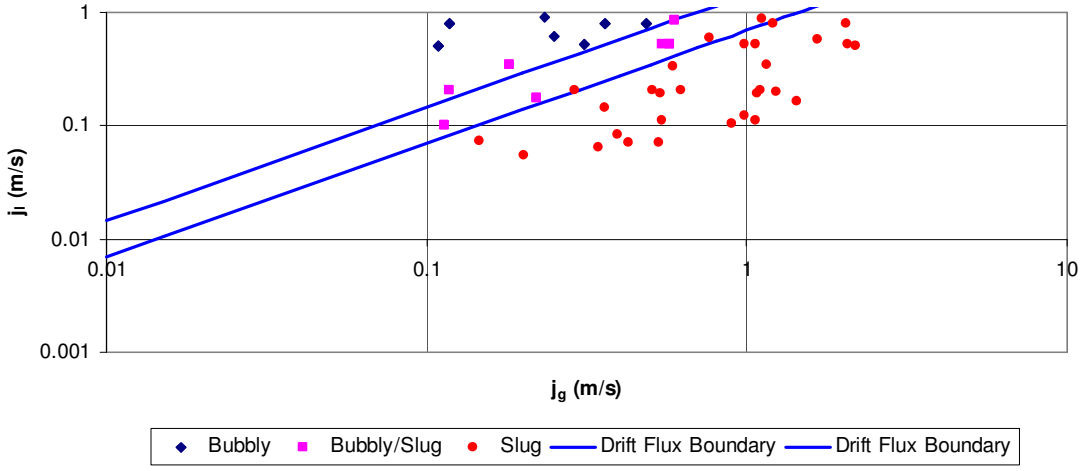

Figure 130: Drift Flux Transition Region ID=12.7 mm

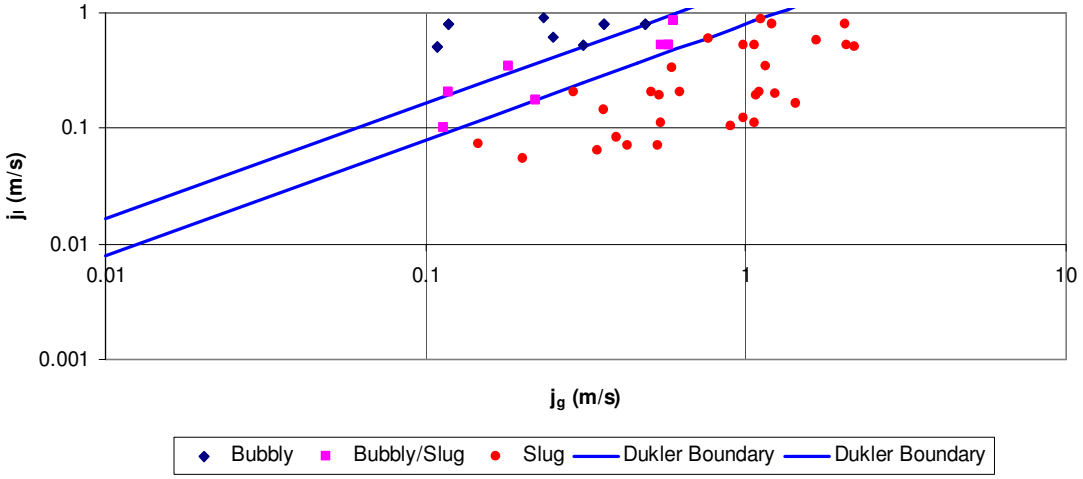

Figure 131: Dukler Transition Region ID=12.7 mm

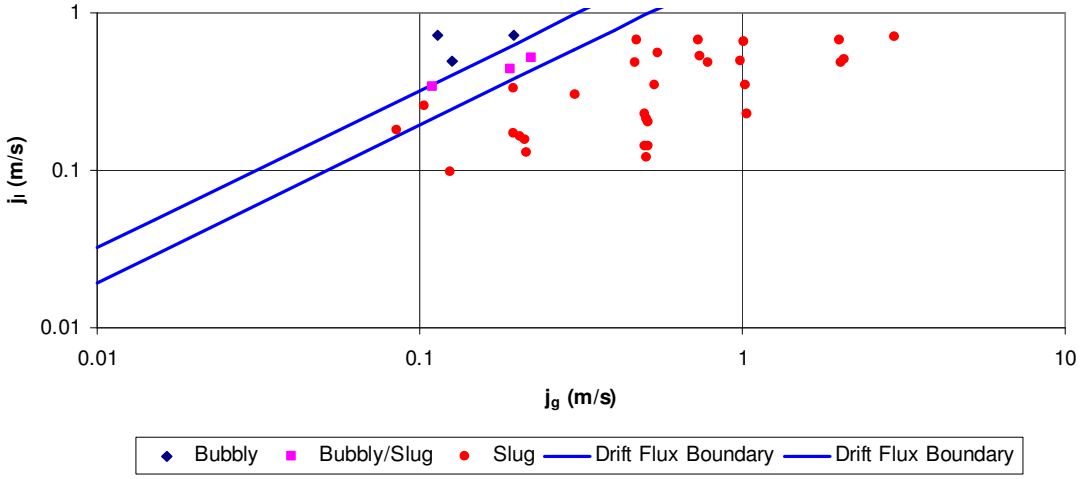

Figure 132: Drift Flux Transition Region ID=24.5 mm

6.8.3 Slug-to-Annular Transition Region

The 9.525 mm data were perfectly modeled by both the Bousman model and the Creare model earlier in this chapter. Only the bubbly and slug points were analyzed earlier so the transition points will now be analyzed. The transition region is very large in the small diameter tube. Each of the two model transition lines were thickened until

they included as many transition data points as possible without touching any of the bubbly or slug flow points. The results are shown in Figure 133 and Figure 134 for the Bousman and Creare models respectively. The transition region was developed by including error bars of 65% in each direction. The Bousman model transition region developed excludes 22 transition data points while the Creare model excludes 19 transition data points. The Creare model provides a slightly better model for this diameter tube.

Reinarts' slug-to-annular transition model fits the data best for both the 12.7 mm tube and the 24.5 mm tube. The transition lines are thickened by applying an error bar of plus and minus 25%. Reinarts' model fits the data well, but does not model the transition region well. As shown in Figure 135 for the 12.7 mm data, most of the transition data are outside of the transition region. Expanding the region to a greater thickness does not help model the region. More data collected within the predicted transition region would be necessary. Reinarts' model fits the transition data better for the 24.5 mm tube as shown in Figure 136. A 25% error region includes more than half of the transition points while only including three slug data points. Again, the model does not provide a well defined transition region. Visual observation shows that the transition data points do not follow the general shape of the transition model.

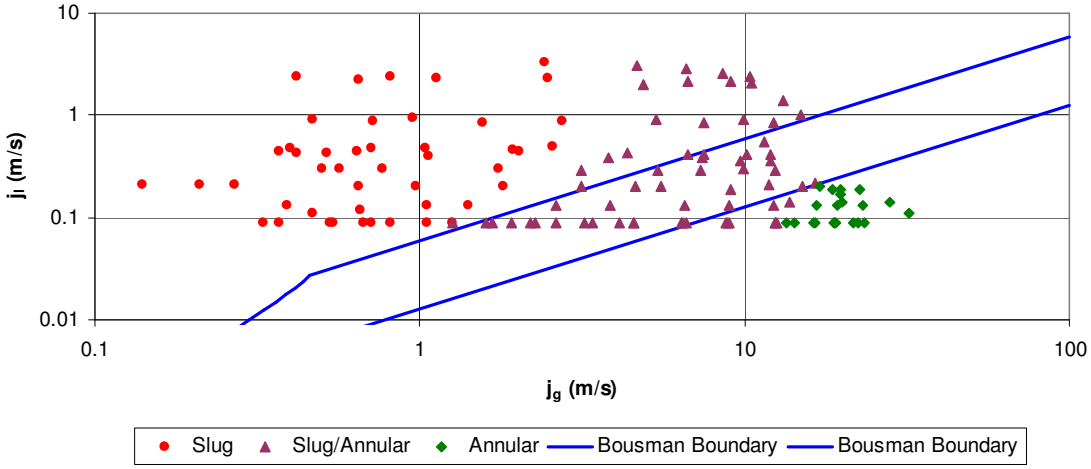

Figure 133: Bousman Transition Region ID=9.525mm

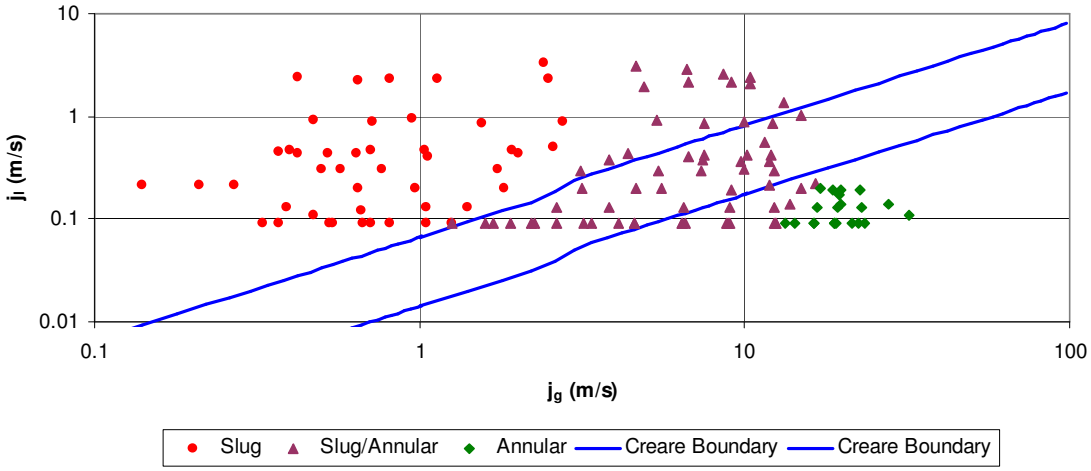

Figure 134: Creare Transition Region ID=9.525mm

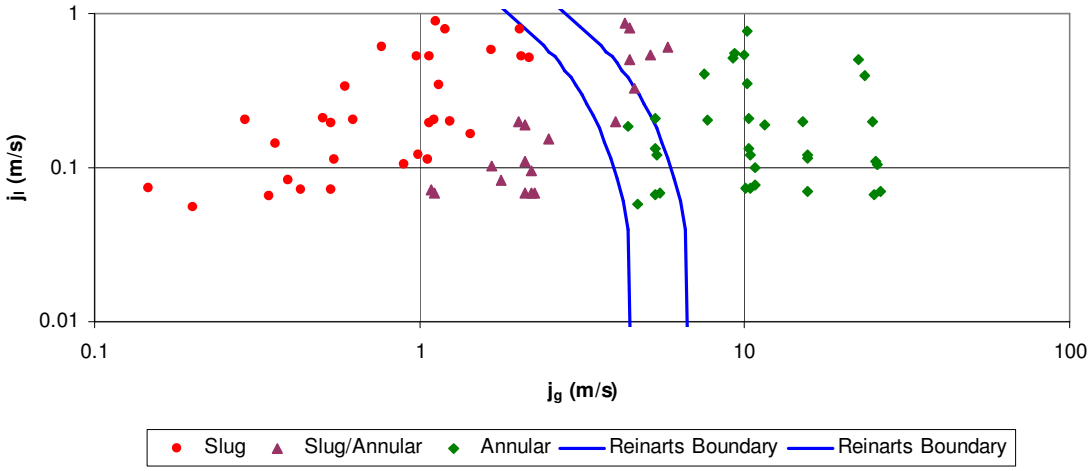

Figure 135: Reinarts Transition Region ID=12.7 mm

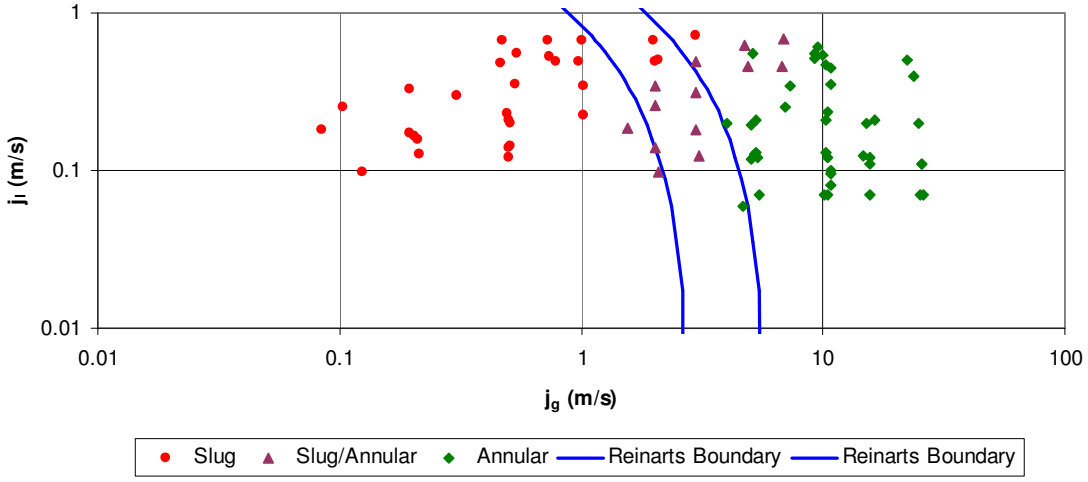

Figure 136: Reinarts Transition Region ID=24.5 mm

6.9 Summary

This chapter presents a comparison of all the models evaluated in this thesis. Visual comparison, squared difference methods, and even distribution methods were applied to find the model or combinations of models that best fits the data. Even distribution of the data caused the drift flux bubbly-to-slug model and the Creare slug-to-annular models' grades to improve. The Creare slug-to-annular model is only slightly behind Reinarts' slug-to-annular model. This chapter also looked at the strengths and weaknesses of each model. The conclusions drawn from this work will form the recommendations for RELAP5-3D flow regime mapping in reduced gravity conditions as well as the recommendations for future studies in this area.

CHAPTER VII

SUMMARY AND CONCLUSIONS

7.1 Introduction

This thesis shows the faults of the RELAP5-3D flow regime maps for use in zero gravity conditions and provides a quantitative method for comparison of various current zero gravity flow regime transition models with the purpose of recommending the best model for use in RELAP5-3D. The results presented in this thesis clearly show that there are many opportunities for future work in the area of reduced gravity flow regime mapping. These opportunities include but are not limited to data collection and model improvements. The results of this work show that several models are valuable in modeling zero gravity air/water flow regimes. Tube diameter has an impact on which model best maps the flow regime. The recommendations made for zero gravity flow regime mapping in RELAP5-3D are presented in this chapter as well as the recommendations for future studies.

7.2 Recommended Flow Regime Models

After all of the comparison studies were completed, the results show that Dukler's bubbly-to-slug flow regime transition model best models data in the smaller diameter tubes. The Drift Flux bubbly-to-slug transition model best models the data in the larger diameter tubes. Both models assume that the transition occurs at a constant void fraction. The results by diameter are presented in Table 14.

The results for the slug-to-annular flow regime transition show that Creare best models the 9.525 mm diameter data while Reinarts best models the 12.7 mm and 24.5 mm diameter data. The slug-to-annular transition regions are not well represented by either model. The Creare model is much more successful modeling the transition region than Reinarts' model. More research is required to determine the actual transition region location. The results for the slug-to-annular models are presented in Table 15.

The recommended flow regime maps for each diameter are shown in Figure 137 through Figure 140. These flow regime maps should take the place of the ones described in Chapter II in zero gravity conditions. The slug-to-annular transition regions shown in Figure 138 and Figure 139 are estimated and as discussed in the previous chapter have low confidence in the accuracy of the region. More research in the transition region specifically is needed.

Table 14: Bubbly-to-Slug Transition Model Recommendation by Inner Diameter

	Recommended Model
9.525 mm	Dukler
12.7 mm	Dukler
25.4 mm	Drift Flux
40 mm	Drift Flux

Table 15: Slug-to-Annular Transition Model Recommendation by Inner Diameter

	Recommended Model
9.525 mm	Creare
12.7 mm	Reinarts
25.4 mm	Reinarts

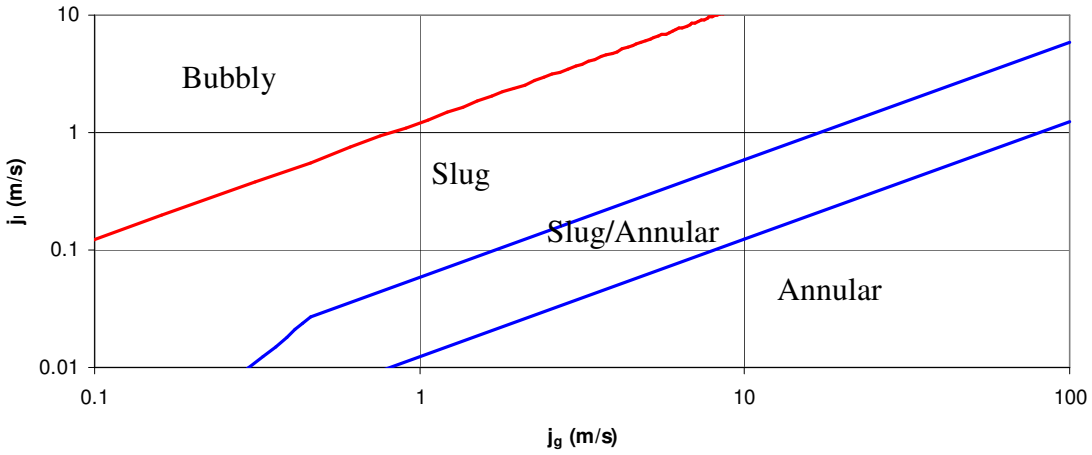

Figure 137: Recommended Flow Regime Map ID=9.525 mm

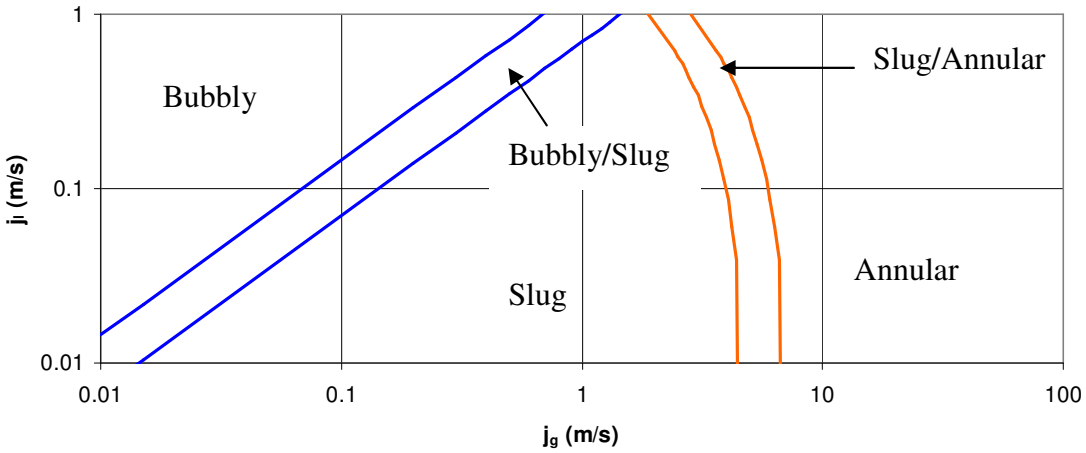

Figure 138: Recommended Flow Regime Map 12.7 mm

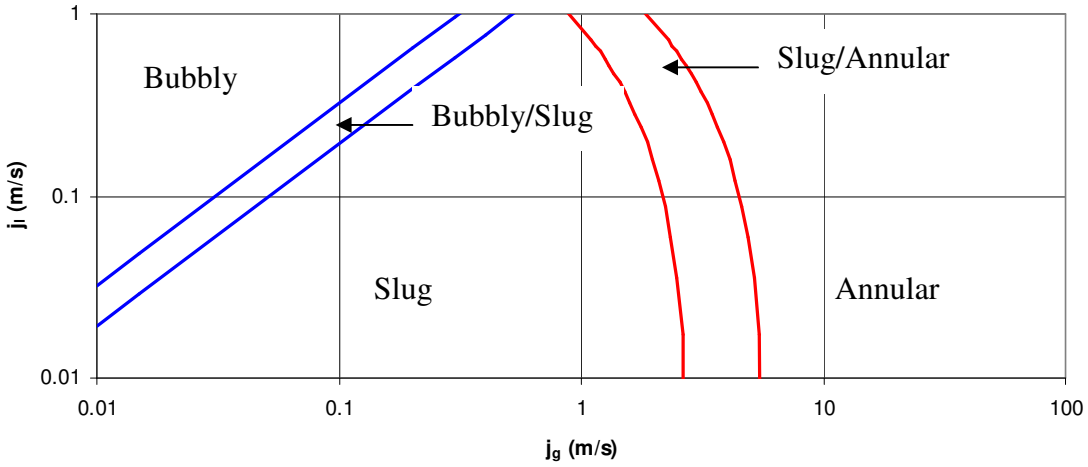

Figure 139: Recommended Flow Regime Map 24.5 mm

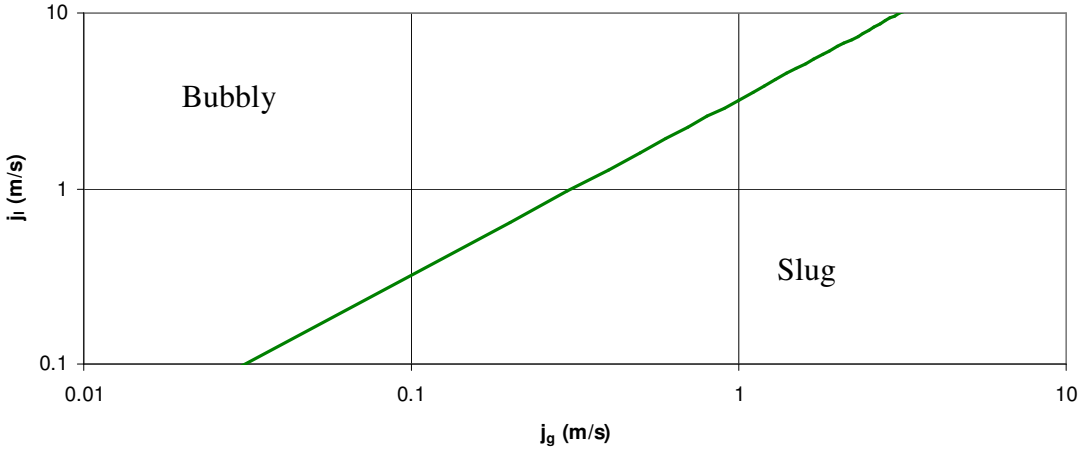

Figure 140: Recommended Flow Regime Map ID=40mm

7.3 Recommendations for Future Study

The recommendations outlined in this work are a direct result of the methodology developed in this thesis work. The main thing to note from these recommendations is that they are made strictly from this methodology. In previous research, qualitative comparisons were made to choose flow regime models. A non-biased approach was needed to compare different flow regime models, and given the data available the outlined approach provides a good start. However, the transition data

that was not directly used in the quantitative comparison calls into question some of the results. The main uncertainty in the recommendations includes the slug-to-annular transition region. While Reinarts' slug-to-annular transition model best fits the slug and annular data, it is visually apparent that the transition data points do not lie along this line or follow the shape of the transition line. Therefore the Reinarts' model provides no transition region. It is reasonable to assume that the transition data should follow the direction of the transition line predicted by a successful model. Visual observation shows that this is not the case for either the Lee or Reinarts' model. This observation will not affect the recommendations made in this work, but it should be noted. Further research could prove that Reinarts' model does not best fit the data based on the transition data points. While the Creare and Bousman models incorrectly identified more of the slug and annular points, a transition region can easily be created by thickening the transition line. Most of the transition data points fell within the transition region created due to the fact that the points followed the general shape of the transition lines. With some model manipulation, one of these two models could possibly be a better slug-to-annular model than Reinarts' model.

A recommendation made from the results of this thesis study is to improve the slug-to-annular models based on comparisons with the data. These improvements would require data collected with a specific purpose. From a visual inspection, the Creare and Bousman model shapes follow the data pattern better than the Reinarts and Lee models. This observation suggests that with improvements, these models could be much more efficient at modeling the data. From visual inspections of the Bousman and Creare slug-to-annular flow regime transition models and the "transition region" created from

thickening the transition line, it appears that in the models would fit the data much better if the transition lines had an increased slope. On all three diameters looked at in this study, an increased slope in the transition line would have yielded better results and most likely changed the recommendations.

There are many parameters utilized in the models that have values developed in fluid research performed in earth's gravity field. These values may be affected by varying gravity fields. Validation of the assumed values for reduced gravity conditions is needed. Parameters that affect slope in both the Creare and Bousman models include the distribution coefficient and the friction factors. There is uncertainty in the Equations for the friction factors, and the values and Equations for the friction factors used in the models were developed in 1969 by Wallis (Ref 14). With the change in technologies and research methods since 1969, a new study of these parameters may yield more accurate results. Data should be collected with special emphasis and with the purpose of determining the annular flow interfacial friction factors for reduced accelerations. It is feasible that further research would yield different values for the friction factors and/or distribution coefficients. While Bousman's research shows a value of 0 for microgravity drift flux, other research suggests non-zero values (Ref 15). This is yet one more parameter that needs specific research. Results from these studies should be incorporated into the various models and then compared again using the methodology outlined in this thesis as well as comparing the way the transition points fall along and beside the transition lines.

Additional general two-phase flow regime mapping data are needed. Flow regime modeling has been developed around data. Models are validated through

comparison and agreement with data. Because data often can contain experimental error, an abundance of data is required for these types of validations. Reduced gravity data collection is extremely difficult to gather. Due to the experimental difficulty, reduced gravity databases are sparse. More data collection is required to gain the same confidence in reduced gravity two-phase flow modeling as that of the 1-g modeling that is commonly used. The data points collected to be used in flow regime modeling efforts should be rigorously analyzed to ensure that only highly reliable data points are incorporated.

As shown in previous sections, equally distributed data points are desperately needed to produce unbiased comparison against the flow regime models. Flow regime data are needed at a wide range of superficial velocities, both liquid and gas velocities to truly map the transition regions. Experiments should be developed where the flow rates can be varied through a wide range of values. Predetermined test matrixes should be developed so that equal distribution across flow velocities could be achieved. Data points should also be repeated multiple times and/or the flow regime identified by multiple individuals or methods due to the fact that identification of flow regime is somewhat subjective and is most likely responsible for some of the discrepancy in the data. High speed imagery should also be collected for later comparison and validation.

Due to the fact that a majority of the flow regime models are based on constant void fraction, more data collection is required to determine the accurate value of the transition void fraction in reduced gravity conditions. How the transition void fraction changes with diameter remains invalidated. While Bousman attempted to collect void fraction data at multiple diameter tubing, the experiment was only successful for the 12.7

mm diameter tube. No other research contains transition void fraction data with air/water. Further air/water research is needed to validate models used in RELAP5-3D due to the fact that refrigerants are not currently available. Further air/water experimentation could possibly be conducted at the International Space Station (ISS) which would ease the time restraint (30 seconds per parabola aboard the plane) and also would provide more space for lengthened test sections and a greater span of tube diameters.

Due to the properties of air/water systems, most reduced gravity experiments choose other mediums for experimentation, such as refrigerants. RELAP5-3D should incorporate these refrigerants into their computer codes to compare to the vastly higher amount of reduced gravity data that is available. Varying gravity fields could then also be compared and studied with refrigerants.

REFERENCES

1. R. Oinuma, "Two-Phase Flow Issues in Space Nuclear Reactor and Nuclear Propulsion Systems" *Proc. Space Nuclear Conf* 2005. San Diego, CA (2005).

2. L. Zhao and K. S. Rezkallah, "*Gas-Liquid Flow Patterns at Microgravity Conditions*" Int. J. Multiphase Flow Vol. 19 No 5. Great Britain (1993).

3. C. Kurwitz, "New Results in Gravity Dependent Two-Phase Flow Regime Mapping" *Proc. Conf on Applications of Thermophysics in Microgravity and Breakthrough Propulsion Physics*, Albuquerque, NM (2002).

4. G. F. Hewitt, "Multiphase Flow: The Gravity of the Situation," *Third Microgravity Fluid Physics Conf*, Cleveland, OH 44135 (1996).

5. T. R. Reinarts, "Prediction of Annular Two-Phase Flow in Microgravity and Earth-Normal Gravity" *AIChE Symposium Series*. Houston, TX (1996).

6. RELAP5-3D Code Development Team, "*RELAP5-3D Code Manual Volume IV: Models and Correlations*" Idaho National Engineering Laboratory, Idaho Falls, ID (2005).

7. J.G. Collier, *Convective Boiling and Condensation,* Clarendon Press, Oxford, NY (2001).

8. C. J. Crowley, "*Unified Flow Regime Predictions at Earth Gravity and Microgravity*" Creare Inc, Hanover, NH, (1989).

9. W. S. Bousman, A. E. Dukler "Studies of Gas-Liquid Flow in Microgravity: Void Fraction, Pressure Drop and Flow Patterns" *Proc. Conf ASME Winter Meeting*, New Orleans, LA (1993).

10. K. M. Hurlbert, *Flow Dynamics for Two-Phase Flows in Partial Gravities,* Disseration. Dept. of Mech. Engr. Univ. of Houston, Houston, TX (2000).

11. Aircraft Operations Division, *Operations User's Guide JSC Reduced Gravity Program User's Guide Rev D , National Aeronautics and Space Administration*, Houston, TX (2000).

12. T. R. Reinarts, *Adiabatic Two-Phase Flow Regime Data and Modeling for Zero and Reduced (Horizontal Flow) Acceleration Fields*, Dissertation. Dept of Nuclear Engineering, Texas A&M University, College Station, TX (1993).

13. W. S. Bousman, *Studies of Two-Phase Gas-Liquid Flow In Microgravity,* Dissertation, Department of Chemical Engineering, University of Houston (1994).

14. C. J. Crowley, M. J. Izenson, *Design Manual for Microgravity Two-Phase Flow and Heat Transfer,* Air Force Space Technology Center Space Division, San Diego, CA (1989).

15. Kurwitz, and F. Best, "A Statistical Comparison of Various Fluids for a Drift Flux Model in Reduced Gravity Two-Phase Slug Flow," *Proc. Conf Applications of Thermophysics in Microgravity and Breakthrough Propulsion Physics*, Albuquerque, NM (2005).

VITA

Name:	Melissa Renee Ghrist
Address:	Department of Nuclear Engineering 3133 TAMU College Station, Tx 77483-3133
Email Address:	melissa.ghrist@gmail.com
Education:	B.S., Nuclear Engineering, Texas A&M University, 2005 M.S., Nuclear Engineering, Texas A&M University, 2008